THESIS APPROVAL

GRADUATE SCHOOL, KASETSART UNIVERSITY

Doctor of Philosophy (Chemistry)
DEGREE

Chemistry
FIELD

Chemistry
DEPARTMENT

TITLE: Productions of the Hydroxyapatite from Calcium Based Natural Sources and Their Application as Drug Delivery

NAME: Miss Upsorn Boonyang

THIS THESIS HAS BEEN ACCEPTED BY

THESIS ADVISOR
(Associate Professor Sutatip Siripaisarnpipat, Ph.D.)

COMMITTEE MEMBER
(Associate Professor Paisan Kongkachuichay, Ph.D.)

COMMITTEE MEMBER
(Associate Professor Atchana Wongchaisuwat, M.S.)

DEPARTMENT HEAD
(Assistant Professor Noojaree Prasitpan, Ph.D.)

APPROVED BY THE GRADUATE SCHOOL ON _____

DEAN
(Associate Professor Gunjana Theeragool, D.Agr.)

THESIS

PRODUCTIONS OF THE HYDROXYAPATITE FROM CALCIUM BASED NATURAL SOURCES AND THEIR APPLICATION AS DRUG DELIVERY

UPSORN BOONYANG

A Thesis Submitted in Partial Fulfillment of
the Requirements for the Degree of
Doctor of Philosophy (Chemistry)
Graduate School, Kasetsart University
2010

Upsorn Boonyang 2010: Productions of the Hydroxyapatite from Calcium Based Natural Sources and Their Application as Drug Delivery. Doctor of Philosophy (Chemistry), Major Field: Chemistry, Department of Chemistry. Thesis Advisor: Associate Professor Sutatip Siripaisarnpipat, Ph.D. 130 pages.

The crocodile bone powder was successfully converted into hydroxyapatite by thermal process. The XRD and FTIR spectra support the type B hydroxyapatite. High purity hydroxyapatites (HAp) were synthesized from coral (*Acropora Formosa*), freshwater shell (*Hyriopsis myersiana*) and crocodile eggshell by hydrothermal process. The *in vitro* bioactivity study in simulated body fluid (SBF) at 37 °C reveals that the bone hydroxyapatite is less bioactive than the hydroxyapatite from calcium based natural source. The size and shape of drug molecule and pore size of hydroxyapatite affect the amount of drug loading in the hydroxyapatite. Thus, percentage drug loading of vancomycin whose structure is large and bulky is less than that of tetracycline. The release profiles for both drugs show that the release behavior consists of two stages: the initial step was fast release, followed by a relatively slow release.

/ /

Student's signature Thesis Advisor's signature

ACKNOWLEDGEMENT

I would like to thank the following individuals for their help and support: Assoc. Prof. Sutatip Siripaisarnpipat, my thesis advisor, for all of the guidance and support that she has shown me throughout the course of my graduate career. Prof. Andreas Stein for his generous mentoring in study of drug delivery system and open access to his laboratory facilities, Prof. Besim Ben-Nissan for his valuable suggestion and comments on biomaterials, Assoc. Prof. Paisan Kongkachuichay for his advice in material characterizations, Assoc. Prof. Atchana Wongchaisuwat for her insightful collaboration on analysis project, current and former members of the Siripaisarnpipat research group, Dr. Tanwawan Duangtongyu, Panana Kitipaisanlnont and Wachirapun Punkrawee, for their friendship and contributions to this work.

In addition, I am grateful for the financial support from: (1) The Royal Golden Jubilee Ph.D. Program (Grant No. PHD/0070/2547), Research Assistantship from the Thailand Research Fund (TRF), (2) The RGJ-CHE-PhD-SW, Research Fund from Walailak University, (3) The Research and Development Institute, Kasetsart University, Commission on Higher Education, Ministry of Education and (4) STRF grant from Department of Chemistry, Faculty of Science, Kasetsart University.

Finally, I must especially thank my parents, Wanida and Samai Boonyang, my elder sister, Siriporn Boonyang, my younger brother, Suriyan Boonyang, my friends for all of the love and support that they have shown me throughout my life. Their strong belief in education has carried me through my years of schooling. They have been a blessing to me, helping me when I needed it most. Thank you for providing a warm and unconditional love that always brightened my day. I would not have reached this point without their balance and perspective. Thank you all.

Upsorn Boonyang

February, 2010

TABLE OF CONTENTS

Page

LIST OF TABLES

LIST OF TABLES (Continued)

Appendix Table **Page**

LIST OF FIGURES

LIST OF FIGURES (Continued)

LIST OF FIGURES (Continued)

LIST OF FIGURES (Continued)

LIST OF FIGURES (Continued)

Appendix Figure

LIST OF SYMBOLS AND ABBRAVIATIONS

BHAp	=	bone hydroxyapatite
HAp	=	hydroxyapatite
β-TCP	=	beta tricalcium phosphate
TC	=	tetracycline
VM	=	vancomycin
IMC	=	indomethacin
EDTA	=	ethylenediaminetetraacetic acid
Tris	=	tris (hydroxymethyl) aminomethane
IgG	=	immunoglobin G
ppm	=	part per million
SBF	=	stimulated body fluid
CPBSz	=	citric-phosphate buffered saline
SEM	=	scanning electron microscopy
ESEM	=	environmental scanning electron microscopy
TEM	=	transmission electron microscopy
EDS	=	energy dispersive spectrometry
SAED	=	selected area electron diffraction
XRD	=	X-ray diffractometry
BET	=	the Brunauer-Emmett-Teller
FTIR	=	fourier transform infrared spectroscopy
ICP-AES	=	inductively coupled plasma atomic emission spectroscopy
FWHM	=	the full width at half maximum
JCPDS	=	the Joint Committee on Powder Diffraction Standards
ASTM	=	the American Society for Testing and Materials

PRODUCTIONS OF THE HYDROXYAPATITE FROM CALCIUM BASED NATURAL SOURCES AND THEIR APPLICATION AS DRUG DELIVERY

INTRODUCTION

Hydroxyapatite is chemically similar to the mineral component of bones and hard tissues in mammals. It is one of few materials that are classed as bioactive, meaning that it will support bone ingrowths and osteointegration when used in orthopaedic, dental and maxillofacial applications. The chemical nature of hydroxyapatite lends itself to substitution, meaning that it is common for non-stoichiometric hydroxyapatite to exist. The most common substitutions involve carbonate, fluoride and chloride substitutions for hydroxyl groups, while defects can also exist resulting in deficient hydroxyapatite.

Chemical Formula

Apatite is a general term for crystalline minerals with a composition of $M_{10}(ZO_4)_6X_2$. Many elements occupy the M, Z, and X sites:

M = Ca^{2+}, Sr^{2+}, Ba^{2+}, Cd^{2+}, Pb^{2+}, etc

Z = P, V, As, S, Si, Ge, etc.

X = F^-, Cl^-, OH^-, O^{2-} , Br^-, vacancy, etc.

Various apatite compounds different in composition can be prepared by the replacement of elements for each site. Natural minerals of apatite compounds are found in igneous rocks, especially pegmatite, and in metamorphosed limestone. Biological apatite is found in bones and teeth of vertebrates.

Hydroxyapatite (HAp) belongs to the apatite family and has the chemical formula $Ca_{10}(PO_4)_6(OH)_2$ and a Ca/P molar ratio of 1.67.

Structure of Hydroxyapatite

Hydroxyapatite crystallizes in hexagonal rhombic prism, space group $P6_3/m$ with unit cell dimensions a = 0.9432 nm and c = 0.6881 nm. This space group is characterized by a sixfold c-axis perpendicular to three equivalents a-axis (a_1, a_2, and a_3) at angle of 120 ° to each other. Its unit cell contains a complete representation of the apatite crystal, consisting of Ca^{2+}, PO_4^{3-}, and OH^- groups. The three dimension crystal structure of HAp is shown in Figure 1. The projection on the c-axis onto the basal plane is shown in Figure 2 (Aoki, 1994). The hydroxyl ions lie at the corners of the project basal plane and occur at equidistant intervals (0.344 nm) along the columns perpendicular to the basal plane and parallel to the c-axis. Six of the 10 calcium ions in the unit cell are associated with the HAp in these columns, resulting in strong interactions among them.

The crystallographic data of HAp are summarized below:

Crystal system	Hexagonal
Space group	$P6_3/m$
Lattice constants	a = 0.9432 nm,
	c = 0.6881 nm
Chemical unit number	Z = 1

The apatite structure is very hospitable in allowing the substitutions of many other ions. Ca^{2+}, PO_4^{3-}, and OH^- groups in apatite can be substituted. Carbonate (CO_3^{2-}) can substitute either for the hydroxyl (OH^-) or phosphate (PO_4^{3-}) group, designate as Type A or Type B substitution, respectively. The substitutions cause morphological changes in precipitated apatite crystals as well as their properties. For example, carbonate substituted apatite is more soluble than carbonate-free synthetic apatite (Wang, 2004b). In addition to the difference in hydroxyl content, there is a size difference between the nano-crystallites in bone HAp and the micro-crystallites in the synthetic material (Takahashi *et al.*, 2001). The theoretical density of hydroxyapatite is 3.156 g/cm^3.

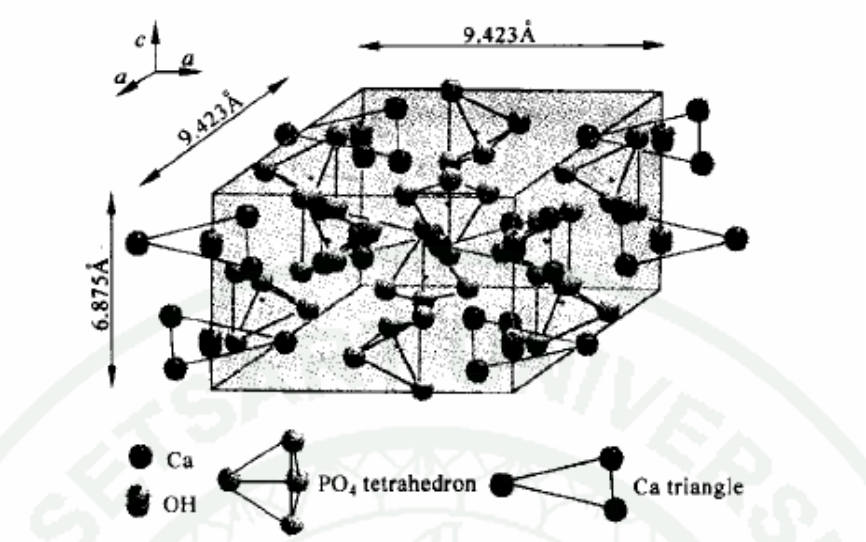

Figure 1 Crystal structure of hydroxyapatite.

Source: Aoki (1994)

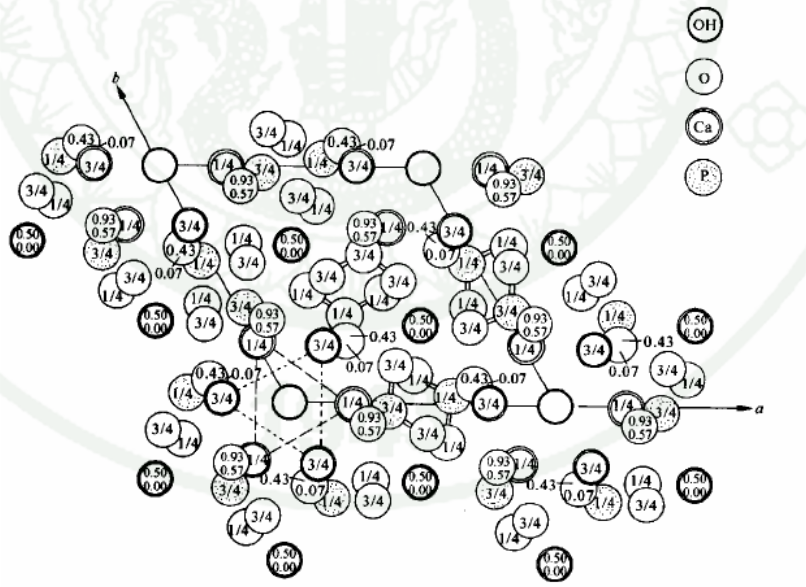

Figure 2 Projected on the basal plane of hydroxyapatite.

Source: Aoki (1994)

Applications of Hydroxyapatite

Hydroxyapatite is one of the major constituents of the inorganic components in human hard tissues (bones and teeth) and the chemical species constituting HAp crystal (Ca, P, O and H) are expected to have no toxicity. The structural chemistry of biological HAp is very complex because the mineral is not compositionally pure (non-stoichiometric), often being calcium-deficient and enriched in CO_3^{2-} which replaces PO_4^{3-} ions in various lattice sites (Mann, 2001). Composition and lists of the properties of biological apatite and hydroxyapatite are showed in Table 1. It has long been widely used as a bone substitute owing to its similarity with material constituents found in hard tissue and its high level of biocompatibility.

The mineral part of calcified tissues (bone, teeth) consists of calcium phosphates with an apatitic structure. They belong to a family of isomorphous compounds which crystallize in the hexagonal system and have the general formula:

$$Ca_{10-X}(HPO_4)_X(PO_4)_{6-X}(OH)_{2-X} \qquad \text{with } 0 \leq x < 2$$

In this family, two compounds hold a particular position, hydroxyapatite (x = 0) and tricalcium phosphate (x = 1). Hydroxyapatite, with an atomic Ca/P ratio of 1.67, is biocompatible and only slightly bioresorbable because of its insolubility. These properties, associated with those of osteoconduction, have led to it being used as a covering for prostheses. Apatitic tricalcium phosphate (TCP), with an atomic Ca/P ratio of 1.50, is also biocompatible but is more soluble than HAp, thus it is quickly biodegraded and replaced by new formed bone (Wood *et al.*, 1990).

In addition, hydroxyapatite is also used in chromatography, in catalysis and water treatment (Christoffersen *et al.*, 1991; Joris and Amberg, 2002).

Table 1 Composition and properties of biological apatite and hydroxyapatite.

	Biological Apatite		Hydroxyapatite
Major Constituent	In enamel (wt %)	In bone (wt %)	(wt %)
Ca	36.00	24.50	39.60
P	17.70	11.50	18.50
Na	0.50	0.70	
K	0.08	0.03	
Mg	0.44	0.55	
F	0.01	0.02	
Cl	0.30	0.10	
CO_3^{2-}	3.20	5.80	
Trace element: Sr,Pb, Ba,Fe, Zn, Cu, etc.			
Ca:P (molar ratio)	1.62	1.65	1.67
Lattice parameter (nm)			
a	0.9441	0.9419	0.9432
c	0.6882	0.6880	0.6881
Crystal size	130 x 30 nm	25 x (2.5–5.0)nm	μm
Elastic modulus (GPa)	14	7 - 30	10
Tensile strength (MPa)	70	50 -150	~ 100

Source: Wang (2004c)

Synthesis of hydroxyapatite

Hydroxyapatite can be synthesized via numerous production routes, using various different reactants. Many synthetic methods were used for the production of HAp such as precipitation, solid-state reaction, sol-gel and hydrothermal reaction. Basically, two staring materials are used as calcium source and phosphate source. The reactions shown below (eq.1, eq.2 and eq.3) are reported in literature. Natural materials like coral, nacre, natural gypsum, eggshell, animal bone have considered as

biowaste which are rich in calcium in the form of carbonate and oxide. An attempt to synthesize HAp using these materials as calcium source was widely studied.

$$10CaCO_3 + 6(NH_4)_2HPO_4 + 2H_2O \rightarrow Ca_{10}(PO_4)_6(OH)_2 + 6(NH_4)_2CO_3 + 4H_2CO_3 \quad (1)$$

$$CaCO_3 + 3Ca_3(PO_4)_2 + H_2O \rightarrow Ca_{10}(PO_4)_6(OH)_2 + CO_2 \quad (2)$$

$$Ca(OH)_2 + 6H_3PO_4 \rightarrow Ca_{10}(PO_4)_6(OH)_2 + 18H_2O \quad (3)$$

The crocodile belongs to a unique group of animals, being a semi-aquatic reptile. The bones are required to bear large loads as crocodile weighs up to a ton. Maintenance of a structure that enables fast movement on land and locomotion in water is required (Seebacher *et al.*, 2003). The crocodile is a reptile which has periods of slow bone growth due to lack of activity during winter. This provides a highly mineralized bone which may provide additional benefits (Lewis *et al.*, 2006). Crocodile bone may show promise as a bioceramic because it has no known complications from BSE (bovine spongiform encephalopathy) or similar diseases which occur with bovine tissue. In addition, Thailand is one of the leading crocodile producers in the world, producing a total of 170,000 units per year (Kasikorn Research Center, 2004).

Crocodile eggshells mainly consist of calcium carbonate as the other eggshells. In Thailand, crocodile eggshells are reused as decorative objects for various occasions. The size of crocodile eggshells is about three times larger than that of hen eggshells. Hence, the conversion into HAp will increase the value of crocodile eggshells. Furthermore, the growing crocodile farming industry has created an increasing abundance of this hydroxyapatite source. The natural species of sea origin, such as corals and seashells, consist of calcium carbonate (aragonite structure) as well. These seashells are just laid to waste and are abundantly available in nature. Therefore they are expected to use as calcium source for hydroxyapatite production. Nacre, known as mother-of-pearl, occurs in the inner layer of mollusk shells. Nacre is a natural composite material consisting of more than 95 wt % of calcium carbonate in

the aragonite structure and 1-5 wt % of organic matter (Zaremba *et al.*, 1998). Nacre is an osteoinductive (bone inducing) material and can imitate bone formation both *in vivo* (Atlan *et al*., 1997, 1999) and *in vitro* (Lopez *et al*., 1992; Silve *et al*., 1992).

As mention above, all biowastes, which are rich in calcium and available in nature, can be used as a source of calcium in the production of hydroxyapatite, thus will increase their values. Therefore these biowaste materials will be the starting materials for the production of hydroxyapatite in this study.

The objective of this work is to propose the economical way of synthesizing HAp from crocodile bone by thermal process and from calcium based natural sources by hydrothermal method. In addition, the *in vitro* bioactivity and antibiotic drug delivery properties of the synthesized hydroxyapatite are studied.

OBJECTIVES

1. Conversion of crocodile bone into hydroxyapatite powder by heat treatment.

2. Synthesis of hydroxyapatite powder from calcium based natural materials such as crocodile eggshells, freshwater shells and corals by hydrothermal process.

3. Characterizations of the synthesized hydroxyapatite powder by X-ray Diffractometry (XRD), Fourier Transform Infrared Spectroscopy (FTIR), Scanning Electron Microscopy (SEM), and Transmission Electron Microscopy (TEM).

4. Investigation of the *in vitro* bioactivity of the synthesized hydroxyapatite in stimulated body fluid (SBF).

5. Study of loading and releasing behaviors of the antibacterial drugs in the synthesized hydroxyapatite powder.

LITERATURE REVIEW

1. Hydroxyapatite

Hydroxyapatite, $Ca_{10}(PO_4)_6(OH)_2$, denoted as HAp, is one of the major constituents of the inorganic components in calcified tissues (bones and teeth). Because of its biocompatibility and osteoconductive properties, it has been extensively investigated for medical applications (Aoki, 1991; Wang, 2004b; Woodard *et al.*, 2007). HAp has been investigated as a bone substitute material (Suchanek and Yoshimura, 1998) due to its similar chemical composition to that of bone, its direct bone bonding ability, and its commercial availability (Wang, 2004a). HAp also has the advantage of absorbability and high binding affinity with a variety of molecules, it had been used in various drug delivery systems (Arm *et al.*, 1996; Cosijns *et al.*, 2007; Descamps *et al.*, 2009; Itokazu *et al.*, 1998; Palazzo *et al.*, 2005; Rauschmann *et al.*, 2005; Slosarczyk *et al.*, 2000) and used as the carrier for protein (Arm *et al.*, 1996; Matsumoto *et al.*, 2004; Mizushima *et al.*, 2006; Zhu *et al.*, 2004). In addition, hydroxyapatite is also used in chromatography, in water treatment (Christoffersen *et al.*, 1991) and protein purification (Schlatterer *et al.*, 2004; Suen *et al.*, 2004).

HAp in the particular form can be produced by using a variety of methods for examples, hydrothermal (Andres-Verg *et al.*, 1998; Ioku *et al.*, 2006; Xu *et al.*, 2001; Yoshimura and Suda, 1994b; Yoshimura *et al.*, 2004; Zhang *et al.*, 2005), sol-gel (Beganskienė *et al.*, 2003; Cheng *et al.*, 2001; Fathi and Hanifi, 2007; Feng, *et al.*, 2005), solid-state reaction (Nasiri-Tabrizi *et al.*, 2009; Rhee, 2002), microwave irradiation (Murugan and Ramakrishna, 2006; Parhi *et al.*, 2004, 2006; Wang *et al.*, 2006), and precipitation (Cao *et al.*, 2005; Monmaturapoj, 2008; Yeong *et al.*, 1999; Zhang *et al.*, 2002). For each method two starting materials are used as a calcium source and a phosphate source. Some calcium and phosphate precursors are listed in Table 2. The hydrothermal method has been widely used for preparation of the HAp. Moreover HAp with good crystalline and homogeneous size and shape were achieved at low temperature (Suchanek and Yoshimura, 1998; Yoshimura and Suda, 1994a).

Table 2 Calcium and phosphate sources for syntheses of hydroxyapatite.

Ca source	PO_4^{3-} source	References
$Ca(OH)_2$	H_3PO_4	(Lee and Oh, 2003a)
$Ca(OH)_2$	$CaHPO_4 \cdot 2H_2O$	(Liu *et al.*, 2003; Nasiri-Tabrizi *et al.*, 2009; Rivera. *et al.*, 2003)
$CaCl_2$	Na_3PO_4	(Parhi *et al.*, 2004)
$Ca(NO)_3$	Na_2HPO_4	(Liu *et al.*, 2004)
$Ca(NO)_3$	$(NH_4)H_2PO_4$	(Cao *et al.*, 2005; Sung *et al.*, 2004)
$Ca(NO)_3$	P_2O_5	(Feng *et al.*, 2005)
$CaCO_3$	$CaHPO_4 \cdot 2H_2O$	(Nasiri-Tabrizi *et al.*, 2009; Toriyama *et al.*, 1996)
$CaCO_3$	$(NH_4)_2HPO_4$	(Rocha *et al.*, 2005; Zhang and Vecchio, 2006)
$CaCO_3$	$Ca_3(PO_4)_2$	(Rivera *et al.*, 1999)
$Ca(CH_3COOH)_2 \cdot H_2O$	H_3PO_4	(Ioku *et al.*, 2002)

Since starting material of HAp production is calcium, many research groups proposed an economical way of synthesizing HAp from natural materials such as corals (Chattopadhyay *et al.*, 2007; Hu *et al.*, 2001; Innes *et al.*, 2003; Roy and Linnehan, 1974; Sivakumar *et al.*, 1996; Xu *et al.*, 2001), seashells (Lemos *et al.*, 2006; Ni and Ratner, 2003; Shen *et al.*, 2006; Vecchio *et al.*, 2007; Zaremba *et al.*, 1998; Zhang and Vecchio, 2006) , eggshells (Lee and Oh, 2003a, 2003b; Nayar and Guha, 2009; Prabakaran *et al.*, 2005; Rivera *et al.*, 1999, 2003; Sanosh *et al.*, 2009; Sasikumar and Vijayaraghavan, 2006), Cuttlefish backbones (Rocha *et al.*, 2005a, 2005b), fish bone (Prabakaran and Rajeswari, 2006) and bovine bone (Herliansyah *et al.*, 2009; Kim *et al.*, 2008; Ooi *et al.*, 2007; Ruksudjarit *et al.*, 2008). Chemical analyses have shown that these natural materials which are otherwise considered as biowaste are rich sources of calcium in the form of carbonates and oxide.

The hydrothermal method was first used for hydroxyapatite formation directly from corals (*Porites*), which is a natural calcium carbonate material with aragonite

structure, by Roy and Linnehan (1974). It was reported that complete replacement of aragonite by phosphatic material was achieved under 270 ºC and 103 MPa by using the hydrothermal process. In 1996, HAp derived from Indian coral using hydrothermal process was reported by Sivakumar *et al.* Coral was subjected to a temperature of 900ºC at which all organic materials were removed and all carbonate phases were decomposed. The calcium carbonate in preheated coral was converted into HAp by chemical exchange reaction with diammonium phosphate under hydrothermal conditions. However, the resultant material was in the form of a powder and required further forming and sintering. The exchange reaction took place under favorable conditions was proposed as the following:

$$10CaCO_3 + 6(NH_4)_2HPO_4 + 2H_2O \rightarrow Ca_{10}(PO_4)_6(OH)_2 + 6(NH_4)_2CO_3 + 4H_2CO_3$$

In 2001, Hu et al. succeeded to convert Australian coral (*Gonipora*) to monophasic hydroxyapatite by using a two-stage process where the hydrothermal method was followed by a hydroxyapatite sol-gel coating process based on alkoxide chemistry. There is little evidence of change in the structure of the coral before and after treatment. The images (Fig 3) show that the pore size ranges from 150–300 μm prior to hydrothermal conversion and 200–250 μm after conversion. The coral maintained its overall structure during conversion to hydroxyapatite. In the other case, the hydrocoral of species *Millepora dichotoma* was converted to HAp using a unique two-step conversion procedure (Innes *et al.*, 2003). After hydrothermal conversions the coralline HAp pores were further dip-coated via alkoxide sol-gel method. Once coated, the nanopores and mesopores were no longer visible (Fig 4). Pore sizes were observed to be around 25-75 μm, which were much smaller than the converted *Gonipora* species (Hu *et al.*, 2001). Xu *et al*., 2001 used a mineraliser, KH_2PO_4, to accelerate the exchange process and to eliminate the formation of intermediary phase. In the absence of the mineraliser, KH_2PO_4, aragonite (coral, *Porites*) was converted at high temperature and pressure into calcite, which was subsequently converted to β-TCP and finally to HAp, as HAp being the most thermo dynamically stable form. Whereas in the presence of KH_2PO_4, the exchange process was stable form. Whereas in the presence of KH_2PO_4, the exchange process was

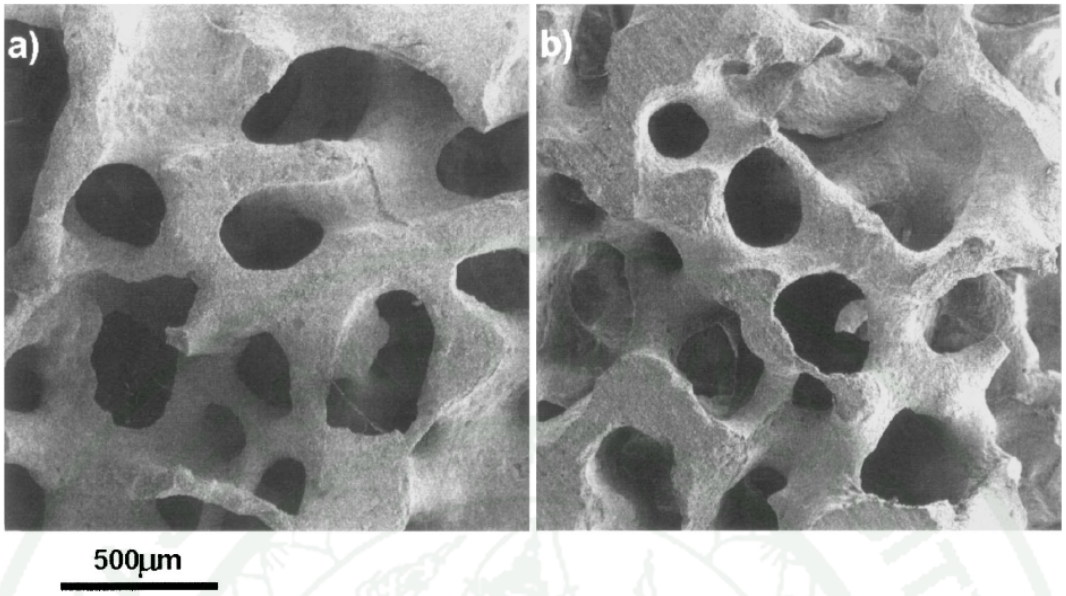

Figure 3 Comparision of the Australian coral (a) in original state and (b) after hydrothermal conversion.

Source: Hu *et al.*, (2001)

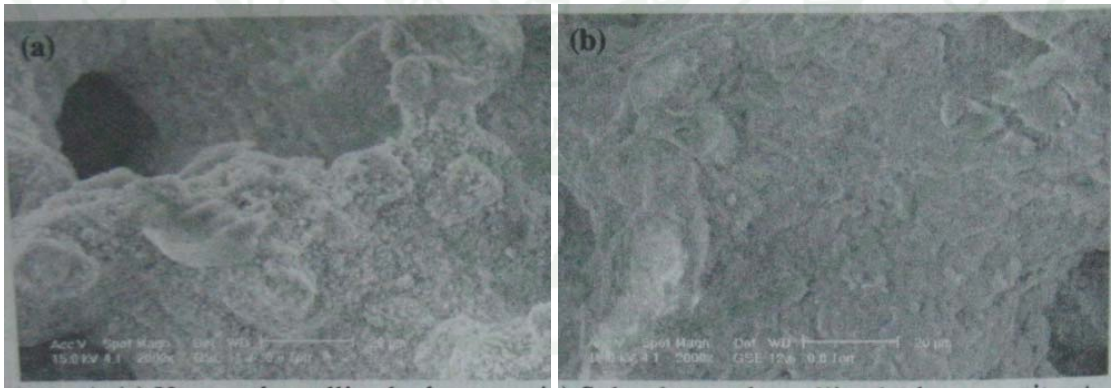

Figure 4 (a) Uncoated coralline hydroxyapatite and (b) sol-gel coated coralline hydroxyapatite at high magnification.

Source: Innes *et al.*, (2003)

completed without the formation of intermediary conversion stages by the direct conversion of aragonite into HAp. The advantages of the use of mineraliser also included the enhanced rate of conversion and better retention of the original structure of the coral. The retained interconnectivity of the coral could directly affect the biological properties (Xu *et al.*, 2001).

There are just few reports about the production of HAp from nacreous aragonite in the literature. Conversion of nacre into HAp was first reported by (Zaremba *et al.*, 1998). The mechanism of hydrothermal reaction of aragonite structural units packed in bulk nacre samples was investigated. It was reported that either aragonite plates or fine powders (<100 μm) of nacreous origin could transform to HAp in a phosphate buffer solution even at room temperature and pH 7.4 (Ni and Ratner, 2003). ESEM (Fig 5) showed that the morphology of nacre chips changed dramatically after soaking in citric-phosphate buffered saline (CPBSz). In 2006, Zhang and Vecchio reported the conversion of conch shells (*Strombus gigas*) and giant clam shells (*Tridacna gigas*) to HAp by the hydrothermal method. The conversion process was accelerated at higher temperature, and the thickness of the HAp layer increased with increasing conversion time. The conversion at 180 ºC with refreshing the diammonium hydrogen phosphate ($(NH_4)_2HPO_4$) solution every 2 days produced samples of good quality. Some different morphologies of HAp were found in the converted shells, which may be caused by porosity in different parts of the original shell (Fig 6 and Fig 7). Dense structures of HAp were created by hydrothermal conversion of conch and clamshells at relative low temperature (~ 200 ºC). The conversion process was accelerated at higher temperature, and the thickness of the HAp layer increased with increasing conversion time. The average fracture stress is ~137-218 MPa, for conch shell samples and ~70-150MPa for original and converted clamshell samples, which is close to the mechanical strength of compact human bone. This indicated that the converted shell samples could be used as implants in load-bearing applications (Zhang and Vecchio, 2006, Vecchio *et al.*, 2007). The nano-powders of pure AB-type carbonated HAp with the size of ~100 nm were produced via hydrothermal transformation of milled oyster shell powders at 200 °C shell powders at 200 °C (Lemos *et al.*, 2006). The osteogenetic activity of

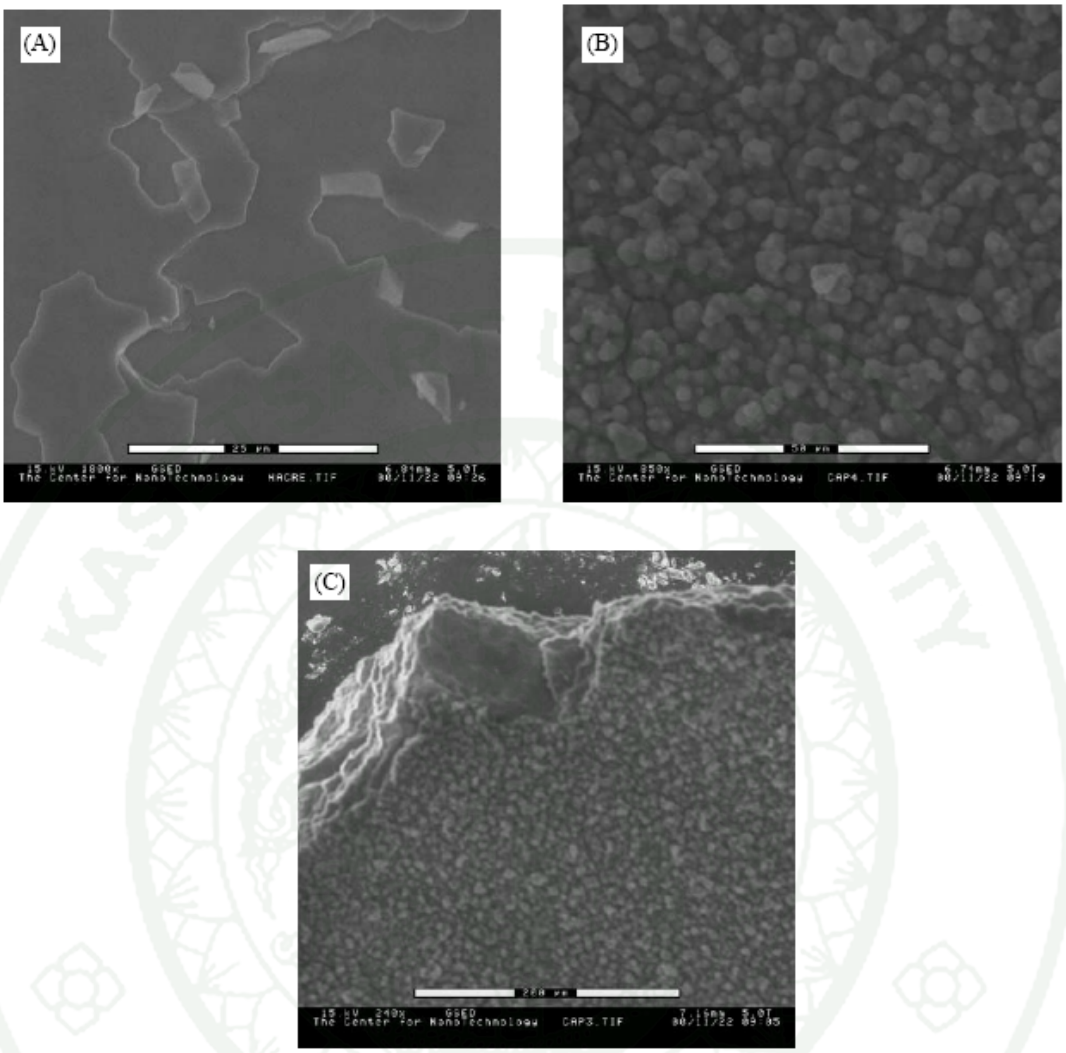

Figure 5 SEM images of nacre: (a) prior to soaking in citric-phosphate buffered saline, scale 25 mm; (b) after soaking for 14 days in citric-phosphate buffered saline, scale 50 mm; and (c) after soaking for 14 days in buffer, scale 200 mm. Freshly cleaved nacre shows areas uncovered by HAp.

Source: Ni and Ratner (2003)

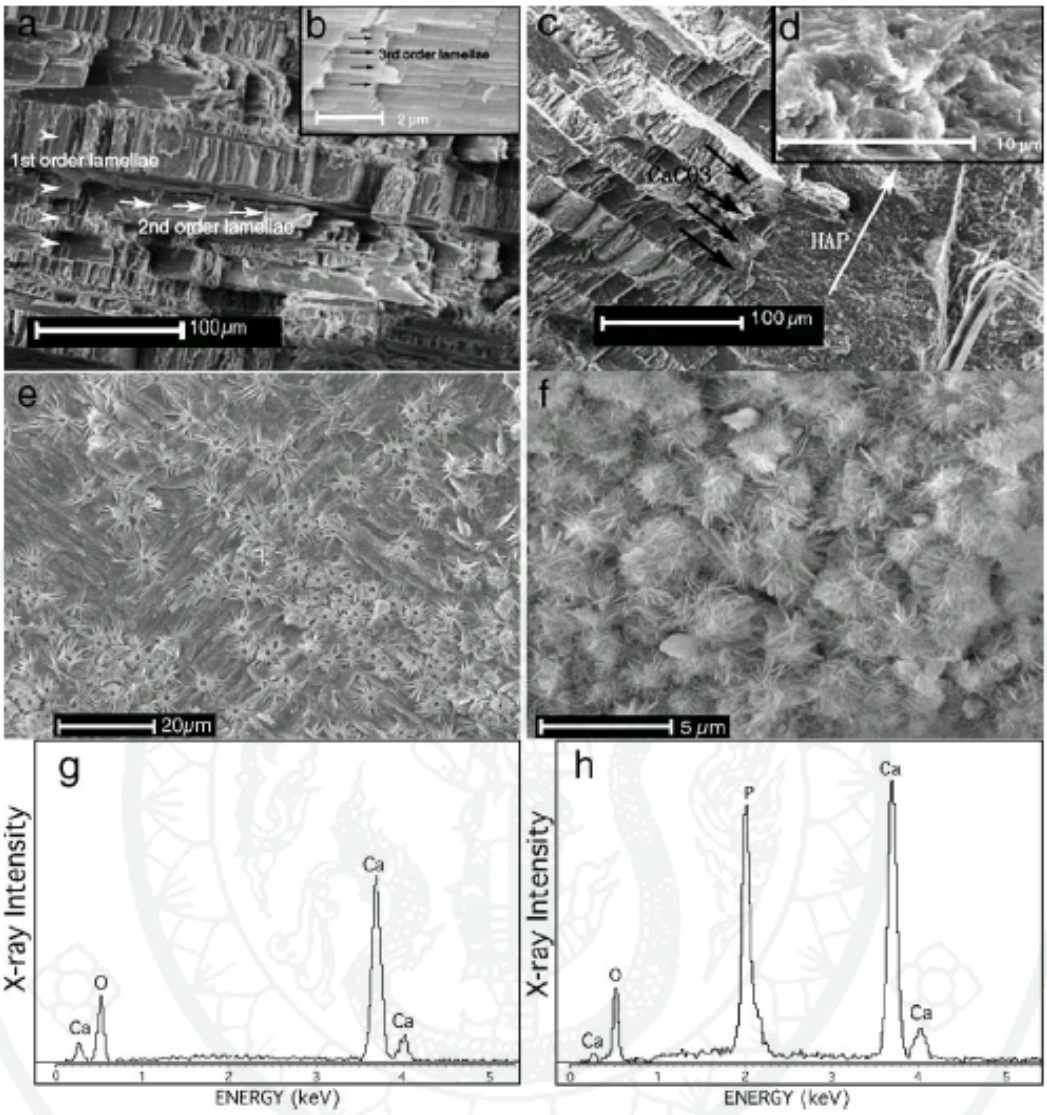

Figure 6 (a) SEM images of conch shell, (b) higher magnification of second-order lamella, (c) SEM image of conch shell converted at 180 ºC for 10 days (d) magnification of HAp part in (c), (e) and (f) SEM images of conch shell converted at 200 ºC for 10 days, (g) the EDS spectrum from $CaCO_3$ portion in (c) and (h) The EDS spectrum of HAp portion in (c).

Source: Zhang and Vecchio (2006)

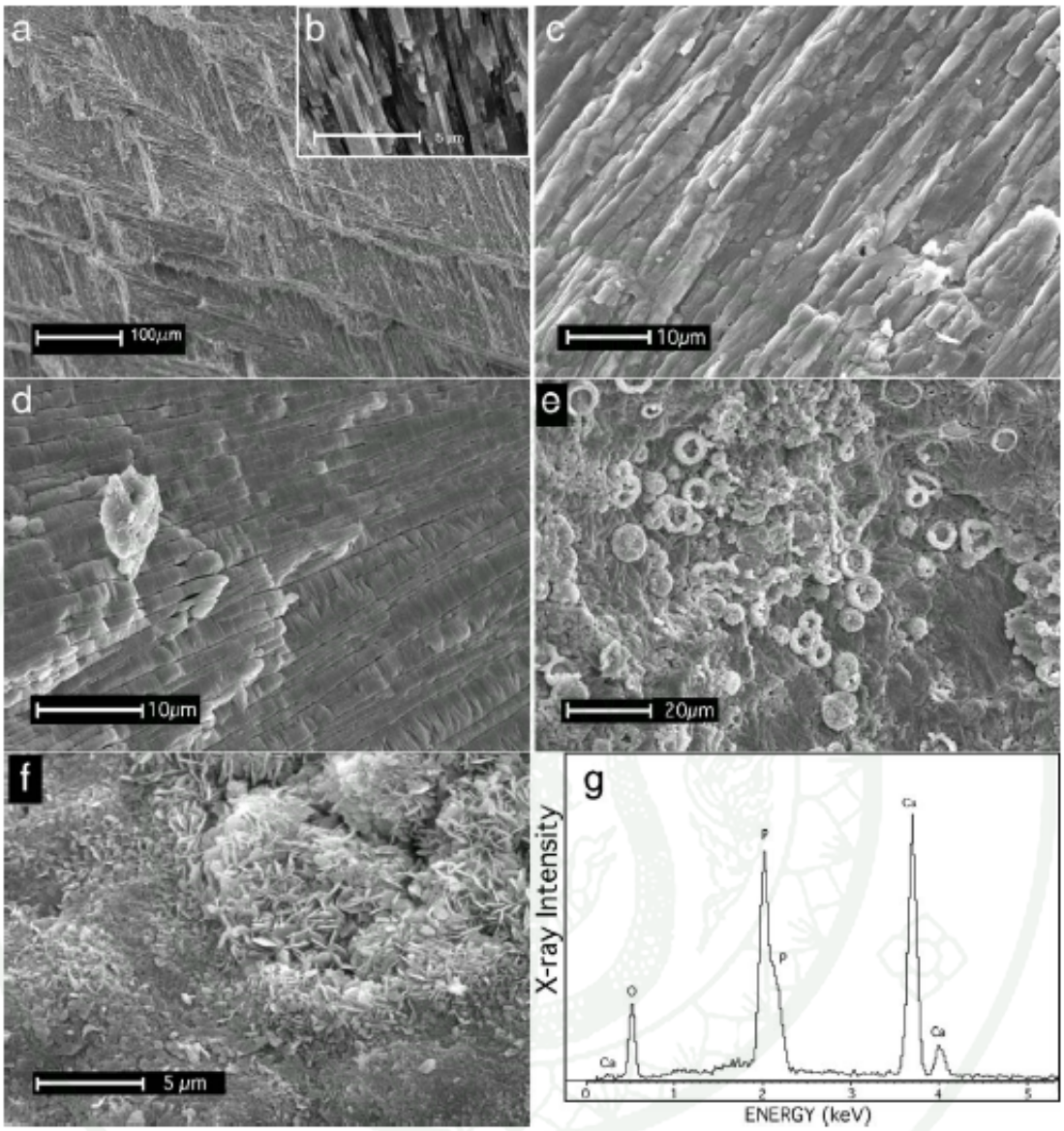

Figure 7 (a) and (c) SEM images of clam shell, (b) a magnification of a layer in (a), (d) and (e) SEM image of clam converted at 180 ºC for 20 days, (f) SEM image of clam converted at 180 ºC for 12 days and (g) EDS spectrum from (d).

Source: Zhang and Vecchio (2006)

pearl was evaluated by soaking in simulated body fluid (SBF) and cell culture. HAp particles were rapidly formed on the surface of pearl after soaking in SBF via a dissolution_binding_precipitation mechanism. Cell culture revealed that pearl could stimulate osteoblast proliferation, which proceeded more quickly and smoothly than that on shell nacre and HAp, and abundant extracellular matrix occupied the whole pearl surface by 5 days (Fig 8). It is concluded that pearl is a superior osteoinductive material with high osteogenetic activity (Shen *et al.*, 2006). Scaffolds of pure AB-type carbonated hydroxyapatite was successfully produced via hydrothermal transformation of aragonite cuttlefish bones at 200 °C. The produced scaffolds preserved the initial structure of the cuttlefish bone, fracturing pore size of ~ 80 μm in width and ~ 100 μm in height. The transformation was complete after 9 h and no intermediate products were registered. The hydroxyapatite crystallites formed had a size of nanoscale (~ 20-50 nm) and were randomly oriented. Bioactivity *in vitro* tests were excellent: (a) rapid and pronounced formation of hydroxyapatite occurred when the scaffolds were immersed in simulated body fluid and (b) outstanding proliferation of osteoblasts was registered (Rocha *et al.*, 2005a, 2005b).

There are several reported studies about the conversion of eggshells, a natural calcium carbonate material with calcite structure, into different Ca precursors for deriving HAp. The porous hydroxyapatite was synthesized at high temperature by first transforming the eggshell into CaO and in a second stage transforming this calcium oxide into hydroxyapatite by the reaction with anhydrous acid calcium phosphate ($CaHPO_4$) at 1100 °C for 3 hours (Rivera *et al*., 1999, 2003). Lee and Oh, 2003 revealed a new wet chemical method using eggshell and phosphoric acid to synthesis the HAp and β-TCP ceramics, which had uniform sized powder (Fig 9) (Lee and Oh, 2003a, 2003b). Stoichiometric, pure and thermally stable HAp powder was synthesized using calcined eggshell and phosphoric acid by precipitation method. FT-IR and XRD analyses indicated the phase purity and crystallinity of the HAp powder. TG-DTA results showed the thermal stability of HAp up to 1300 °C (Prabakaran *et al*., 2005). Nanocrystalline hydroxyapatite was synthesized from eggshells at low temperature. The $(NH_4)_2HPO_4$ solution was added to the eggshell solution whose pH

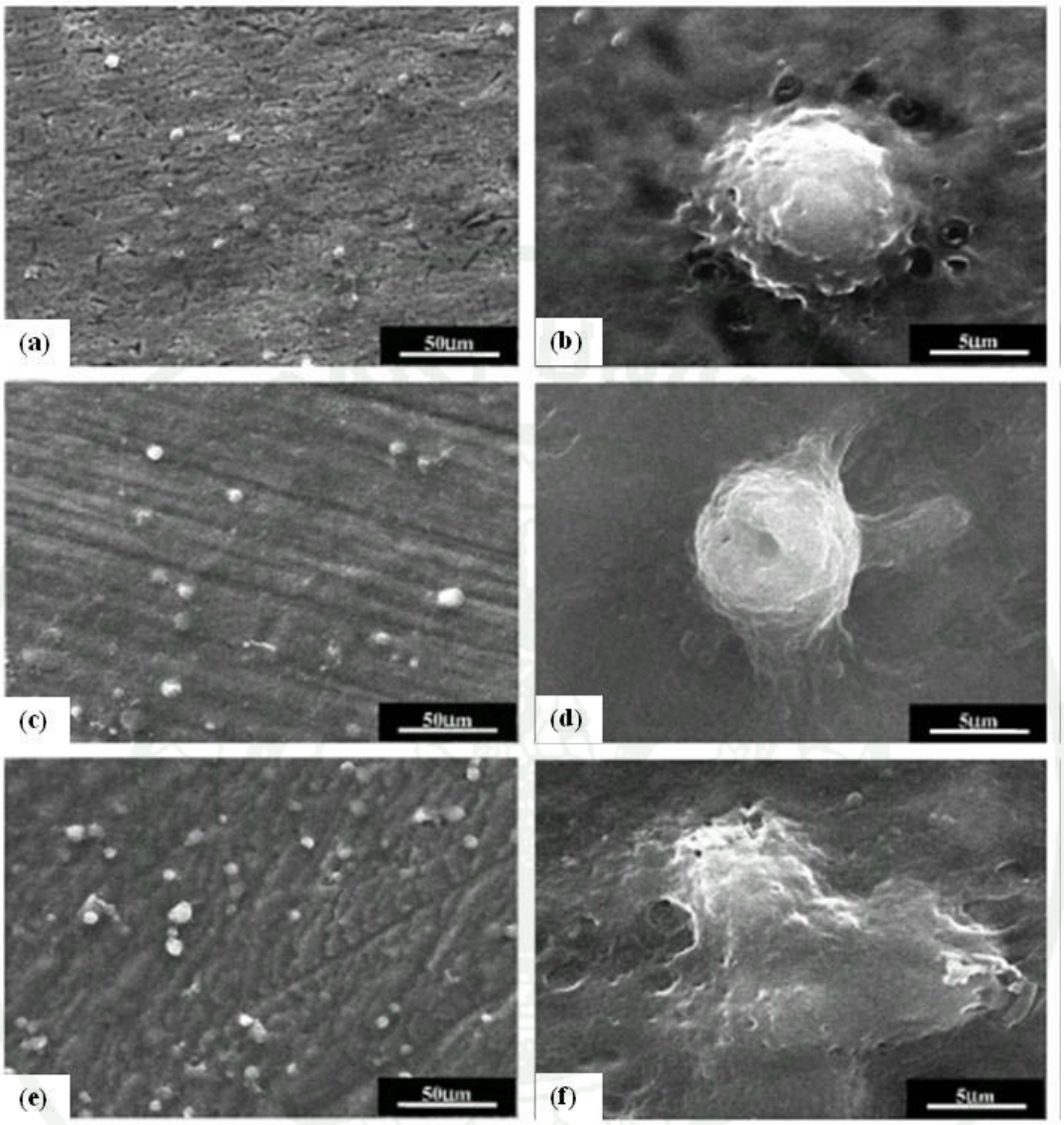

Figure 8 SEM images of osteoblasts on the surface of different materials after 5 days' culture. (a, b) HAp; (c,d) nacre; (e, f) pearl. After culture, the surfaces of all specimens were covered by osteoblasts and abundant mineralized extracellular matrix as compared with the original surface, and the osteoblasts shrunk into spheroids due to fixation with neutral formalin. Lower magnification images (a, c, e) and higher magnification images (b, d, f) showed that osteoblasts on pearl surface proliferate most quickly and adhere to the surface most firmly as compared with nacre and HAp.

Source: Shen *et al.*, (2006)

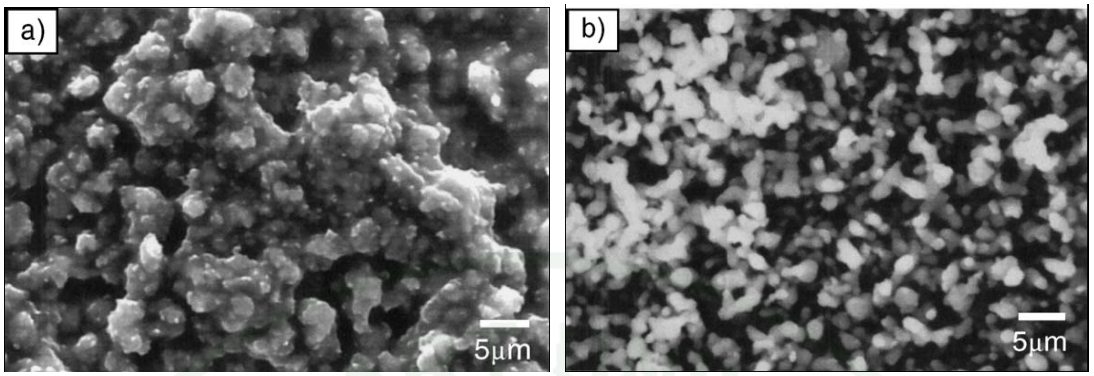

Figure 9 SEM micrographs of (a) as-milled and dried mixture and (b) synthesized β-TCP powder fired at 900 ºC for 1 h, derived from 1:1.5 mixing ratio.

Source: Lee and Oh (2003a)

was adjusted to 9.5. The precipitating hydroxyapatite was dissolved in conc. HNO_3 and the pH of solution was adjusted to 1. The resultant solution was stirred until the formation of transparent gel at 70 ºC. The gel formed underwent combustion with a bright flame in a muffle furnace at 250 ºC, resulting in a black coloured precursor. After sintering the black precursor at 900 ºC for 2 hours, the pure white nanocrystalline hydroxyapatite was obtained (Sasikumar and Vijayaraghavan, 2006). In other study reported by Nayar group, eggshells were dissolved in hydrochloric solution prior to the mixing with phosphate precursors. The problem with this technique was the uneasy removal of chloride ions (Nayar and Guha, 2009). While Sanosh *et al*. reported a simple sol–gel precipitation technique to synthesize nano hydroxyapatite powders using calcium oxide derived from chicken eggshells. TEM micrographs showed high amorphicity (Fig 10a) while powders calcined at 700 °C showed prolate spheroidal morphology (Fig 10b) with particle sizes varying between 30 and 50 nm. SAED analysis (Fig 10c) revealed the polycrystalline nature of this calcined powder (Sanosh *et al.*, 2009).

In several reports, HAp were prepared from animal bones. Most of the researches in bovine hydroxyapatite were focused on the heat treatment (annealing) for bone synthesizing HAp because bovine bone has a high potential as a raw material

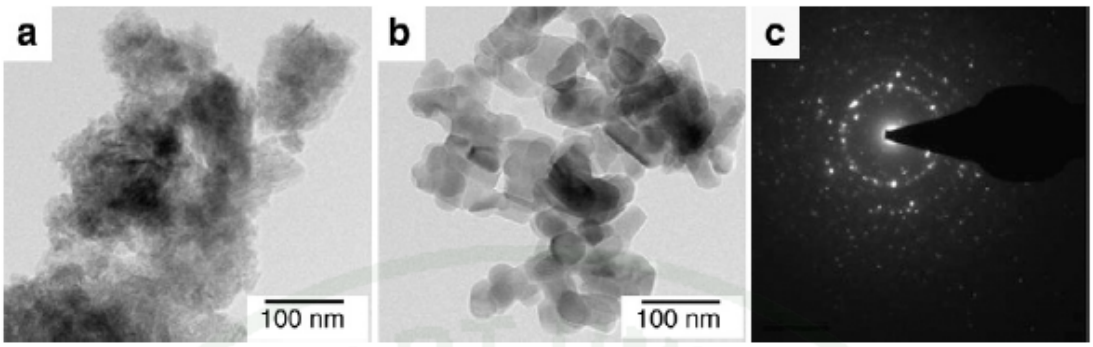

Figure 10 TEM images of HAp powders (a) dried at 65 ºC (b) calcined at 700 ºC (c) SAED of HAp powders calcined at 700 ºC.

Source: Sanosh *et al.*, (2009)

of natural HAp due to its similar morphologically and structurally similar to human bone, easy to obtain, lower cost and availability in unlimited supply. Ooi *et al*., 2007 prepared highly pure HAp directly from bovine bone through heat treatment (annealing) above 600 ºC in air. However, a small amount of β-TCP was present in the bone matrix when annealed at 1100 ºC and 1200 ºC, due to the partial decomposition of the HAp phase. Additionally, the crystallinity of the HAp phase in bovine bone increases with increasing annealing temperature (Ooi *et al.*, 2007). Nanocrystalline HAp powder was synthesized from natural bovine bone by a vibro-milling method. The bovine bone had been deproteinized by hot water before it was calcined at 800 ºC for 3 h. The resulting product was crushed into small pieces and milled in a ball mill pot for 24 h. Then the HAp powders were reground by vibro-milling method using ethanol as a milling media and optimum milling time of about 2-4 h. The as-prepared powders were confirmed to be pure nanocystalline HAp powder with their Ca/P ratio is close to that of stoichiometric HAp. The SEM images of all as-prepared HAp powders were given in Figure 11. It was clearly seen that the nanoneedle-like shape of HAp powder with diameter less than 100 nm was obtained from the powders using vibro-milling time of more than 2 h. The more the vibro-milling time was employed, the better distributuion of the nanoneedle-like HAp crystals was obtained (Ruksudjarit *et al*., 2008).

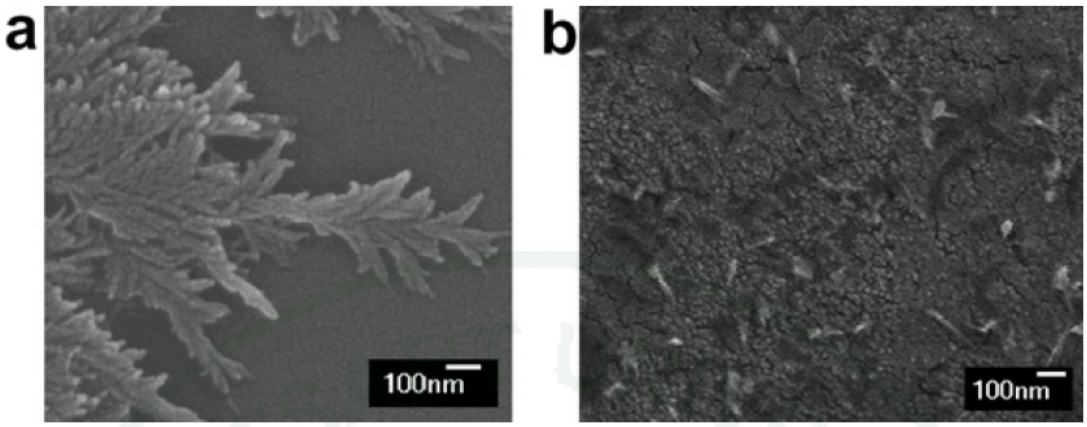

Figure 11 SEM micrographs of HAp powders at various vibro-millng time, (a) 2 h (b) 8 h.

Source: Ruksudjarit *et al.*, (2008)

2. Study of *in vitro* bioactivity

The artificial materials considered for implants are tested by *in vivo* methods (in live animal organism) and by *in vitro* ones (in media simulating the body fluid).

In 1990 a team of Japanese researchers at Kyoto University devised a pre-clinical *in vitro* laboratory test which reproduce the *in vivo* surface structural changes that took place when ceramics and glasses were implanted in the body. The test involved immersing the candidate bioceramic in a 'simulated body fluid, consisting of a variety of salts, whose ionic composition approximated that of human body fluid (Table 3) (Kokubo *et al*., 2006). Typical immersion periods ranged from 30 minutes to seven days at 37 ºC. Infrared spectroscopy and/or electron microscopy were then used to determine whether a layer of hydroxyapatite had precipitated onto the surface and also the fluid composition was monitored over time to determine the kinetics.

The tests were focused on their physical, chemical and mechanical properties and thus provided the basic information allowing the suitability of a material for

Table 3 Ion concentrations of the simulated body fluid and human blood plasma.

Ion	Concentration (mmol/dm^3)	
	Simulated body fluid (SBF)	Human blood plasma
Na^+	142.0	142.0
K^+	5.0	5.0
Mg^{2+}	1.5	1.5
Ca^{2+}	2.5	2.5
Cl^-	147.8	103.0
HCO_3^-	4.2	27.0
HPO_4^{2-}	1.0	1.0
SO_4^{2-}	0.5	0.5

Source: Kokubo *et al*., (2006).

implanting into the human organism to be assessed. The simulated body fluid is a metastable solution that has inorganic ion concentrations similar to those of human extracellular fluid, in order to reproduce formation of apatite on bioactive materials *in vitro*. This fluid can be used for not only evaluation of bioactivity of artificial materials *in vitro*, but also coating of apatite on various materials under biomimetic conditions. The simulated body fluid is often abbreviated as SBF or Kokubo solution. The ion concentrations of SBF are given on Table 3.

The pH of SBF is adjusted to pH 7.25 at 36.5 ^oC, by using 50 mM of tris (hydroxymethyl) aminomethane and approximately 45 mM of HCl. When apatite-forming ability of the specimen is not so high, pH of SBF is sometimes adjusted to pH 7.40.

3. Drug Delivery System

During the last two decades, significant progress has been made in the area of drug delivery systems. Drug delivery in the future will require sophisticated devices

that are controlled, self-regulated, and can release drugs only at target sites. With the recent developments, HAp has attracted much attention in the field of implantable drug delivery system for treatment of bone infections. Hydroxyapatite has the advantage of being biocompatible, bioresorbable and highly binding to a variety of molecules (e.g. proteins, enzymes, antibody fragments, nucleic acids, and some sub-classes of immunoglobin G (IgG)). This has opened the potential for using HAp to deliver a large variety of drugs in many clinical applications.

Bone and cartilage injuries occur due to various reasons including degenerative, surgical, and traumatic processes, which significantly compromise quality of life. Currently, millions of patients are suffering from bone and cartilage defects, reportedly with over 450,000 bone grafts and approximately 250,000 knee arthroplasty procedures performed per year in united state alone. Artificial implants, such as the total hip replacement, are successful for a limited time, but all orthopaedic implants lack three of most critical characteristics of living tissues: (1) the ability to self-repair; (2) the ability to maintain a blood supply; and (3) the ability to modify their structure and properties in response to environment factors mechanical load. These artificial joint replacements are at risk of infection if a small amount of bacteria succeeds in colonizing the foreign material. Bacteria stick to the surface and become sessile by forming biofilm (Belt *et al.*, 2001). Periprosthetic infection results if some of the bacteria in biofilm convert to planktonic forms and induce infection of the adjacent tissue. The use of local antibiotic delivery systems, including antibiotic-loaded bone cement is well accepted adjunct for the treatment of an established infection.

In bone reconstruction surgeries, osteomyelitis caused by bacteria infection is the main complication. Conventional treatments include systemic antibiotic administration, surgical debridement, would drainage and implant removal. Accordingly, the removal of the implant is mandatory for the treatment and cure of implant sepsis in most cases. After removing implants, it has been the current trend to insert antibiotic-impregnated bone cement in the form of beads or spacers. These approaches, however, are rather inefficient and the patients would suffer for extra

surgeries (Duncan and Masri, 1994). A new method to solve this problem is to introduce a local drug release system into the implant site. The advantages of this treatment include high delivery efficiency, continuous action, reduced toxicity and convenience to the patients (Sudo *et al.*, 2008). In 1994, the relationship between the drug release properties *in vitro*, the location of drug in the cement device, and the physicochemical properties of the device were studied (Fig 12) (Otsuka *et al.,* 1994). The local-drug delivery system base on $CaO\text{-}SiO_2\text{-}P_2O_5$ glass containing 2% and 5% of indomethacin (IMC) as anti-inflammable drug were released into simulated body fluid at pH 7.25, 37 °C; the IMC was released from bioactive cement over a long term and controlled by homogeneous and heterogeneous systems, which did not interfere with the hardening process in the formation of cement. Thirty percent of drug in this hardening cement was excluded and the drug release continues slowly more than 300 h (Higuchi, 1961).

At present, the studies on controlled drug delivery systems mainly focus on biopolymers (Rossi *et al.*, 2004). However, they may not be suitable for bone repair as filling materials since most of the biopolymers are not able to chemically bond to living bone. The mixing bone cement with antibiotic-loaded polymethyl-methacrylate beads as an antibiotic carrier system was usually performed (Neut *et al.*, 2001; Wahlig *et al.*, 1978). One problem inherent in the local insertion of a compound is that it entails subsequent surgery for replacement with an auto graft. Implantable drug delivery systems for local drug release in bone tissue are the most promising therapeutic concepts in orthopedic surgery. The antibiotic load-bone cement is interested in bone repair due to it can not only generate the new bone, but also for prophylaxis against infection. Accordingly, hydroxyapatite ceramics have excellent biocompatibility, act as bone substitute and do not need to removed, thus can be used as a drug carrier, which is most advantageous since it will not elicit any inflammation, immunological and irritating responses with living tissues (Ogiso, 1998).

Basically, there are many studied reporting on the *in vitro* release kinetics of HAp containing antibiotic drugs, such as pentoxifylline (Slosarczyk *et al.*, 2000), riboflavin sodium phosphate (Cosijns *et al.*, 2007), ibuprofen-lysine and

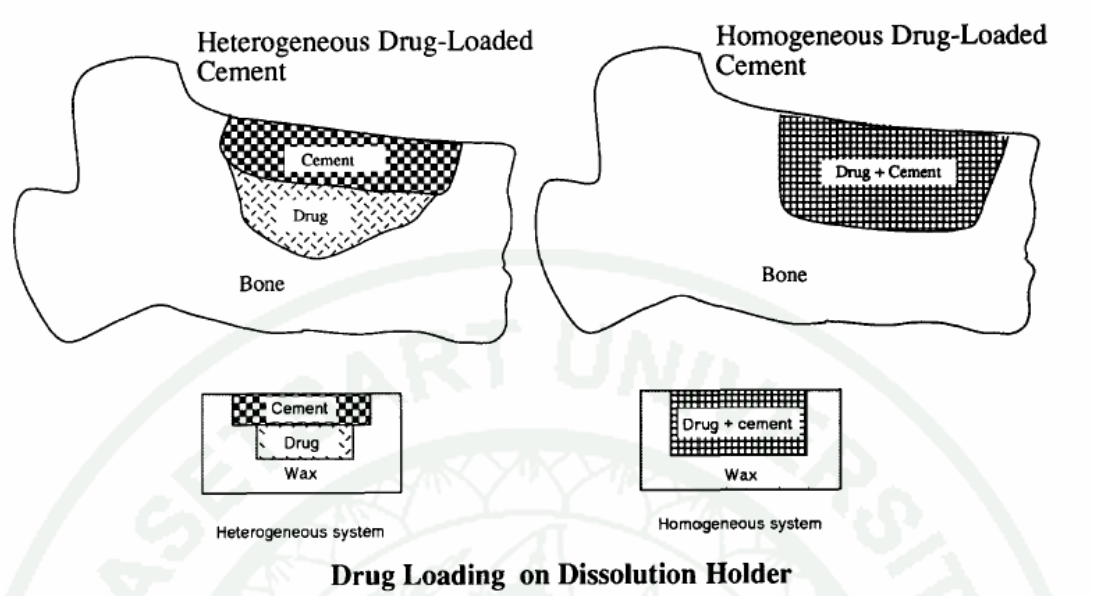

Figure 12 The use of bioactive bone cement as a drug delivery system.

Source: Otsuka *et al.*, (1994)

hydrocortisone sodium succinate (Palazzo *et al.*, 2005), isepamicin (Itokazu *et al.*, 1998), vancomycin (Gautier *et al.*, 2001; Gbureck *et al.*, 2008; Joosten *et al.*, 2005), gentamicin (Sivakumar *et al.*, 2002; Teller *et al.*, 2006).

It was reported that the rate of pentoxifylline release from the hydroxyapatite carriers to the phostphate buffer at 37 °C varied depending on the microstructure of the hydroxyapatite ceramics used for their preparation (Ślósarczyk *et al.*, 2000). The HAp microspheres containing ciprofloxacin with controlled morphology were synthesized by a spray-drying step. Agglomerated microspheres were prepared by a wet granulation process using a granulator. The *in vitro* release of ciprofloxacin from the agglomerated microspheres was fast and complete within 1 hour. Implants were prepared by direct compression of granules on a carver press. Implants have a lower release rate that can be sustained for several days (Pham *et al.*, 2002).

In 2005, Joosten *et al*., investigated HAp cement as a carrier for vancomycin in the treatment of chronic osteomyelitis due to *Stephylococcus aureus* strains with

various mechanisms of resistance. The HAp cement was mixed with drug at 80, 160, and 240 mg/g. Then the kinetic of release with three different concentrations of vancomycin is shown in Figure 13. The released quantities were initially 1512.12 ± 318.45 μg/ml up to 1936.6 ± 335.85 μg/ml. These amount released from standard test cylinders *in vitro* clearly exceeded the minimum inhibitory concentration for the pathogens (Joosten *et al*., 2005). The release kinetics of vancomycin from calcium phosphate dihydrate (brushite) matrices and polymer/brushite composites were compared using different fluid replacement regimes, a regular replacement (static conditions) and a continuous flow technique (dynamic conditions). The use of a constantly refreshed flowing resulted in a faster drug release due to a constantly high diffusion gradient between drug loaded matrix and the eluting medium. Drug release was modeled using the Weibull, Peppas and Higuchi equations. The results showed that drug liberation was diffusion controlled for the ceramics matrices, whereas ceramics/polymer composites led to a mixed diffusion and degradation controlled release mechanism (Gbureck *et al*., 2008).

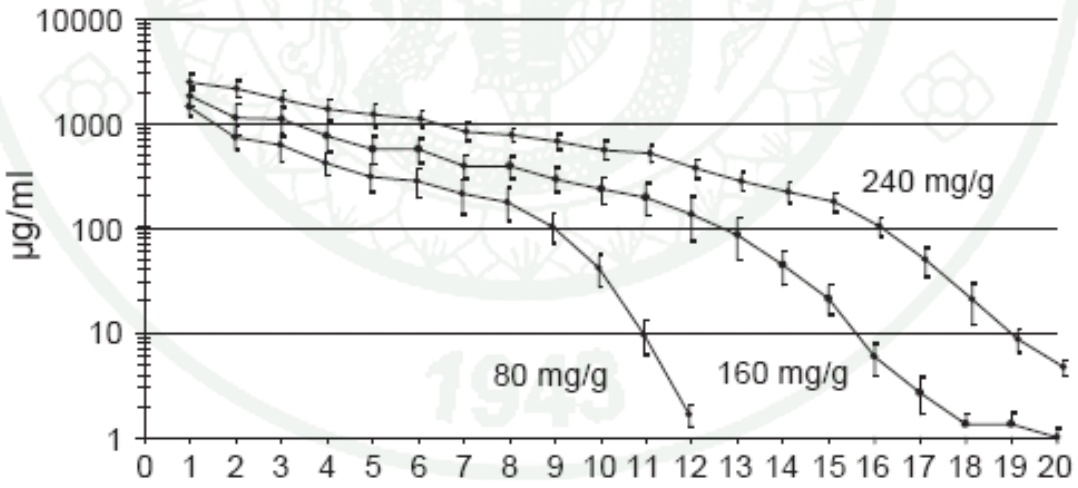

Figure 13 Releases of vancomycin from standard cylinders of HAp cement *in vitro*. Three different concentrations of vancomycin were used.

Source: Joosten *et al.*, (2005)

Recently, hydroxyapatite has excellent biocompatibility and interlinked pore structure, antibiotics could be loaded into pores. When filling grafts in osteomyelitis, the antibiotic-loaded HAp is useful not only as an antibiotic carrier but also strut bone graft.

MATERIALS AND METHODS

This part describes syntheses, characterization and bioactivity and drug delivery studies of the synthesized compounds and is made up of 4 sections: (1) chemicals, apparatus and instruments; (2) conversion of crocodile bone into hydroxyapatite; (3) syntheses of hydroxyapatite from calcium based naturals materials by hydrothermal technique; (4) characterization methods.

Materials

1. Chemicals, apparatus and instruments

1.1 Chemicals

1. Tricalcium phosphate (reagent grade; BDH company)
2. Sodium chloride (reagent grade; BDH company and Mallinckrodt baker Inc.,)
3. Sodium hydrogen carbonate (analytical reagent grade; Mallinkrodt baker Inc.,)
4. Potassium chloride (analytical reagent grade; UNIVA and Mallinckrodt baker Inc.,)
5. di-Potassium hydrogen phosphate (analytical reagent grade; Fluka and Mallinckrodt baker Inc.,)
6. Magnesium chloride hexahydrate (analytical reagent grade; Sigma-Aldrich and Mallinckrodt baker Inc.,)
7. Calcium chloride (reagent grade; BDH company and Mallinckrodt baker Inc.,)
8. Sodium sulfate(analytical reagent grade; Carlo Erba and Fisher Scientific)
9. Tris-hydroxymethyl aminomethan (reagent grade; Sigma-Aldrich and Aldrich Chemical Company)

10. Hydrochloric acid (analytical reagent grade; Fisher Scientific)
11. Sodium hypochlorite (reagent grad; Ajex Finechem)
12. Tetracycline hydrochloride (laboratory use; Acros)
13. Vancomycin hydrochloride (intravenous use; Abbott Laboratories)
14. Hydroxyapatite (Calcitite®HA2040, Centerpulse Dental Inc.)
15. Nitric acid (analytical reagent grade; Fisher Scientific)

1.2 Apparatus and instruments

1. Hydrothermal apparatus

Two sets of hydrothermal apparatus are used in this study. One is Parr Model 4842 reactor equipped with temperature controller, denoting as apparatus set 1 (Fig 14). The other consists of Teflon-lined stainless steel autoclave equipped with thermal couple, and high temperature oven, denoting as apparatus set 2 (Fig 15). The temperature inside the autoclave in the latter was proved to be the same as the temperature of oven within thirty minutes.

2. High temperature electric furnace

High temperature electric furnace was locally made by King Mongkut's University of Technology Thonburi.

3. High temperature oven

Oven model Venticell 111 and oven model Venticell 65

4. Orbital shaker

IKR ® orbital shaker model KS 130 basic

5. Vacuum suction apparatus

Vacuum suction apparatus EYELA model Aspirator A-35

6. Magnetic stirrer

Magnetic stirrer JENWAY model 1002 stirrer

Figure 14 Apparatus set 1: Parr Model 4842 reactor equipped with temperature controller.

(a) **(b)**

Figure 15 Apparatus set 2: (a) The Teflon-lined stainless steel autoclave and (b) high temperature oven**.**

7. Fourier Transform Infrared Spectrophotometer (FTIR)

Bruker Model Equinox 55 Spectrophotometer

8. X – ray Diffractometer (XRD)

X-ray diffractometer model Miniflex Rigaku/Destop X- ray Diffractometer system at King Mongkut's University of Technology Thonburi. And Bruker-AXS Microdiffractometer at University of Minnesota

9. Transmission Electron Microscopy (TEM)

Transmission Electron Microscope: JEM 1220 at RDI (Kasetsart University) and FEI Tecnai 12 at University of Minnesota.

10. Scanning Electron Microscopy (SEM)

Scanning electron microscope: JEOL model JSM 6310F at National Metal and Materials Technology Center, JSM 5600 LV at Research and Development Institute, Kasetsart University. Field Emission Gun Scanning Electron Microscope JEOL 6500 at University of Minnesota and Environmental Scanning Electron Microscope FEI XL30 ESEM.

11. Autosorb

Surface area analysis (BET) model Autosorb 1 at Thailand Institute of Scientific and Technological Research.

12. UV/VIS Spectrophotometer

Jasco V-530 UV/VIS/NIR spectrophotometer

13. pH/mV/ºC meter

EUTECH instruments model pH/Ion 510

14. Water-bath

Water bath with Temperature controller

15. Centrifuge

Becton Dickinson, ADAMS ® compact II centrifuge

16. Ultrapure Deionizer

Utrapure deionizer ELGA model Optima reservoir 75Liter Volume

17. Inductively Coupled Plasma

Inductively Coupled Plasma Atomic Emission Spectrometer model Perkin-Elmer PLASMA-1000

Methods

1. Conversion of crocodile bone into hydroxyapatite by thermal process.

The fresh crocodile bones of *Crocodylus siamensis* were obtained from Sriracha Farm (Asia) Co. Ltd., Thailand. Two parts of bones which are tibia and tail were used (Fig 16). The fresh bone samples were boiled in water for 6 hours for easy removal of flesh, bone marrow and tendon. The tibia bones were cut into small pieces (Fig 17). The bone samples were boiled again in distilled water and cleaned well to remove macroscopic and microscopic adhering impurities.

1.1 Characterization of crocodile bone

The cleaned bone samples were soaked in NaOCl with sonication for several hours to remove all impurities inside the bones. After rinsing with distilled water, the cleaned bones were dried at 125 °C overnight.

Elemental analysis was performed by inductively coupled plasma atomic emission spectrometer (ICP-AES) using a Model Perkin–Elmer PLASMA-1000, to determine the trace and rare earth elements. The bones were rinsed with tap water, brushed cleaned and rinsed with de-ionized water. The cleaned bone samples were then cut using drill with diamond disc. These samples were treated in ultrasonic bath with de-ionized water and dried in an oven at 125 ◦C. The treated bone samples were ashed (8 h, 550 °C). The ashing step ensures the complete destroying of the organic part of the bone sample and decreases the fluctuation in the plasma. One gram of ashed bone was placed in an erlenmeyer flask. After adding 8 ml of conc. HNO_3, the sample was kept standing about 2 h at room temperature for pre-decomposition. Then, 2 ml of $HClO_4$ were added with heating. After cooling, the resulting solutions were diluted to 100 ml with de-ionized water and was analyzed using ICP-AES.

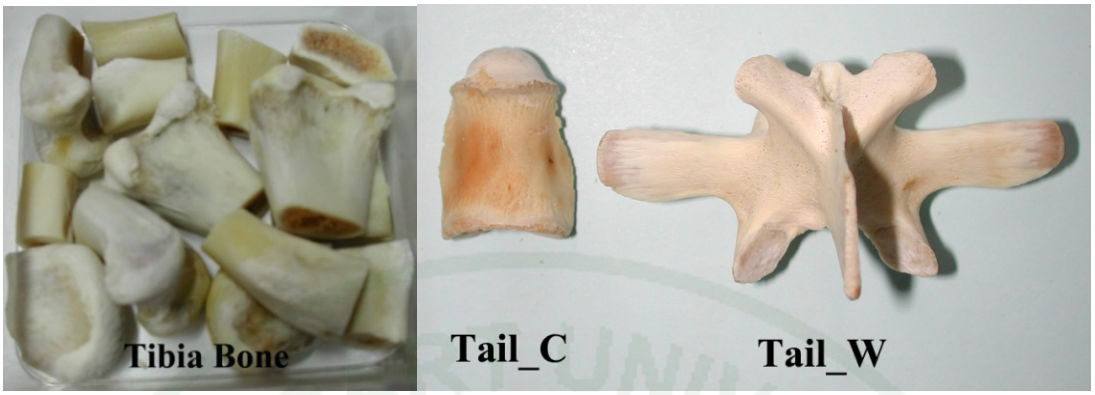

(a) (b)

Figure 16 The crocodile bone; (a) Tibia bone (b) Tail Bone.

Figure 17 The cleaned crocodile bone.

The phase of the cleaned bone was examined by X-ray diffraction pattern, and FTIR spectra. The thermal stability and microstructure of bone were observed from thermogram and SEM micrographs, respectively.

1.2 Conversion of crocodile bone into hydroxyapatite by thermal process.

The cleaned bone samples were soaked in water and cleaned well to remove the visible tissue and substances on the bone surface and then stored in refrigerator until use. The cleaned bone samples were heated in an electric furnace

under ambient condition, at four different temperature ranging from 550 ºC to 900 ºC using a heating rate of 10 ºC/min with 4 h holding time. After calcination, calcined bone samples were grounded. These samples were coded with correspond to their heating temperature as shown in Table 4. One portion of each calcined bone powder was washed with de-ionized water to remove the CaO phase and dried at 100 ºC for overnight. The other portion was characterized for phase analysis by X-ray diffraction analysis and Fourier Transform Infrared Spectroscopy. The microstructures were examined by Scanning Electron Microscopy and Transmission Electron Microscopy.

Table 4 Sample codes

Bone	Heating temperature (ºC)	Calcined bone*	Calcined bone washed with water**
Tibia	550	HTib_550	HTib_550W
	650	HTib_650	HTib_650W
	750	HTib_750	HTib_750W
	900	HTib_900	HTib_900W
Tail_C	550	HTC_550	HTC_550W
	650	HTC_650	HTC_650W
	750	HTC_750	HTC_750W
	900	HTC_900	HTC_900W
Tail_W	550	HTW_550	HTW_550W
	650	HTW_650	HTW_650W
	750	HTW_750	HTW_750W
	900	HTW_900	HTW_900W

* HA_B denoted as A = type of bone: Tib = tibia bone, TC = tail_C and TW = tail_W and B = calcined temperature.

** W = washed with water

2. Syntheses of hydroxyapatite from calcium based natural materials by hydrothermal technique.

The Ca-based natural materials used in this study consist of corals, shells and crocodile eggshells. Calcium phosphate ($Ca_3(PO_4)_2$ are used as phosphate source in all syntheses. Stag horn corals of *Acropora Formosa* (Fig 18) were obtained from Chulabhorn Research Institute, Thailand. Freshwater shells of *Hyriopsis myersiana* (Fig 19) were obtained from Kanchanaburi research center. Crocodile eggshells (Fig 20) were obtained from Sriracha Farm (Asia) Co. Ltd.

Figure 18 Stag horn coral (*Acropora Formosa*)**.**

Figure 19 Freshwater shell (*Hyriopsis myersiana*)**.**

Figure 20 The crocodile eggshell.

2.1 Synthesis of hydroxyapatite from corals.

Stag horn corals (*Acropora Formosa*) were cleaned by brush to remove all dirt adhered on the surface and then washed with water several time. After drying the corals were crushed and grounded in an agate mortar into powder and used as calcium source. The phase of coral samples were examined by X-ray diffraction pattern and FTIR spectra. The microstructure was observed by SEM micrographs.

Assuming that the whole matter of the coral consists of $CaCO_3$, mixtures of coral powder, and $Ca_3(PO_4)_2$ were prepared in order to set the molar ratio of Ca/P = 1.67. The mixtures were placed in Teflon bottles containing 30 cm^3 distilled water. After stirring well, the bottles were placed in stainless steel autoclave. The autoclave were then sealed and placed in apparatus set 1. The temperature was set at 250°C and periods of heating time varied from 8 to 12 h. After cooling, the products were collected by filtration, washed with water several times and dried in an oven at 110 °C for 1 h. The sample codes and reaction conditions are summarized in Table 5.

The synthesized products were characterized for phase analysis by X-ray diffraction analysis, and Fourier Transform Infrared Spectroscopy. The microstructures were examined by Scanning Electron Microscopy.

Table 5 The sample codes and the reaction conditions of the hydrothermal treatment.

Condition	Size	Time (h)	Temperature (°C)	Product code*
Hydrothermal Set 1				
Coral	unsieved	8	250	C_8_250
	unsieved	10	250	C_10_250
	unsieved	12	250	C_12_250
shell	unsieved	8	250	Sh_8_250
	unsieved	10	250	Sh_10_250
	unsieved	12	250	Sh_12_250
eggshell	unsieved	8	250	E_8_250
	unsieved	10	250	E_10_250
	unsieved	12	250	E_12_250
Hydrothermal Set 2				
Coral	L	8, 12, 16	150	CL_X_150
	M	6, 8, 10	150	CM_X_150
	S	4, 6, 8	150	CS_X_150
	unsieved	20	150	C_20_150
	unsieved	20	200	C_20_200
Shell	L	8, 12, 16	150	ShL_X_150
	M	6, 8, 10	150	ShM_X_150
	S	4, 6, 8	150	ShS_X_150
	unsieved	20	150	Sh_20_150
	unsieved	20	200	Sh_20_200
Eggshell	L	8, 10, 12	150	EL_X_150
	M	6, 8, 10	150	EM_X_150
	S	4, 6, 8	150	ES_X_150

*AB_X_C: A = abbreviation of calcium source (C= coral, Sh = shell and E = eggshell).
B = the exact size of natural material powder where L > 150 μm, 150 μm ≤ M > 53 μm and S ≤ 53 μm.
X = reaction time, C = reaction temperature

2.2 Synthesis of hydroxyapatite from freshwater shells.

Freshwater shells (*Hyriopsis myersiana*) were cleaned by brushing their outer surfaces to remove the dirt adhered. The shell were cut into small pieces and then washed with distilled water. After drying, the shells were crushed into powder by an agate mortar. The phase of freshwater shell samples were examined by X-ray diffraction pattern and FTIR spectra. The microstructures were observed by SEM micrographs.

It was found that the freshwater shells contain 97 % of calcium carbonate (Siripaisarnpipat, 2005). Assuming that the whole matter of the shells consist of $CaCO_3$, mixtures of shell powder and $Ca_3(PO_4)_2$ were prepared in order to set the molar ratio of Ca/P = 1.67. The mixtures were placed in Teflon bottles containing 30 cm^3 distilled water. After stirring well, the bottles were placed in stainless steel autoclave. The autoclave were then sealed and placed in apparatus set 1. The temperature of oven was set at 250°C and periods of heating time varied from 8 to 12 h. After cooling the products were collected by filtration, washed with water several times, and dried in an oven at 110 °C for 1 h. The sample codes and reaction conditions are summarized in Table 5.

The synthesized products were characterized for phase analysis by X-ray diffraction analysis, Fourier Transform Infrared Spectroscopy and the microstructures were examined by Scanning Electron Microscopy.

2.3 Synthesis of hydroxyapatite from crocodile eggshells

The inner membrane of eggshells was taken off. The eggshells were cleaned by brushing their outer surfaces to remove the dirt adhered. The crocodile eggshells were washed with distilled water. After drying, the shells were crushed into powder by an agate mortar. The phase of crocodile eggshell samples were examined by X-ray diffraction pattern and FTIR spectra. The microstructure was observed by SEM micrographs.

Assuming that the whole matter of the crocodile eggshells consist of $CaCO_3$, mixtures of eggshell powder and $Ca_3(PO_4)_2$ were prepared in order to set the molar ratio of Ca/P = 1.67. The mixtures were placed in Teflon bottles containing 30 cm^3 distilled water. After stirring well, the bottles were placed in stainless steel autoclave. The autoclave were then sealed and placed in apparatus set 1. The temperature of oven was set at 250°C and periods of heating time varied from 8 to 12 h. After cooling the products were collected by filtration, washed with water several times, and dried in an oven at 110 °C for 1 h. The sample codes and reaction conditions are summarized in Table 5.

The synthesized products were characterized for phase analysis by X-ray diffraction analysis (XRD), Fourier Transform Infrared Spectroscopy (FTIR) and the microstructures were examined by Scanning Electron Microscopy (SEM).

2.4 Effect of particle sizes of sample powder on the reaction time.

In order to examine the effect of particle sizes of the sample powder on the reaction time, a set of experiments using different sizes of eggshell powder was performed. The corals, freshwater shells and crocodile eggshells fine were grounded and sieved selecting grains with sizes ranging in three different sizes denoting as L (> 150 μm), M (150 μm ≤ M > 53 μm), and S (≤ 53 μm).

Mixtures of sample powder with exact size and $Ca_3(PO_4)_2$ were prepared with the mole ratio of Ca/P = 1.67. The mixtures were mixed with water and placed in Teflon-lined stainless steel autoclave. The autoclave were then sealed and placed in a high temperature oven (apparatus set 2). The temperature of oven was set at 150 °C and period of heating time varied from 8 to 12 h. After cooling, the products were collected by suction filtration, washed with water several times and dried in an oven at 110 °C, 1h. The sample codes and reaction conditions are summarized in Table 5. The synthesized products were characterized for phase analysis by X-ray diffraction analysis.

3. Characterization techniques

3.1 X – ray Diffractometry (XRD)

Phase purity and structural features of the HAp samples was examined by powder X–ray diffraction technique. The intensity data were collected in 0.02º steps in the 2θ range of 20º to 60º, operating with a monochromatic Cu Kα radiation at the wavelength of 1.5406 Å in Guiner geometry, divergence slit of 1º, receiving slit width of 0.1 mm and scan rate at 2º/min. The phase were identified by comparing the experimental XRD patterns to standards complied by the Joint Committee on Powder Diffraction Standards (JCPDS) using the cards 09-432 for HAp, 71-2396 for aragonite and 72-1937 for calcite.

3.2 Fourier Transform Infrared Spectroscopy (FTIR)

Chemical analysis of functional groups were carries out by FTIR spectrophotometer **(**Bruker Model Equinox 55 Spectrophotometer) using KBr pellets over the range between 4000 and 400 cm^{-1} with resolution of 2 cm^{-1}.

3.3 Scanning Electron Microscopy (SEM)

Morphology of samples were observed by using one of following instrument: (1) scanning electron microscope JEOL model JSM 6310F at National Metal and Materials Technology Center, (2) Scanning Electron Microscope: JSM 5600 LV at Research and Development Institute, Kasetsart University, (3) Field Emission Gun Scanning Electron Microscope JEOL 6500 at University of Minnesota.

3.4 Transmission Electron Microscopy (TEM)

The powder sample was ultrasonically dispersed in water to form very dilute suspensions and then a few droplets were put on copper grids coated with carbon film for further examination by Transmission Electron Microscope: JEM 1220

at Research and Development Institute, Kasetsart University and FEI Tecnai 12 at University of Minnesota.

3.5 Autosorb

Surface area analysis (BET) Powder surface area was measured using five-point BET surface area analysis. Powders were dried in a sample holder at 120 ºC in N_2 atmosphere for 12 h before BET surface area analysis.

4. Study of *in vitro* bioactivity of hydroxyapatite

4.1 Preparation of simulated body fluid (SBF)

Since SBF is a solution highly supersaturated with respect to apatite. It is not easy to prepare clear SBF with no precipitation. Therefore, a detailed recipe for preparation of SBF was reported in 1995 by Cho *et al*., (Cho *et al.*, 1995). The recipe for preparing SBF in this report follows the refined recipe given by Kokubo *et al*., (Kokubo and Takadama, 2006).

4.1.1 Cleaning

All PE bottles including flasks, beakers etc. were immersed in dilute nitric acid solution for one day, then washed with distilled water and rinsed with de-ionized water for several times.

4.1.2 Ion concentrations of SBF

The nominal ion concentrations of SBF in comparison with those in human blood plasma are listed in Table 3. The ion concentrations of SBF in this study are prepared according to those values in Table 3. The actual weights of all ions in SBF used in this study are listed in Table 6.

Table 6 Order and amount of reagents for preparing 1000 ml of SBF, pH 7.40

Order	Reagent		Amount
1	NaCl	Assay min. 100.0 %, Mallinckrodt baker Inc., Paris, Kentucky,USA	7.996 g
2	$NaHCO_3$	Assay min. 100.3 %, Mallinckrodt baker Inc., Paris, Kentucky,USA	0.350 g
3	KCl	Assay min. 100.1 %, Mallinckrodt baker Inc., Paris, Kentucky,USA	0.224 g
4	K_2HPO_4	Assay min. 99.7 %, J.T. baker Inc., Phillipsburg, NJ,USA	0.174 g
5	$MgCl_2 \cdot 6H_2O$	Assay min. 99.8 %, Mallinckrodt baker Inc., Paris, Kentucky,USA	0.305 g
6	1 M HCl	87.28 ml of Approximately 37% HCl is diluted to 1000 ml with volumetric flask	40 cm^3
7	$CaCl_2 \cdot 2H_2O$	Assay min. 99.8 %, Mallinckrodt baker Inc., St.Louis , NY,USA	0.369 g
8	Na_2SO_4	Fisher Scientific, Fairlawn, NJ,USA	0.071 g
9	$(CH_2OH)_3CNH_2$ (Tris)	Assay min. 99.9+ %, Aldrich Chemical Company Inc., USA	6.057 g

4.1.3 Preparation procedure of SBF

The preparation procedure follows the procedure given by Kokubo. Since SBF is supersaturated with respect to apatite, an inappropriate preparation method can lead to the precipitation of apatite in the solution. Always make sure that the preparing solution is kept colorless and transparent and that there is no deposit on the surface of the bottle. If any precipitation occurs, stop preparing SBF, abandon the solution, restart from washing the apparatus and prepare SBF again.

In order to prepare 1000 ml of SBF, first of all, put 700 ml of ion-exchanged and distilled water with a stirring bar into 1000 ml plastic beaker. Set it in the water bath on the magnetic stirrer and cover it with a watch glass or plastic wrap. Heat the water in the beaker to 37 ºC under stirring. Dissolve only the reagents of 1st to 8th order into the solution at 37 ºC one by one in the order given in Table 6. Taking care of the indications in the following list.

(a) In preparation of SBF, glass containers should be avoided, but a plastic container with smooth surface and without any scratches is recommended, because apatite nucleation can be induced at the surface of a glass container or the edge of scratches. If the container has scratches, replace it by a new one.

(b) Never dissolve several reagents simultaneously. Dissolve a reagent only after the preceding one (if any) is completely dissolved.

(c) Since the reagent $CaCl_2$, which has great effect on precipitation of apatite, takes usually granular form and takes much time to dissolve on granule at a time, completely dissolve one before initiation of dissolution of the next.

(d) Measure the volume of 1M-HCl by cylinder after washing with 1M-HCl.

(e) Measure the hygroscopic reagents such as KCl, $K_2HPO_4 \cdot 3H_2O$, $MgCl_2 \cdot 6H_2O$, $CaCl_2$, Na_2SO_4 in as short a period as possible.

(f) The reagents of 9^{th} (Tris) and 10^{th} order (small amount of HCl) are dissolved in the following process of pH adjustment.

Set the temperature of the solution at 37 ºC. If the volume of the solution is less than 900 ml, add ion exchanged and distilled water up to 900 ml in total. Insert the pH electrode into the solution. Just before dissolving the Tris, the pH of the solution should be 2.0 ± 1.0.

With the solution temperature between 35 ºC and 38 ºC, preferably to 37 ºC, dissolve the reagent Tris into the solution little by little taking careful note of the pH change. After adding a small amount of Tris, wait until the reagent already introduced is dissolved completely and the pH has become constant; then add more Tris to raise the pH gradually. When the pH becomes 7.30, make sure that the temperature of the solution is maintained at 37 ºC. With the solution at 37 ºC, add more Tris to raise the pH to under 7.45. Do not add a large amount of Tris into the solution at a time, because the radical increase in local pH of the solution can lead to the precipitation of calcium phosphate. If the solution temperature is not within 37 ºC, add Tris to raise the pH to 7.30, stop adding it and wait for the solution temperature to reach 37 ºC. The pH shall not increase over 7.45 at 37 ºC, taking account of the pH decrease with increasing solution temperature (the pH falls about 0.05/ºC at 37 ºC).

When the pH has risen to 7.45, stop dissolving Tris, then drop 1M-HCl by syringe to lower the pH to 7.42, taking care that the pH does not decrease below 7.40. After the pH has fallen to 7.42, dissolve the remaining Tris little by little until the pH rise to 7.45. If any Tris remains, add the 1M-HCl and Tris alternately into the solution. Repeat this process until the whole amount of Tris is dissolved keeping the pH within the range of 7.42–7.45. After dissolving the whole amount of Tris, adjust the temperature of the solution to 37 ºC. Adjust the pH of the solution by dropping 1 M-HCl little by little at a pH of 7.42 at 37 ºC and then finally adjust it to 7.40 exactly at 37 ºC on condition that the rate of solution temperature increase or decrease is less than 0.1 ºC/min. Remove the electrode of the pH meter form the solution, rinse it with ion-exchanged and distilled water and add the washings into the solution. Pour the pH-adjusted solution from the beaker into 1000 ml volumetric flask. Rinse the surface of the beaker with ion-exchanged and distilled water and add the washings into the flask several times, fixing the stirring bar with a magnet as if to prevent it from falling into the volumetric flask. Add the ion-exchanged and distilled water up to the marked line (it is not necessary to adjust exactly, because the volume becomes smaller after cooling), put a lid on the flask and close it with plastic film. After mixing the solution in the flask, keep it in the water to cool it down to 20 ºC.

After the solution temperature has fallen to 20 ºC, add the distilled water up to the marked line.

4.1.4 Preservation of SBF

The SBF should be preserved in a plastic bottle with a lid put on tightly and kept at 5-10 ºC in a refrigerator. The SBF shall be used within 30 day after preparation.

4.2 Procedure of apatite-forming ability test (*In vitro* bioactivity test)

The *in vitro* biomineralization capability of the synthesized HAp was tested by immersion of sample in simulated body fluid (SBF) at body temperature, as described in Kokubo method (Kokubo and Takadama, 2006). The ion composition of SBF is listed in Table 6. The synthesized HAp powders were conformed in 0.1 g/disk (13x1 mm) by uniaxial (2.75MPa) and isostatic pressure (3MPa). The *in vitro* bioactivity study was performed by soaking the HAp pellets in SBF at 37ºC for different periods of time (1, 2, 3, 4, 5 and 6 days) with refreshing the SBF solution everyday. The HAp pellet was placed in the SBF as shown in Figure 21. After soaking, samples were remove from the SBF solution and washed with distilled water several time and air dried at room temperature. The surfaces of the samples were characterized by SEM-EDS and micro XRD.

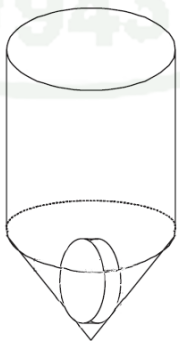

Figure 21 The hydroxyapatite pellet in the SBF.

5. The *in vitro* study of antibiotic drug delivery property of hydroxyapatite

In this study two antibiotic drugs were selected as the model drugs which differ in molecular weight and molecular shape (Fig 22). One is tetracycline, the other is vancomycin. Tetra cycline is polyketide antibiotic and indicated for use against many-bacterial infections. Vancomycin is a glycopeptides antibiotic used in the prophylaxis and treatment of infections caused by gram-positive bacteria. The *in vitro* study of antibiotic drug delivery starts with loading of drug in the HAp micropore by immersion in the drug solution. The estimation of drug uptake by the

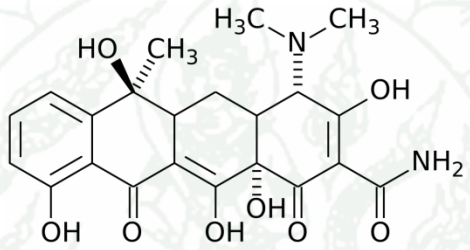

(a)

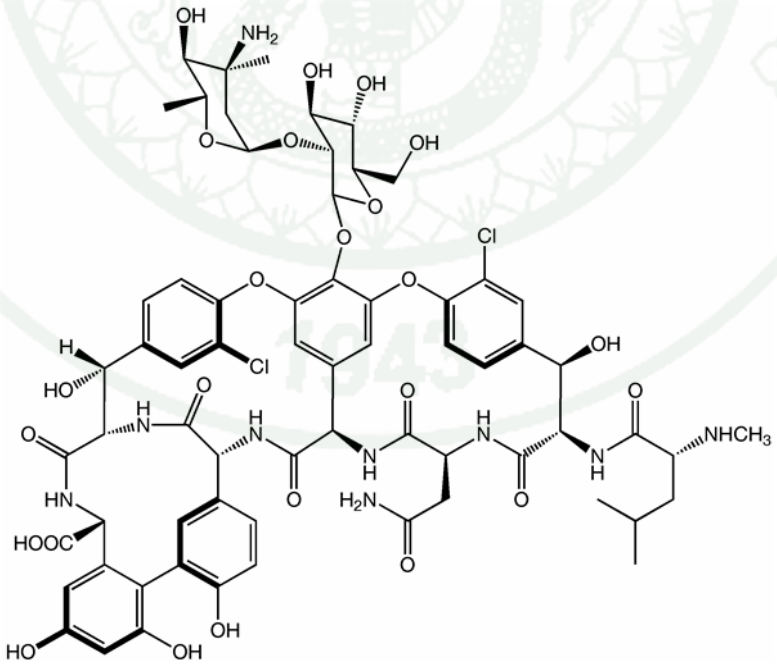

(b)

Figure 22 Chemical structure of (a) tetracycline and (b) vancomycin.

HAp was carried out through an indirect method, by finding the difference in drug concentration before and after loading. Percentage of drug loading was calculated using the formula.

$$\% \text{ drug loading } = \frac{x - y}{x} 100$$

where x and y represent the initial and final drug concentrations, respectively.

The drug concentrations in the solution were measured spectrophotometrically at a wavelength of 364 nm and 284 nm for tetracycline and vancomycin, respectively. *In vitro* release of drug from HAp was carried out at 37 °C in SBF solution. The release medium was collected every two hours and replaced with a fresh SBF solution each time. The amounts of released drug were then measured spectrophotometrically at 366 nm and 284 nm for tetracycline and vancomycin, respectively.

The following samples are used for *in vitro* study: HTib_750w, HTW_750w, ES_6_150, EM_6_150 and EL_6_150. The physicochemical properties of these samples were measured by N_2 sorption analysis.

5.1 Calibration curves for the determination of drug concentration

Standard solutions with TC concentrations of 10, 20, 30, 40, 50 and 60 ppm were prepared in aqueous solution and SBF solution. Similarly, the standard aqueous solutions with VM concentrations of 20, 40, 60, 80 and 100 ppm and the standard SBF solution with VM concentration of 10, 20, 30, 40, 50, 60, 80 and 100 ppm were prepared. The drug concentrations in the standard solution were measured spectrophotometrically at wavelength of 364 nm for tetracycline in water, 366 nm for tetracycline in SBF and 284 nm for vancomycin in aqueous and SBF solution. Since tetracycline is active to the light, all experiments involved tetracycline must be light protected.

5.2 Drug loading

2 g of HAp was placed in a PE centrifuge tube containing 5 ml of 2000 ppm solution of tetracycline hydrochloride. After mild stirring 24 hrs at room temperature, the HAp were separated by centrifugation. The tetracycline concentration in centrifugate was determined by measuring spectrophotometrically at 364 nm. The HAp residue was washed quickly with deionized water, filtered by vacuum suction and dried. The amount of tetracycline in filtrate was determined spectrophotometrically. The experiment was performed in duplicate. In most case, the dilution of centrifugate was carried out in order to keep the sample concentration within the calibration curve. Similar procedure was done for vancomycin drug. The vancomycin concentration in centrifugate was determined by measuring spectrophotometrically at 284 nm. The FTIR spectra of all drug loaded HAp were recorded.

5.3 Drug releasing

0.4 g of drug loaded HAp was immersed in 5 ml SBF in PE centrifuge tube. The release medium was collected by centrifugation at predetermined time intervals of 2 h and replaced with a fresh SBF each time. The releasing tetracycline concentration in centrifugate was determined by measuring spectrophotometrically at 366 nm. The dilution of centrifugate was carried out in order to keep the sample concentration within the calibration curve. The release medium was collected every two hours until no more drug was detected or the drug concentration is below the lowest concentration in the calibration curve.

Similar procedure was performed for vancomycin. The vancomycin concentration in centrifugate was determined by measuring spectrophotometrically at 284 nm.

RESULTS AND DISCUSSION

1. Conversion of crocodile bone into hydroxyapatite

1.1 Characterizations of crocodile bone

1.1.1 Inductively couple plasma analysis

Crocodile bone is composed of high calcium content. There is a wide variation of concentrations in the 15 elements (Table 7). Results showed that calcium had the highest concentration, followed by magnesium. The lowest concentrations were of cobalt, followed by cadmium. Calcium content in the crocodile bone is 38.30 (% w/w), according to be reported in human dental enamel which ranges from 34 to 39 (% w/w) (Webb *et al*., 2005). The content of each trace impurity especially heavy metals is well below the specified limit of ASTM F 1185-88: Standard specification for composition of ceramic hydroxyapatite for surgical implant.

1.1.2 XRD phase analysis

The X-ray diffractogram of commercial hydroxyapatite and cleaned crocodile bone are shown in Figure 23. The XRD pattern of cleaned crocodile bone and commercial hydroxyapatite show the presence of hydroxyapatite phase. The XRD lines in the pattern of the crocodile bone are not as sharp as those of commercial hydroxyapatite indicating the lower crystallinity of bone.

1.1.3 FTIR analysis

The FTIR spectrum of crocodile bones is shown in Figure 24. A large number of bands in the spectrum shown in Table 8 match the bands in the hydroxyapatite reference spectrum (hydroxyapatite commercial) and are in close agreement with reported data (Ooi *et al.*, 2007). Additional absorption peaks

corresponding to a N-H stretching band around 2920-2960 cm^{-1} and amine bands at 1500 – 1750 cm^{-1} were observed. These sets of bands are characteristic of macromolecules of protein in the crocodile bone matrix. They disappeared when the crocodile bone was calcined at 650 °C.

Table 7 Concentration distribution of fifteen elements in ashed bone sample.

Elements	Concentrations			
	(µg/ml)	mg/100 ml	(mg/1 g bone)	(% w/w)
As	< 0.050	< 0.0050	< 0.0050	<0.00050
Ca	3830	383.00	383.00	38.30
Cd	< 0.003	< 0.0003	< 0.0003	<0.00003
Co	< 0.006	< 0.0006	< 0.0006	<0.00006
Cr	0.075	0.0075	0.0075	0.00075
Cu	0.073	0.0073	0.0073	0.00073
Fe	0.211	0.0211	0.0211	0.00211
Hg	< 0.030	< 0.0030	< 0.0030	< 0.00030
Mg	136.0	13.60	13.60	1.36
Mn	0.022	0.0022	0.0022	0.00022
Ni	< 0.010	< 0.0010	< 0.0010	<0..0010
Pb	< 0.040	< 0.0040	< 0.0040	<0.00040
Sn	0.400	0.0400	0.0400	0.00400
Sr	6.730	0.6730	0.6730	0.0673
Zn	0.681	0.0681	0.0681	0.00681

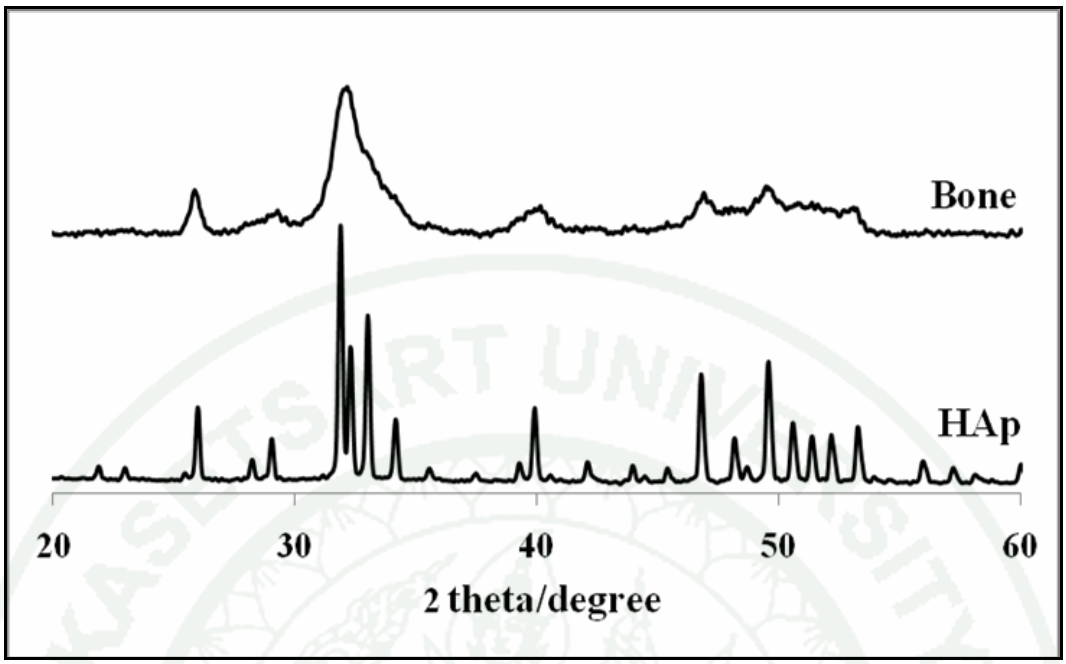

Figure 23 The X-ray diffractogram of commercial HAp and cleaned crocodile bone.

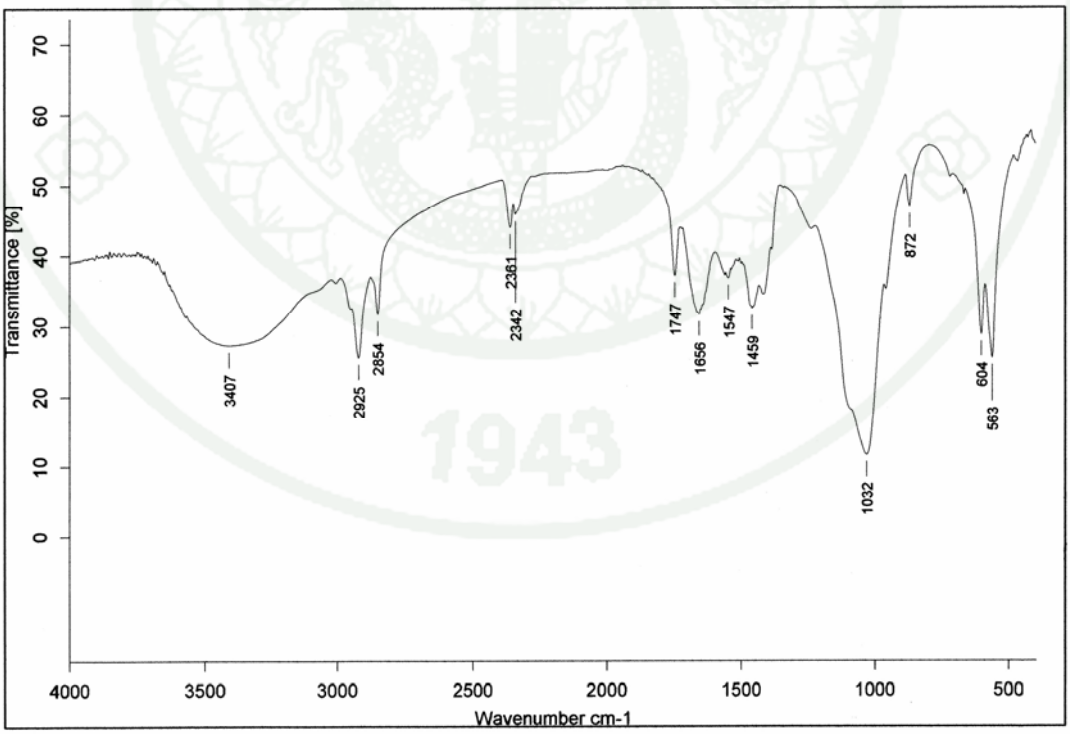

Figure 24 FTIR spectrum of crocodile bones (*Crocodylus siamensis*) treated with NaOCl.

1.1.4 Thermal gravimetric analysis

The TG analysis of crocodile bones treated with NaOCl are shown in Figure 25. The first loss at between 50 – 110 °C is attributed to water evaporation (w %). A continuous weight loss was observed between 200 – 800 °C, which is associated with the burning of organic substances. Additionally, in carbonated apatites, the carbonate is liberated from the HAp structure between 500 – 900 °C producing H_2O and CO_2 (Tadic and Epple, 2004). There was no significant weight loss at above 900 °C, indicating that all organic materials such as fat, collagen, lipids, proteins and tissue were completely removed.

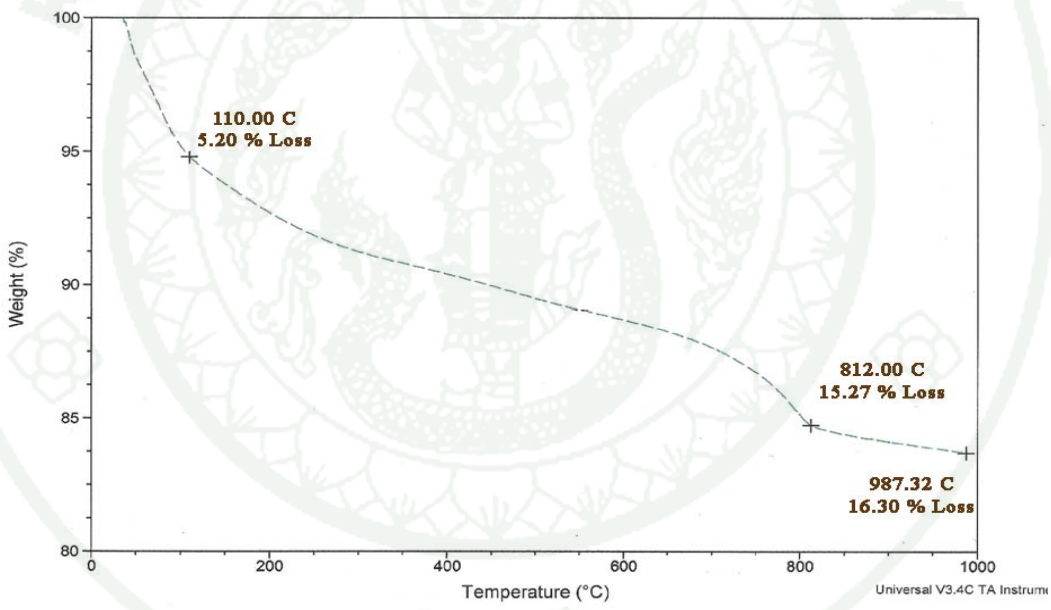

Figure 25 The thermogravimetric curve of cleaned bone samples.

1.1.5 Microstructure analysis

The SEM micrograph cross section of crocodile bone display a layered structure (Fig 26 (a-b)). The environmental scanning electron microscope images (Fig 27) show that the large pores are presented in the crocodile bone. The pore structure appeared random rather than uniform as pores of various sizes were

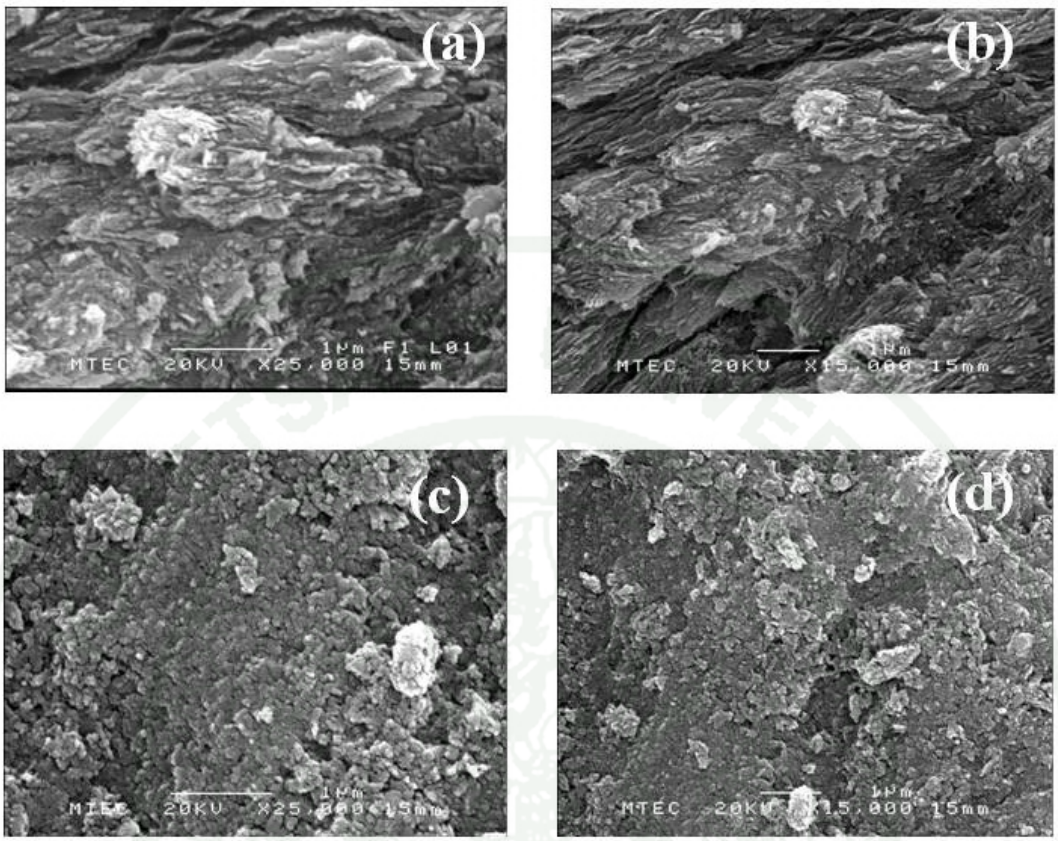

Figure 26 SEM micrographs cross section at (a) high and (b) low magnification of the bone (*Crocodylus siamensis*) and SEM micrographs of the bone surface (*Crocodylus siamensis*) at (c) high and (d) low magnification.

present in the same portion of bone. The majority of pores observed varied between the ranges of approximately 10 – 500 μm in diameter. The bovine sample used for comparison showed only the haversian canals of about 30 μm in diameter, these were extremely uniform in arrangement (Fig 27 (c-d)). These images show promise for the use of hydroxyapatite derived from the crocodile bone due to the approximately pore size for osteointegration (Lewis *et al*., 2006).

1.2 Conversion of crocodile bone into hydroxyapatite by thermal process

A direct observation during the calcination at different temperatures was the color change of the samples. The color of crocodile bone is light yellow. Upon

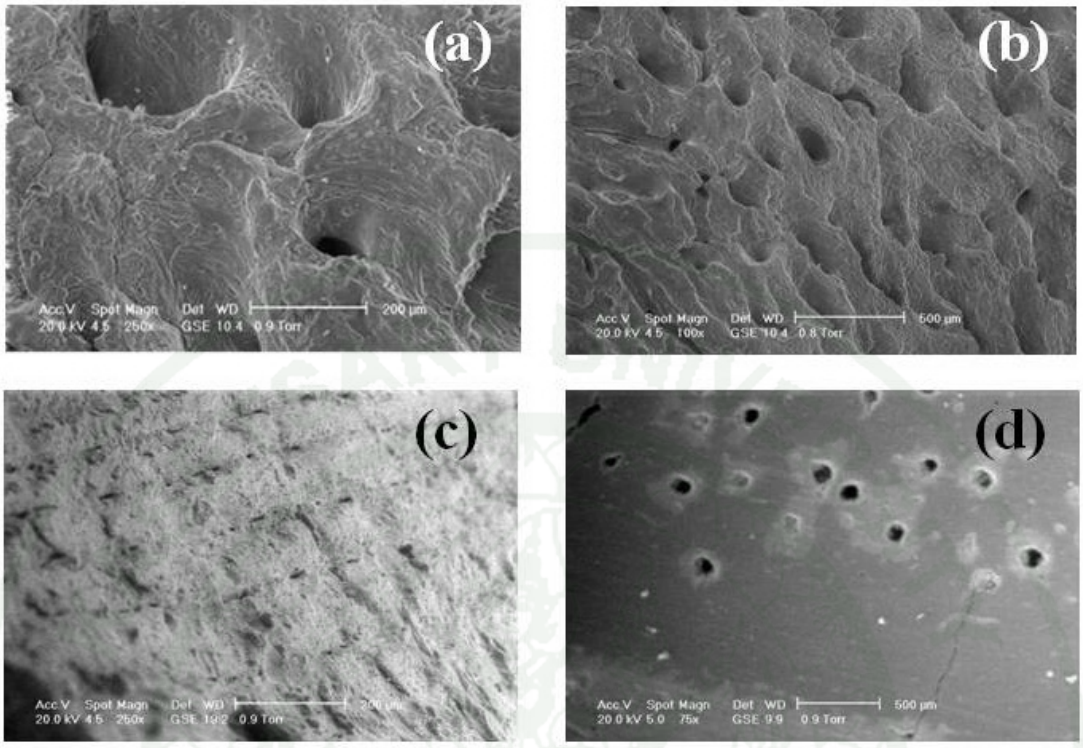

Figure 27 The ESEM images of (a) The pores present in the cortiacal bone of the tail in *Crocodylus siamensis* (scale bar is 200µm) (b) The transition from trabecular to cortical bone in the tail of *Crocodylus siamensis* (scale bar is 500µm) (c-d) Bovine bone: The small, uniformly sized pores (30 -100 µm) within cortical section of bovine bone. (scale bars are 200µm and 500 µm respectively).

Source: (Lewis *et al.*, 2006)

calcination at temperatures of 550 ºC, 650 ºC, 750 ºC and 900 ºC, the colors of the bone samples changed to dark grey, light grey, white and white, respectively. This series of color change was believed to be associated with the burn out process of organic matrix such as protein and collagen in the crocodile bone. The dark colors observed for bone samples calcined below 750 ºC indicated the incomplete removal of organic compositions. At temperatures higher than 750 ºC, the samples are white in color, suggesting complete removal of organic substances.

Figure 28 presents the XRD patterns of crocodile bone and calcined bone. The XRD pattern of HTib_550 shows the presences of low crystalline hydroxyapatite phase in the bone matrix. As the heating temperature increased to 750 ºC, the intensity of HAp characteristic peaks gradually increased. The XRD patterns of bone calcined at 750 ºC and 900 ºC were similar and exhibited a substantial increase in peak height and a decrease in peak width, thus indicating an increase in crystallinity. In addition the calcium oxide phase was observed (Fig 28). Calcium oxide results from the decomposition of the carbonate content of the original bone material. Trace of CaO is easily removed by changing to soluble calcium hydroxide as in eq. 4.

$$CaO + H_2O \rightarrow Ca(OH)_2 \quad (4)$$

The XRD spectra for the calcined bone samples which were washed with water give no calcium oxide peak (Fig 29). All XRD patterns obtained for calcined crocodile bones are in agreement with the XRD patterns in JCPDS file no. 09-0432.

The FTIR spectra of bones calcined at 550 – 900 °C are shown in Figure 30. FTIR analysis showed that the characteristic bands of macromolecules of proteins and organic materials in crocodile bone matrix (2925 and 1500 – 1750 cm^{-1}) are gradually decreased in intensity as the heating temperature increased. They disappeared when the bone was calcined at 750 °C, thus indicating the complete removal of organic material. It is in good agreement with the observed color change from black to grey and finally white. This was also confirmed by TG analysis, which showed no significant weight loss beyond this temperature. There are no significant differences observed in the FTIR spectra of bones calcined from 750 °C to 900 °C suggesting no phase changes due to thermal effect.

In general, the FTIR spectrum of HAp consists of characteristic peaks of phosphate (PO_4^{3-}), hydroxyl (OH^-) and carbonate (CO_3^{2-}) ions as shown below:

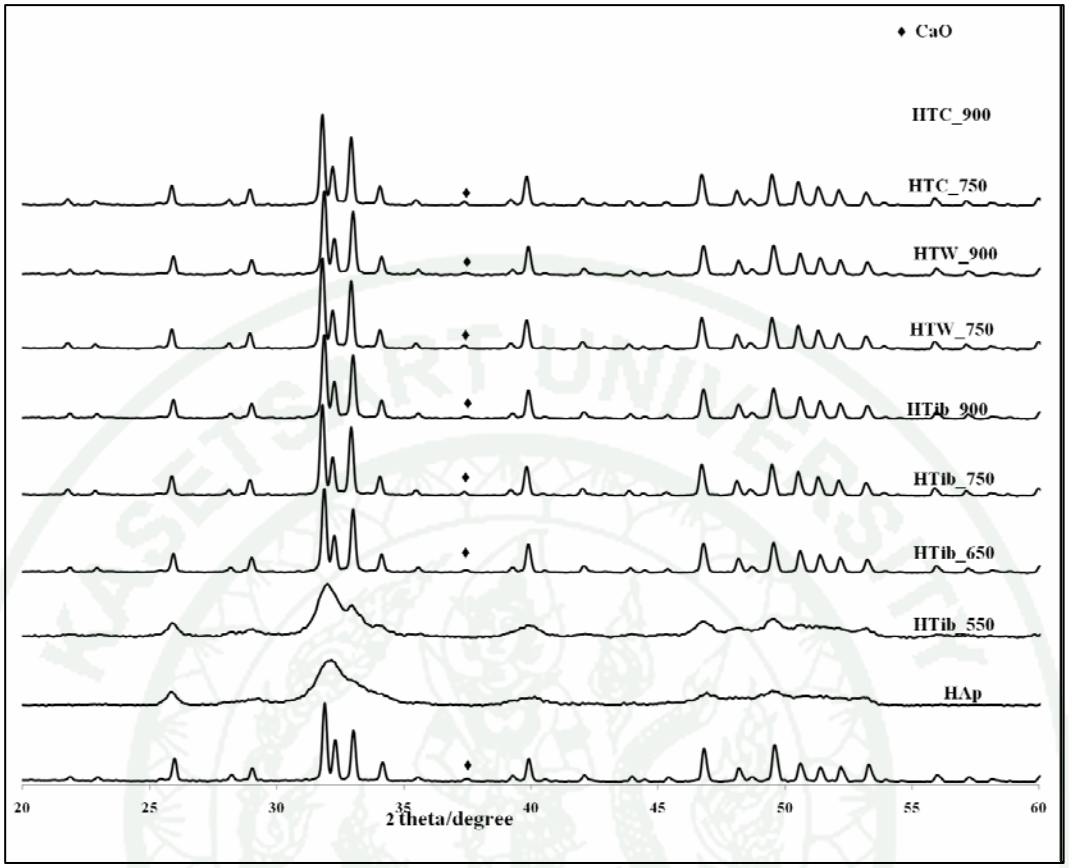

Figure 28 X-ray diffraction patterns of crocodile bone calcined between 550 ºC and 900 ºC.

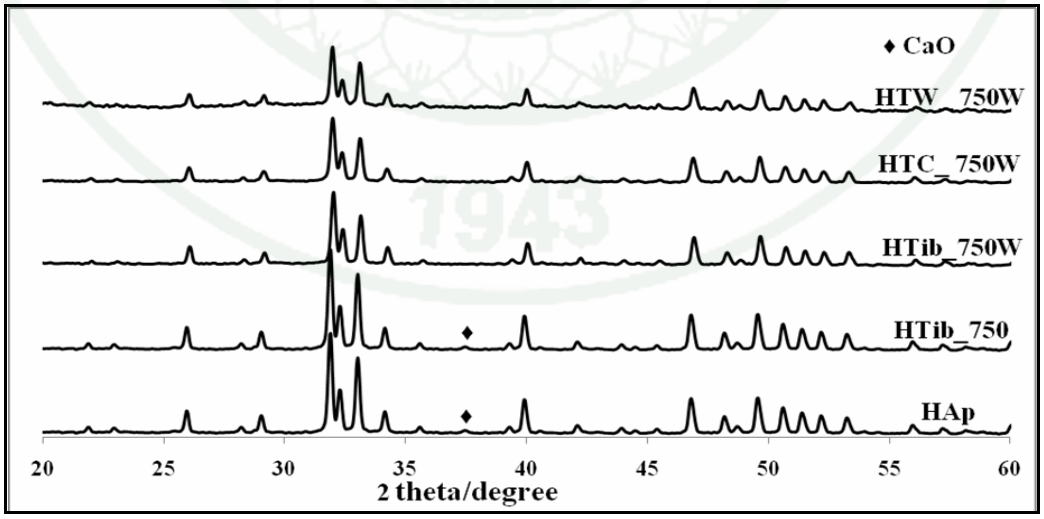

Figure 29 X-ray diffraction patterns of crocodile bone calcined at 750 ºC after washed with water.

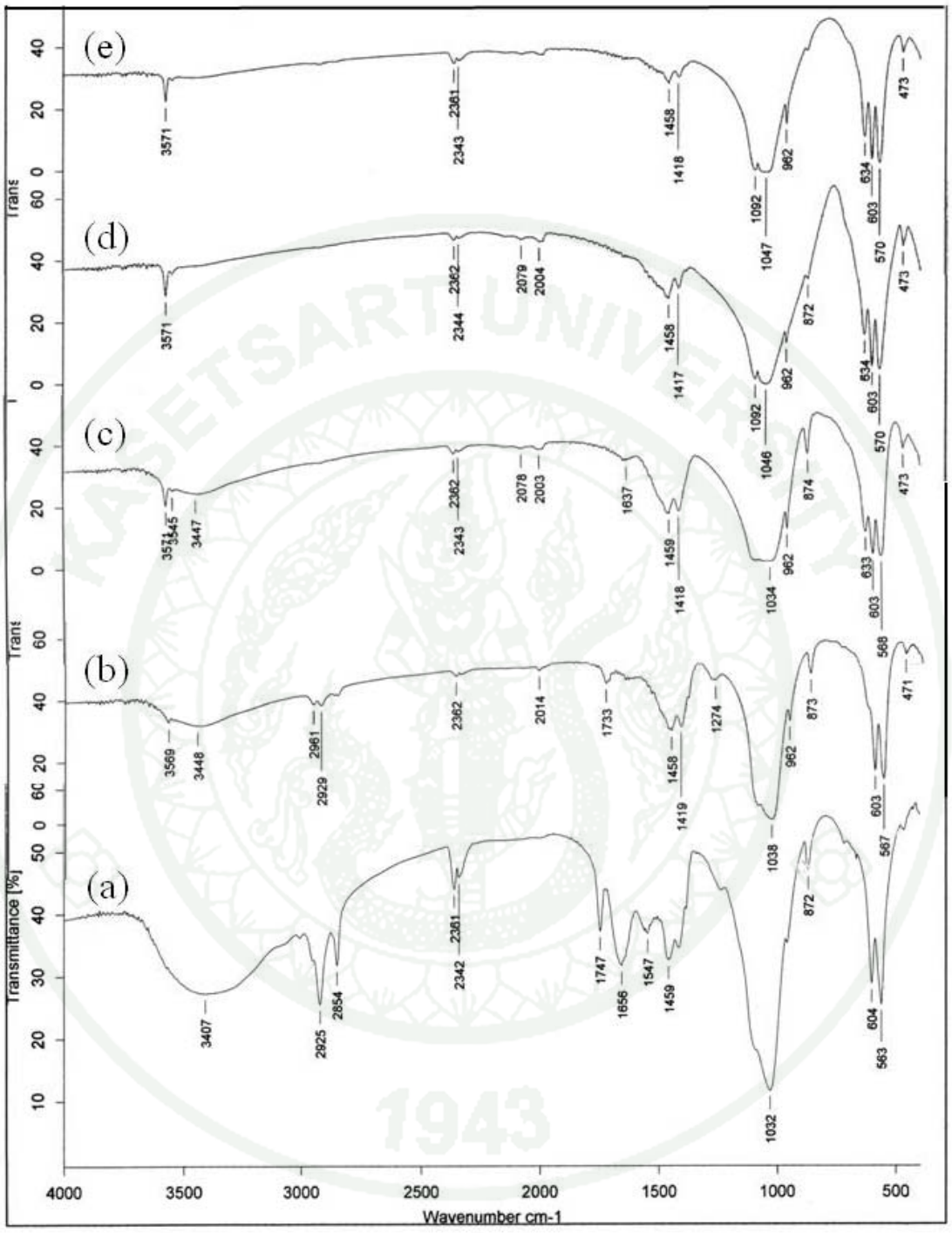

Figure 30 FTIR spectra of (a) calcined bone soaked in NaOCl (b) HTib_550 (c) HTib_650 (d) HTib_750W and (e) HTib_900W.

phosphate (PO_4^{3-}): 470 – 475, 560 – 600, 950 – 965 and 1030 – 1095 cm^{-1}

hydroxyl (OH^-): 630 – 635, 3430 – 3450 (broad) and 3560 – 3575 (sharp) cm^{-1}

carbonate (CO_3^{2-}): 870 – 880 and 1420 – 1460 cm^{-1}

All FTIR spectra illustrates phosphate, hydroxyl and carbonate characteristic peaks (Table 8). A comparison between the FTIR spectra of cleaned crocodile bone and calcined bone is listed in Table 8.

Figure 31 (a, c and e) shows representative SEM pictures of bones calcined at 750 °C and Figure 27 shows SEM picture of crocodile bones. The microstructures of the former appeared not as dense as the latter due to the absence of organic materials in the crocodile bone matrix. The TEM images of the calcined bone showed the presence of hexagonal crystals with various sizes (Fig 31 (b,d and f)).

The analysis of the crystallite size (L_c) of the HAp has been done for all samples using the Scherrer's equation:

$$L_c = \frac{k\lambda}{\beta \cos\theta}$$

Where L_c = mean size of the ordered (crystalline) domains, which may be smaller or equal to the grain size.

k = Scherrer constant (k = 0.94)

λ = x-ray wavelength (λ = 0.1542 nm for cu Kα radiation)

θ = Bragg angle (°)

β = the full width at half maximum (FWHM) of the diffraction peak under consideration (rad).

The single peak near 26 º in the XRD pattern is chosen for the determination of the FWHM distance (Table 9 and Appendix Figure 1). This peak corresponding the *c* crystallographic axis (Fathi, M. H. *et al*., 2008).

Table 8 FTIR characteristic peaks for calcined bone.

Code	PO_4^{3-} vibration				CO_3^{2-} vibration		O-H vibration		
	υ_2	υ_4	υ_1	υ_3	υ_2	υ_3	δ_1	υ_1	υ_2
Crocodile bone[1]									
Crocodylus Porosus	469	566, 605	962	1038	873	1419, 1475	-	3449	-
Crocodylus Siamensis	469	565, 605	961	1044	873	1421, 1475	-	3454	-
Bovine bone[2]									
Heated bovine bone	-	560	962	1049, 1090	875	1410, 1450	630		3570
Calcined bone									
HTib_550	471	567, 603	962	1038	873	1419, 1458	-	3448	3569
HTib_650	473	568, 603	962	1034, 1092	874	1418, 1459	633	3447	3571
HTib_750W	473	570, 603	962	1046, 1092	872	1417, 1458	634	-	3571
HTib_900W	473	570, 603	962	1046, 1092	872	1418, 1458	634	-	3571

Source: [1] Lewis *et al.,* (2006)

[2] Ooi *et al.,* (2007)

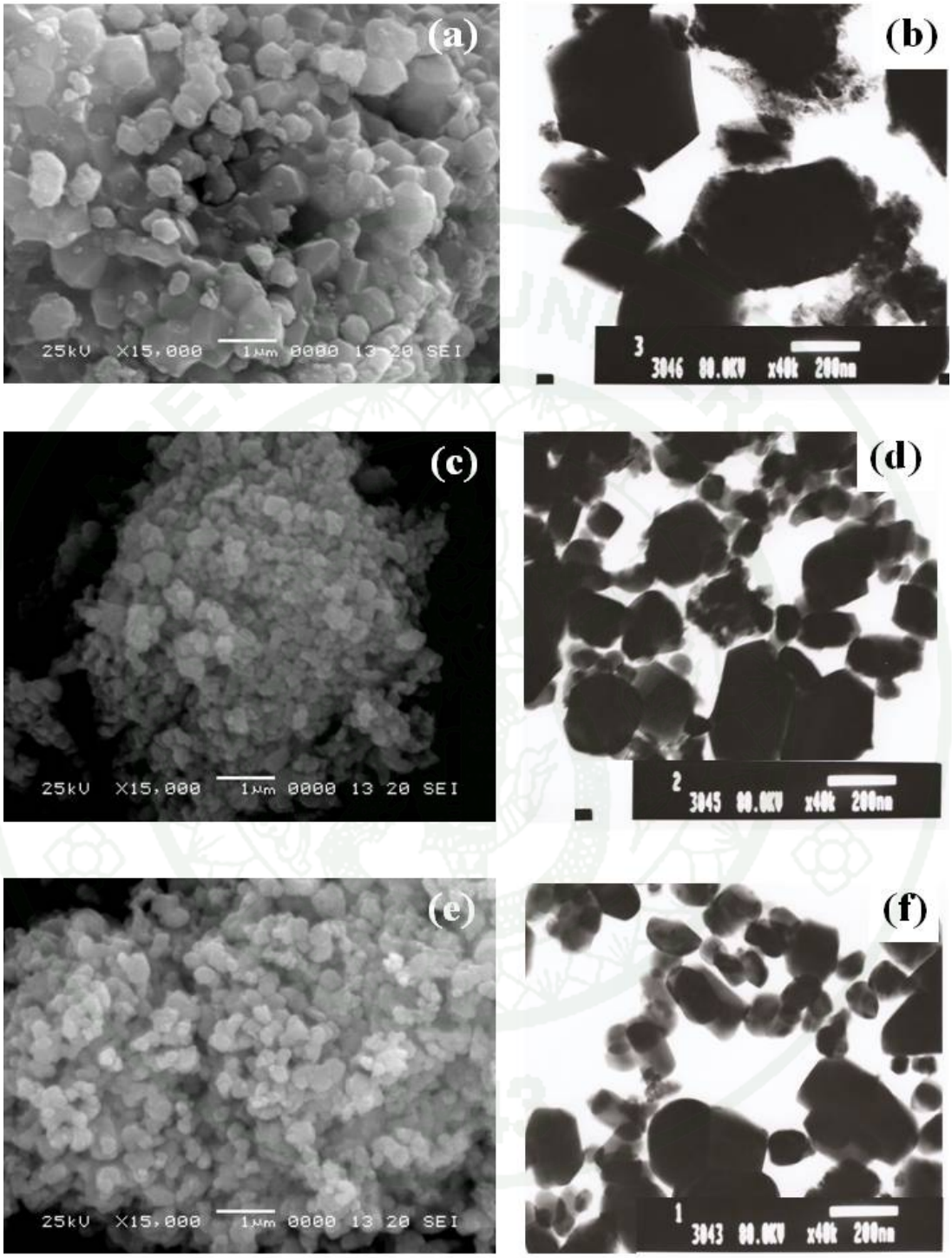

Figure 31 SEM and TEM images of the HAp from bone (a, b) HTib_750W (c, d) HTC_750W and (e, f) HTW_750W respectively.

Table 9 The crystallite size of calcined HAp.

Samples	FWHM	Crystallite size (nm)
HTib_650W	0.0084	17.75
HTib_750W	0.0040	37.06
HTib_900W	0.0036	41.57
HTC_750W	0.0041	31.57
HTC_900W	0.0044	34.09
HTW_750W	0.0041	31.17
HTW_900W	0.0042	35.51

2. Synthesis of hydroxyapatite from calcium based natural materials by hydrothermal process

2.1 Synthesis of hydroxyapatite from corals

The XRD pattern of stag horn corals (Fig 32) shows mainly aragonite structure of $CaCO_3$. After hydrothermal reaction at 250 ºC for 8 h, the corals changed to crystalline hydroxyapatite. The XRD patterns of the coralline hydroxyapatite are shown in Figure 33. All peaks in all figures are indexed to hexagonal lattice of HAp crystal. The wide and high peaks reveal that the synthesized hydroxyapatite has a very small size and excellent crystal quality**.** The patterns show clearly that the coral was successfully converted into hydroxyapatite by hydrothermal treatment for only 8 h at 250 ºC. When the reaction time increased to 12 h, the XRD pattern showed sharp peaks revealing an increase in crystallinity. However, the trace of calcium oxide phase was observed in C_12_250 sample. This result shows the decomposition of the carbonate at the longer reaction time.

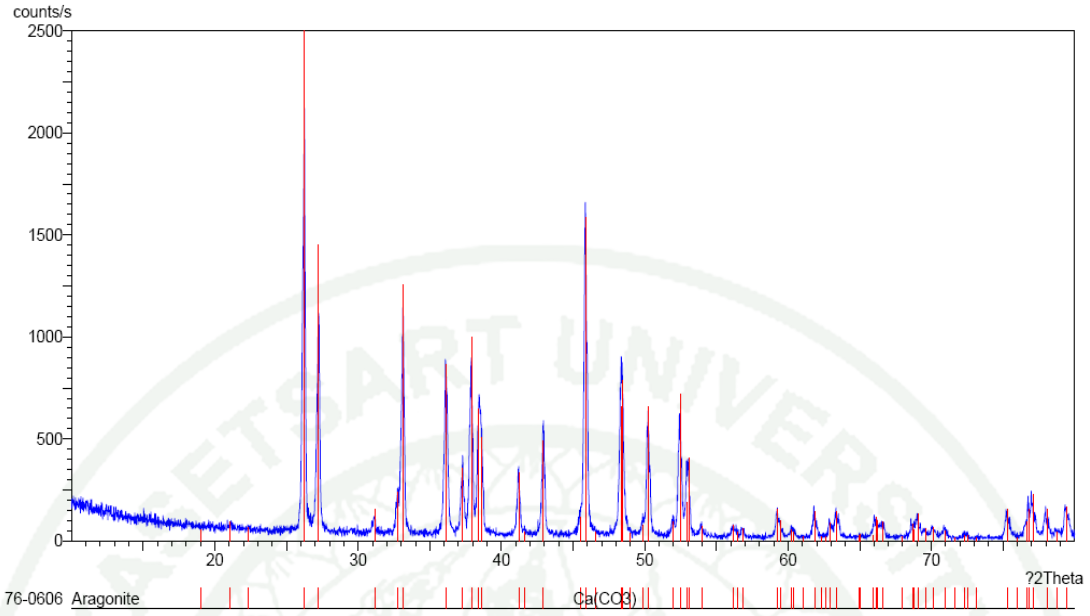

Figure 32 The XRD patterns of Stag horn coral powder compared with aragonite structure (JCPDS file 76-0606**)**.

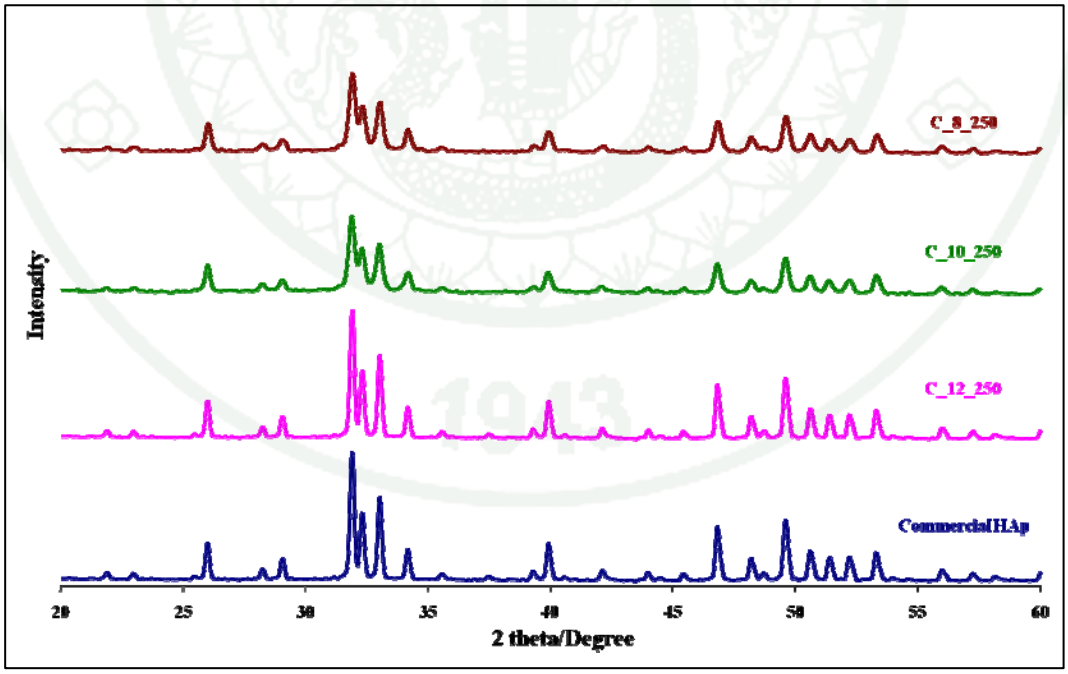

Figure 33 The comparison of the synthesized HAp from stag horn coral at 250ºC for various reaction times.

The FTIR spectrum of stag horn coral shows no evidence of the characteristic bands of the functional groups of HAp phase (Fig 34). The main IR spectrum correspond to the carbonate ion: 700, 713 cm^{-1}(ν_4) , 861 cm^{-1} (ν_2), 1083 cm^{-1}(ν_1), 1470 cm^{-1} (ν_3). The strong IR band at 1783 cm^{-1} corresponds to the C=O groups of the carbonate ion.). The spectrum is characteristic of aragonite (Ni and Ratner, 2003; Vagenas *et al.*, 2003). The FTIR characteristic peaks of coralline hydroxyapatite from corals are shown in Table 10 and Figure 35. All FTIR spectra illustrated phosphate, hydroxyl and carbonate characteristic peaks of hydroxyapatite. Type B carbonated hydroxyapatite was produced as revealed by the CO_3^{2-} bands at 1420 and 1458 cm^{-1}. The FTIR as well as XRD results support a success in the conversion of coral into coralline hydroxyapatite by hydrothermal method.

The morphology of the coralline hydroxyapatite was examined using scanning electron microscopy. The images in Figure 36 demonstrate the agglomerated particles of rod-like morphology. The particle size ranges from 100 – 200 nm.

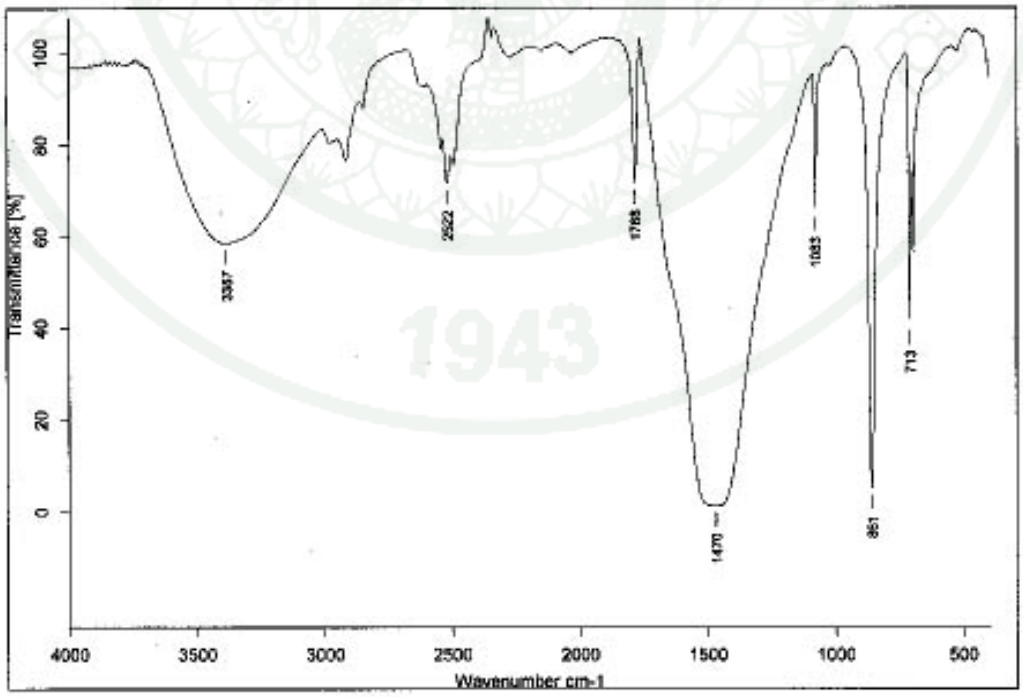

Figure 34 FTIR spectrum of stag horn coral.

Table 10 FTIR characteristic peaks for synthesized products.

Code	PO_4^{3-} vibration				CO_3^{2-} vibration		O-H vibration		
	υ_2	υ_4	υ_1	υ_3	υ_2	υ_3	δ_1	υ_1	υ_2
C_8_250	474	567, 603	963	1042, 1093	878	1420, 1458	633	3447	3571
C_10_250	473	566, 603	963	1037, 1093	875	1421, 1459	633	3434	3571
C_12_250	474	566, 603	963	1040, 1093	878	1422, 1457	633	3433	3571
Sh_8_250	474	597, 603	963	1037, 1093	869	1421, 1459	633	3432	3571
Sh_10_250	474	567, 603	963	1041, 1093	869	1459	633	3468	3571
Sh_12_250	474	567, 603	963	1041, 1093	878	1421, 1459	633	3432	3571
E_8_250	473	566, 603	963	1034, 1093	878	1421, 1459	633	3433	3571
E_10_250	473	567, 603	963	1036, 1093	878	1421, 1458	633	3449	3571
E_12_250	474	567, 603	963	1043, 1093	878	1421, 1458	633	3449	3571

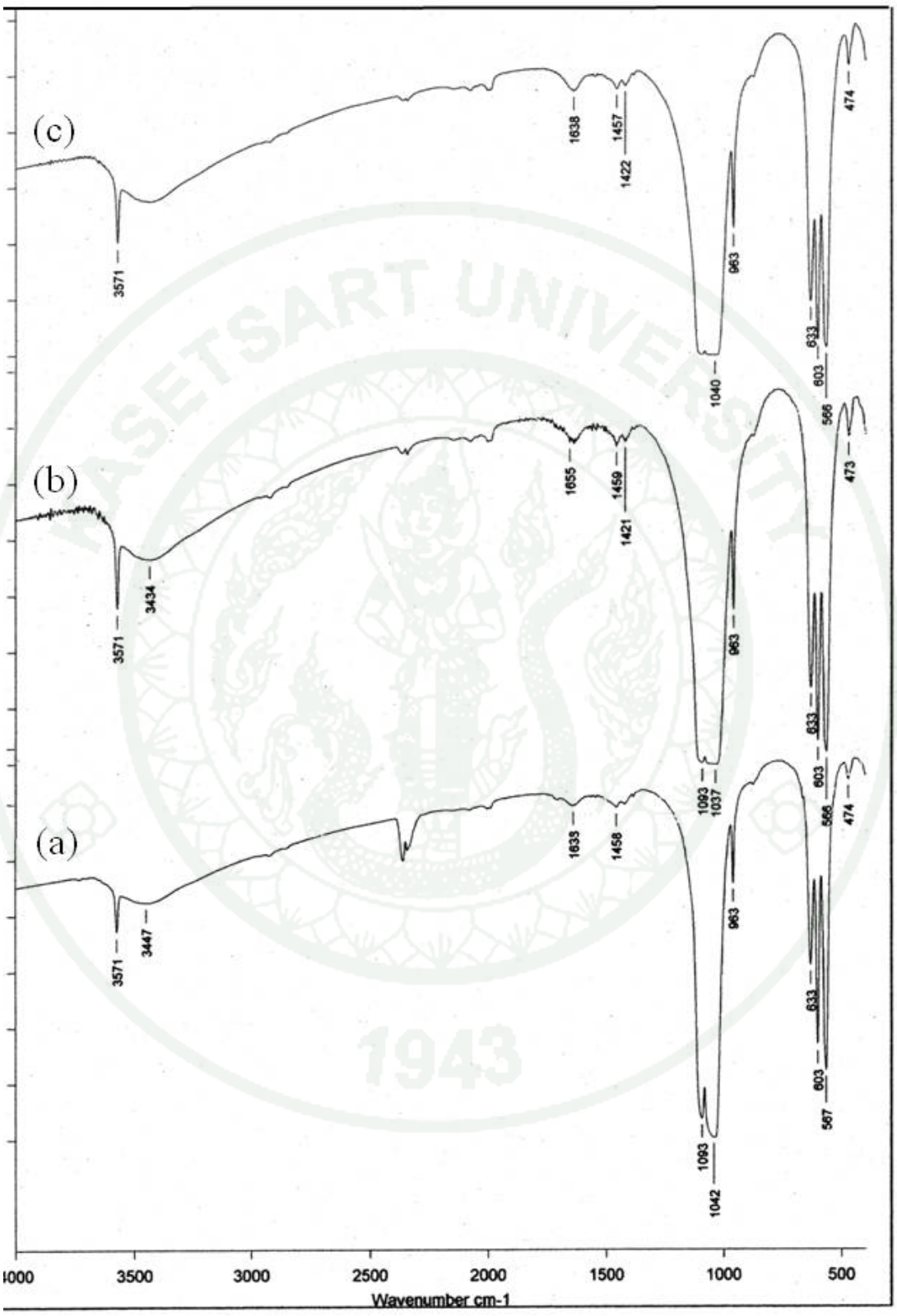

Figure 35 FTIR spectra of (a).C_12_250, (b) C_10_250 and (c) C_8_250.

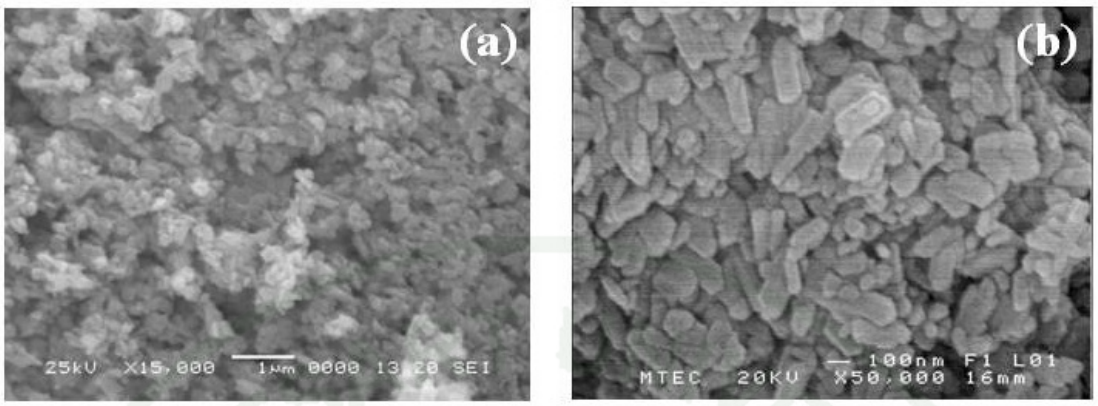

Figure 36 Typical SEM micrographs of synthesized products (a) C_10_250 and (b) high magnification images of C_10_250.

2.2 Synthesis of hydroxyapatite from freshwater shells

The XRD pattern of freshwater shells shows mainly aragonite structure of $CaCO_3$ and small amount of calcite structure (Fig. 37).

The XRD patterns of synthesized hydroxyapatite from freshwater shell in comparison with the commercial hydroxyapatite were reported in Figure 38. The patterns show clearly that the shell powders were successfully converted into hydroxyapatite by hydrothermal treatment for only 8 h at 250 ºC. By increasing the reaction time to 12 h, the XRD pattern shows sharp peaks reveal an increase in crystallinity. However, the trace of calcium oxide phase was observed in Sh_12_250 sample. This result shows the decomposition of the carbonate occurs at the longer reaction time as found in coralline hydroxyapatite.

The FTIR spectrum of freshwater shell (Fig. 39) shows the carbonate ion characteristic peak at 700, 713 cm^{-1} (ν_4), 861 cm^{-1} (ν_2), 1083 cm^{-1} (ν_1), 1472 cm^{-1} (ν_3). The strong band at 1788 cm^{-1} corresponds to the C=O groups of the carbonate ion. After hydrothermal treatment, the formation of hydroxyapatite is evident according to the characteristic peaks of the PO_4 tetrahedra (474, 567, 603, 963, 1037 – 1041 and 1093 cm^{-1}), the hydroxyl (633, 3432 and 3571 cm^{-1}) and carbonate (869 –

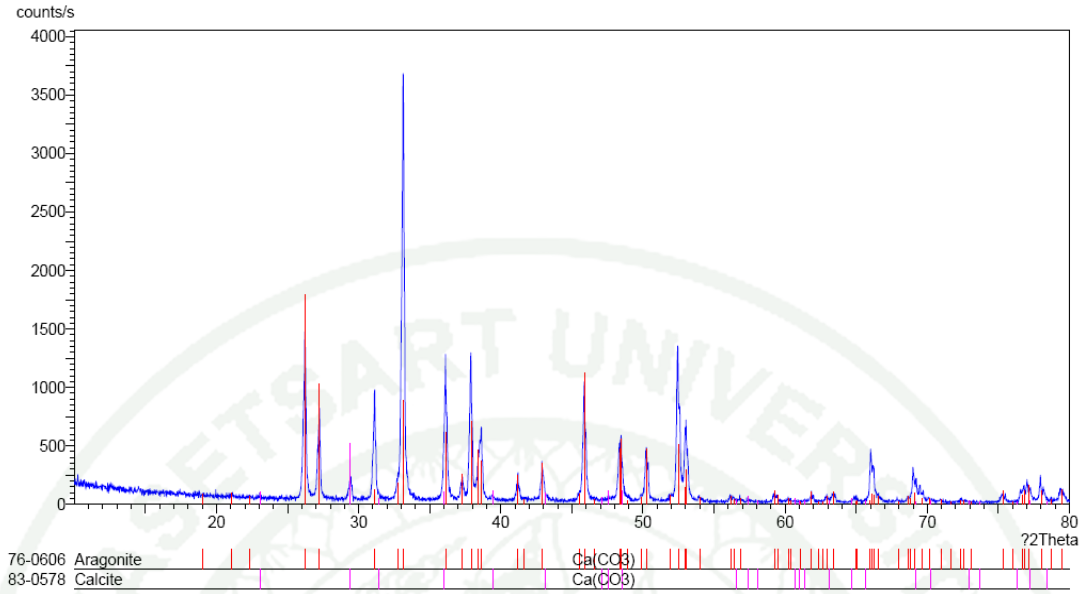

Figure 37 The XRD pattern of freshwater shell powder compared with aragonite structure (JCPDS file 76-0606**)** and calcite structure (JCPDS file 83-0578).

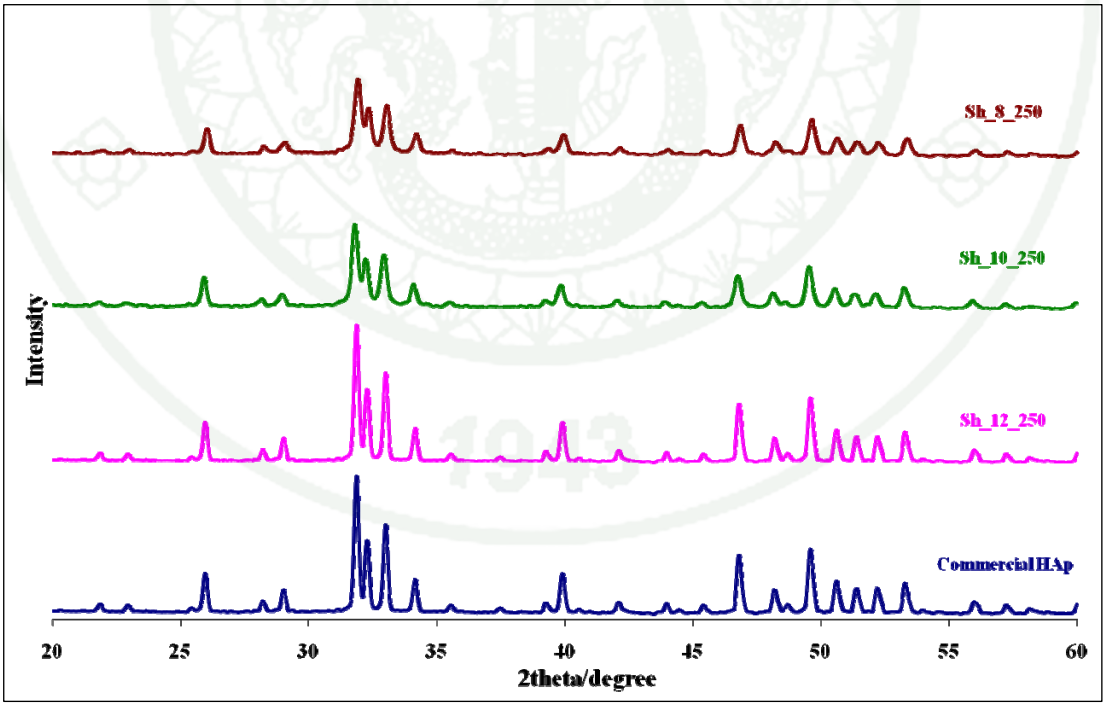

Figure 38 X-ray Diffraction patterns of the synthesized HAp from freshwater shell at 250ºC for various reaction times.

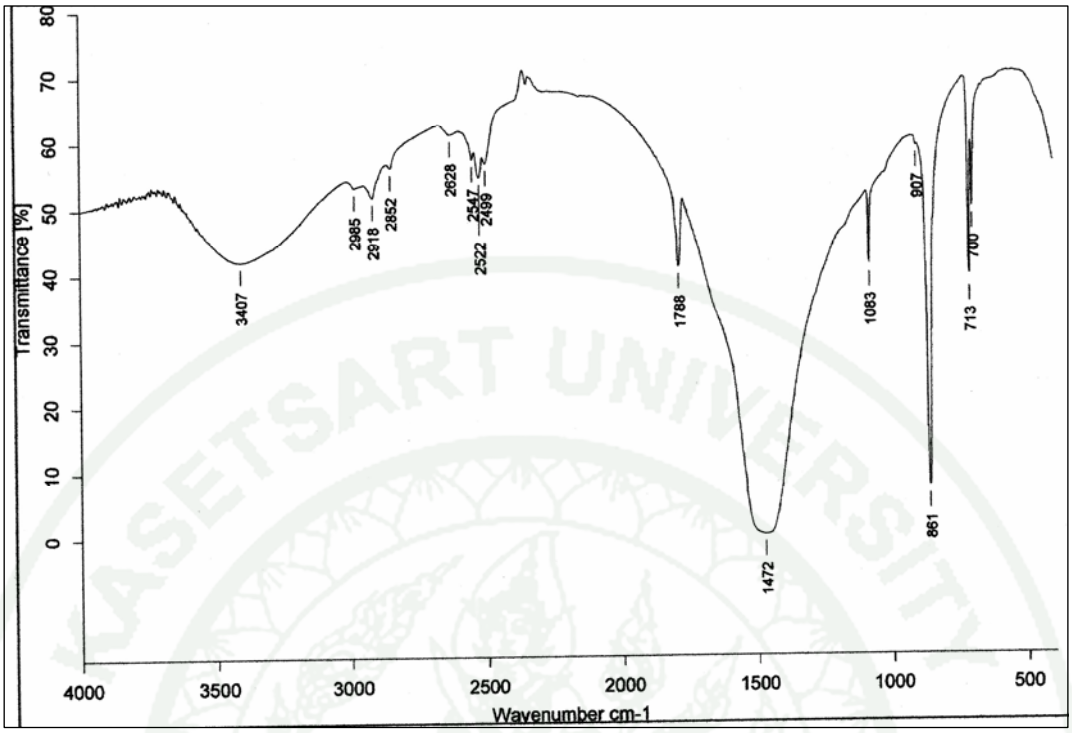

Figure 39 FTIR spectrum of freshwater shell.

878, 1421, 1459 cm^{-1}) (Fig 40). The CO_3^{2-} bands at 1421 and 1459 cm^{-1} indicate the presence of type B carbonated hydroxyapatite.

The inner surface and cross section morphologies of freshwater shell are shown in Figure 41 a –b. The SEM observations revealed a well-stacked lamellar microstructure. Nacreous sheets are arranged step-like. Individual plates are rhombic in outline. Figure 42 show that the nano-sized hydroxyapatite powders were obtained after hydrothermal.

2.3 Synthesis of hydroxyapatite from crocodile eggshells

The XRD pattern of crocodile eggshells shows mainly calcite structure of $CaCO_3$ (Fig 43). In the case of hydrothermal treatment at 250 ºC for 8 and 10 h of crocodile eggshells, the hydroxyapatite and the $CaCO_3$ (calcite) were detected in the obtained samples (Fig 44). The results indicated that the $CaCO_3$ in eggshells remained. After 12 h treatment time the calcite phase was not detected but the trace

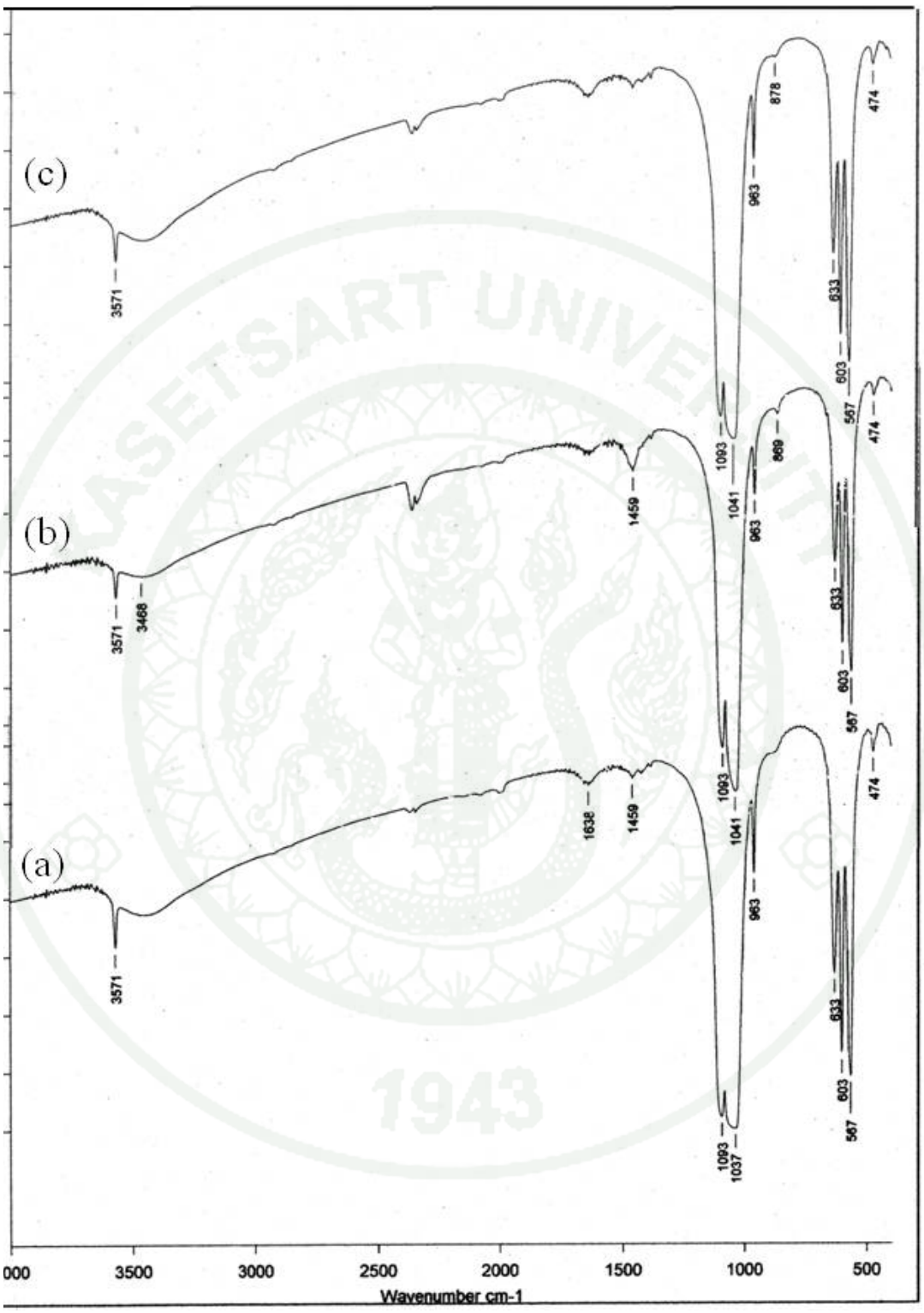

Figure 40 FTIR spectra of (a).Sh_12_250, (b) Sh_10_250 and (c) Sh_8_250.

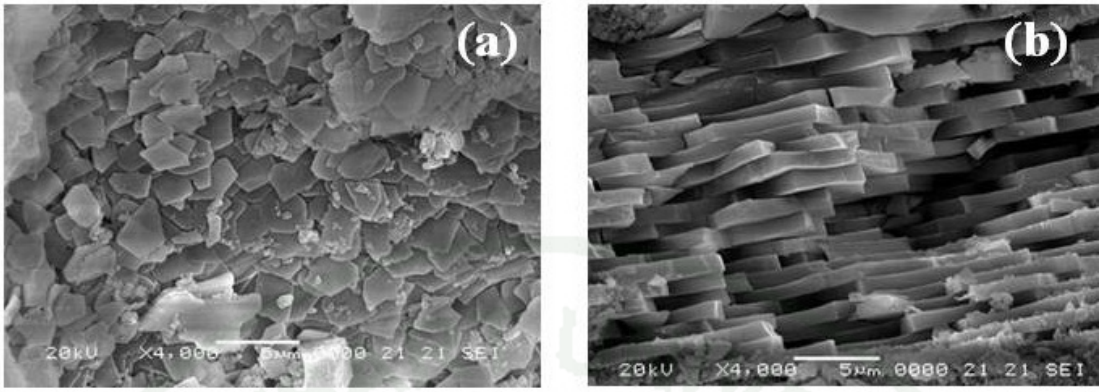

Figure 41 SEM images of freshwater shell (a) outer surfaces and (b) cross section.

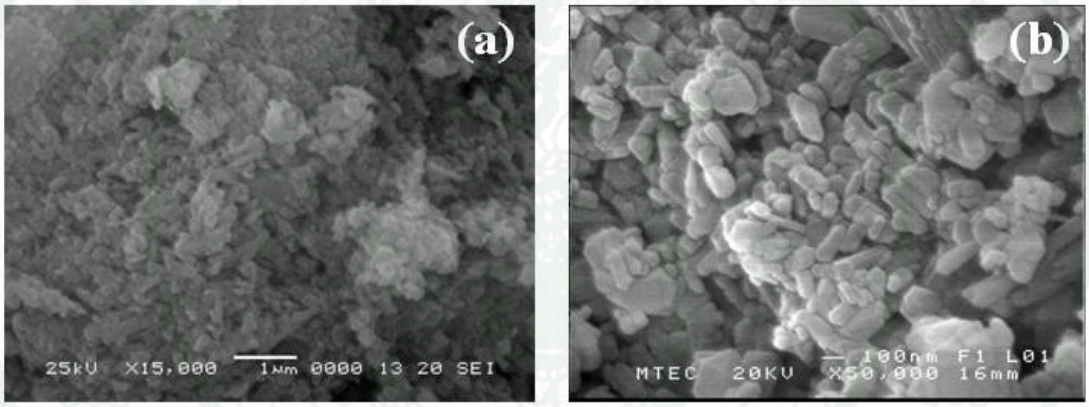

Figure 42 SEM micrographs of synthesized products (a) Sh_10_250 and (b) high magnification images of Sh_10_250.

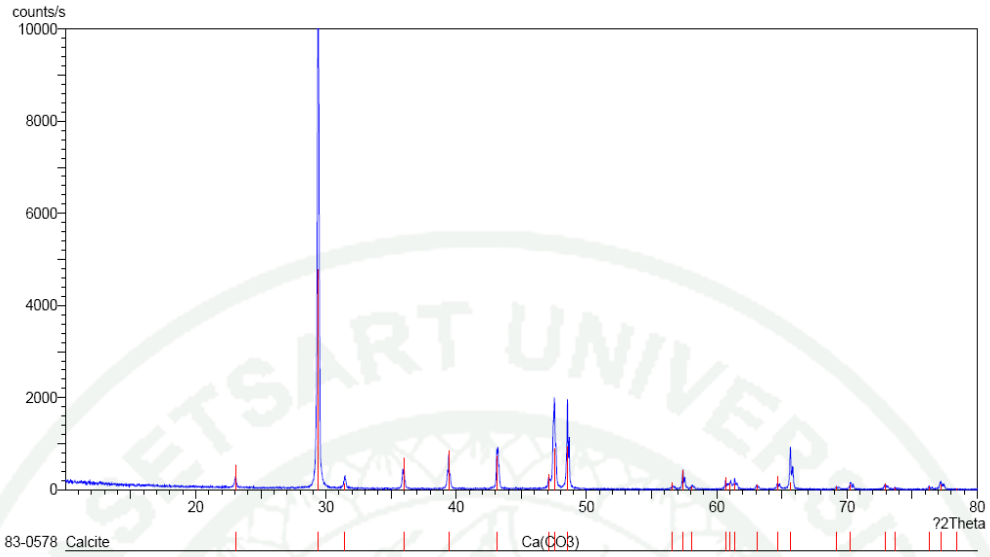

Figure 43 The XRD pattern of crocodile eggshell powder compared with calcite structure (JCPDS file 83-0578).

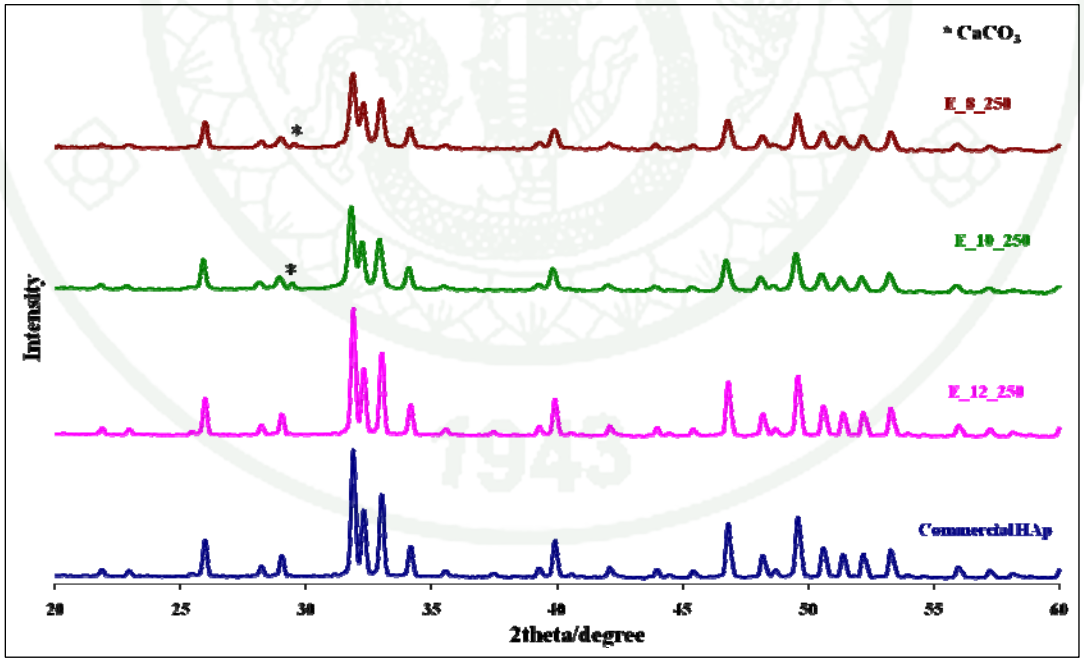

Figure 44 X-ray Diffraction patterns of the synthesized HAp from crocodile eggshell at 250ºC for various reaction times.

of CaO phase was observed. This indicated that the decomposition of the carbonate occurs at the longer reaction time as observed in the syntheses of hydroxyapatite from coral and freshwater shell.

The typical FTIR spectrum of synthesized product is given in Figure 45 and the characteristic peaks for all synthesized HAp are listed in Table 10. The characteristic peaks of HAp are assigned to the PO_4 tetrahedral (1043, 1093 cm^{-1}, 603, 566 cm^{-1}, 963 cm^{-1} and 473 cm^{-1}) and the OH group (3571, 633 cm^{-1}). Another interesting feature of the FTIR spectra of Figure 45 is the evolution of CO_3 bands have been observed at 878 cm^{-1} and 1632, 1547, 1458 and 1421 cm^{-1}. The hydrothermal conditions should favor the orientation of carbonates to the HAp lattice as the sharpening of the CO_3 bands centered at 878 cm^{-1} and at 1632, 1547, 1458 and 1421 cm^{-1} (Rocha *et al.*, 2005).

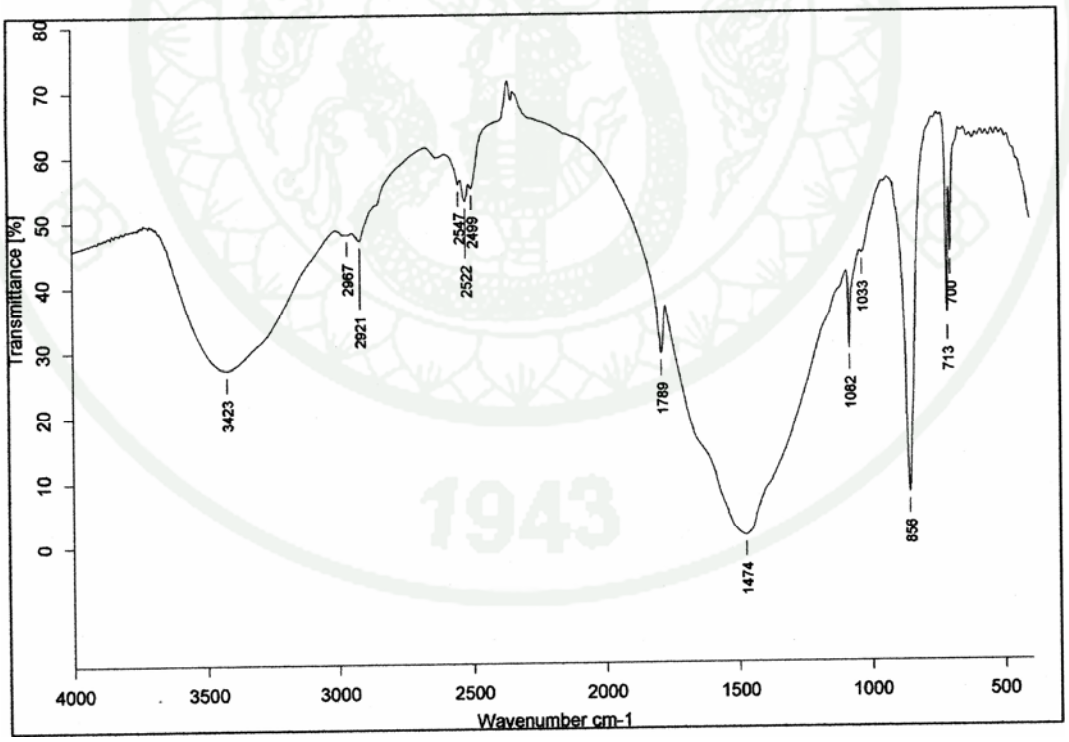

Figure 45 FTIR spectrum of crocodile eggshell.

The morphology of raw crocodile eggshells and the prepared HAp are shown in Figure 46 (Boonyang *et al.*, 2010). The SEM image of external surface of crocodile eggshell illustrates the plate-like crystals which were irregularly stacked on each other (Fig 47a). The internal surface consisted of the broken whiskers which were irregularly oriented (Fig 47b). The morphology of prepared HAp (Fig. 48a, b) show the cluster of agglomerated plate-like crystals.

2.4 Effect of particle sizes of sample powder on the reaction time.

The XRD patterns of the synthesized hydroxyapatite from coral are shown in Figure 49. All peaks in all figures are indexed to hexagonal lattice of hydroxyapatite crystal. The patterns show clearly that the coral with exact size S and M were successfully converted into hydroxyapatite by hydrothermal treatment for only 6 h at 150 ºC. In the case of CL_8_150 and CL_12_150 traces of aragonite phase were found indicating that $CaCO_3$ in coral remained. When the reaction time increased to 16 h, the XRD pattern shows only HAp phase. This result indicates that the large size coral powders required more reaction time than the small ones.

The XRD patterns of the synthesized HAp from freshwater shell are shown in Figure 50. The patterns show that the shell powder with exact size S and M were successfully converted into HAp by hydrothermal treatment for only 6 h at 150 ºC. In the case of ShL_8_150 and ShL_12_150 traces of aragonite phase were found indicating the presence of aragonite $CaCO_3$. When the reaction time increases to 16 h, the XRD pattern shows only HAp phase. This result indicated that the reaction time for larger size powders is higher than that for the smaller ones.

The XRD patterns of the synthesized HAp from crocodile eggshell are given in Fig 51. The patterns show that the shell powder with exact size S and M were successfully converted into HAp by hydrothermal treatment for only 6 h at 150 ºC. The diffraction data were in good agreement with JCPDF file 9-432 for HAp. For hydrothermal reaction at 150 ºC for 6 and 8 h using eggshell powder with L size, two crystalline phases corresponding to the HAp structure and to the calcite structure

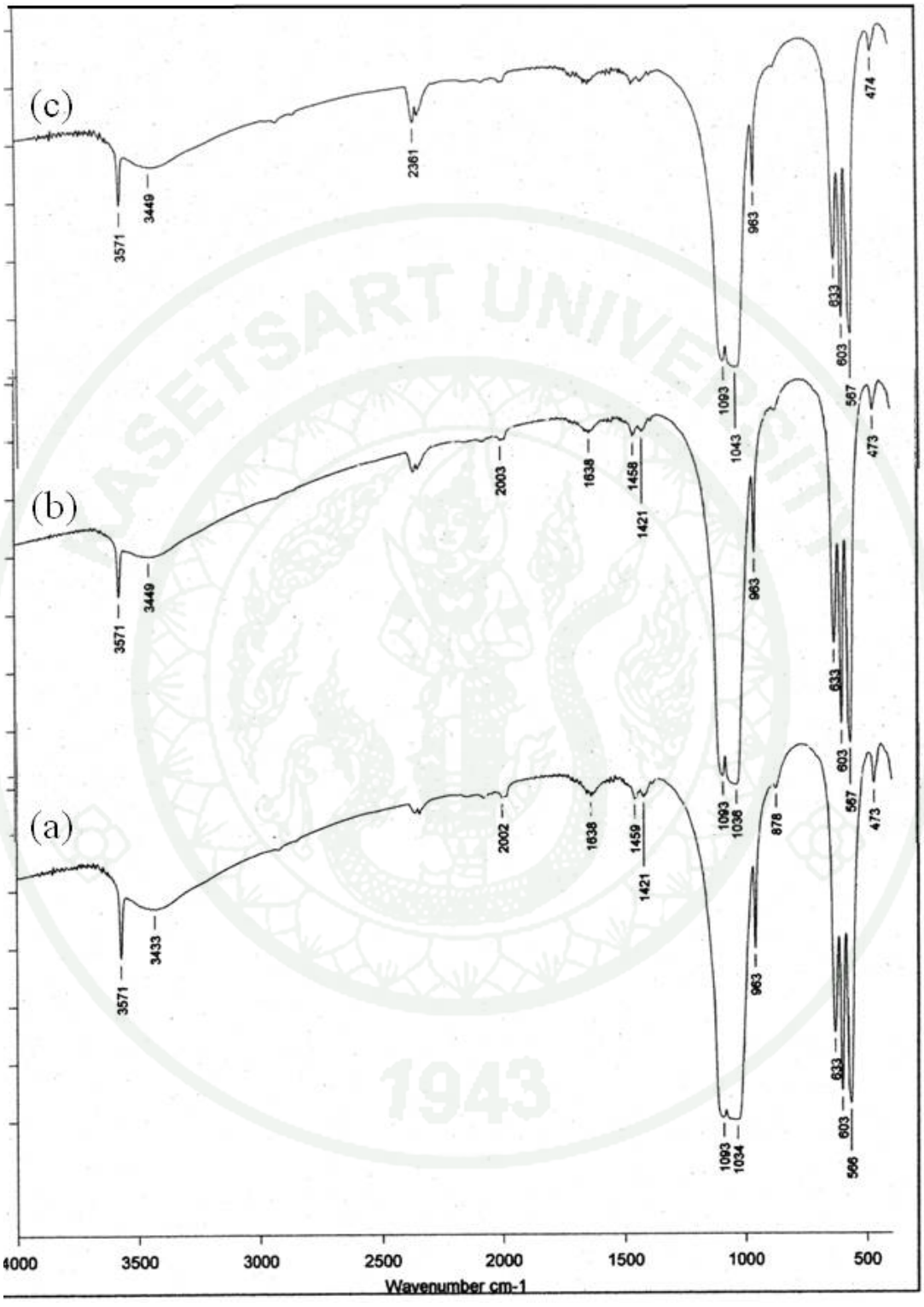

Figure 46 FTIR spectrum of (a).E_12_250, (b) E_10_250 and (c) E_8_250.

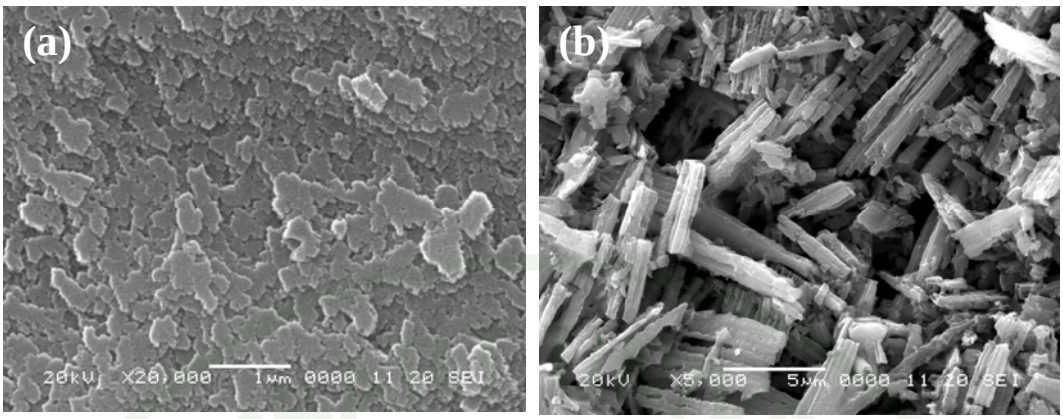

External surface Internal surface

Figure 47 SEM micrograps of (a) external and (b) internal surface of crocodile eggshell.

Source; Boonyang *et al.*, (2010)

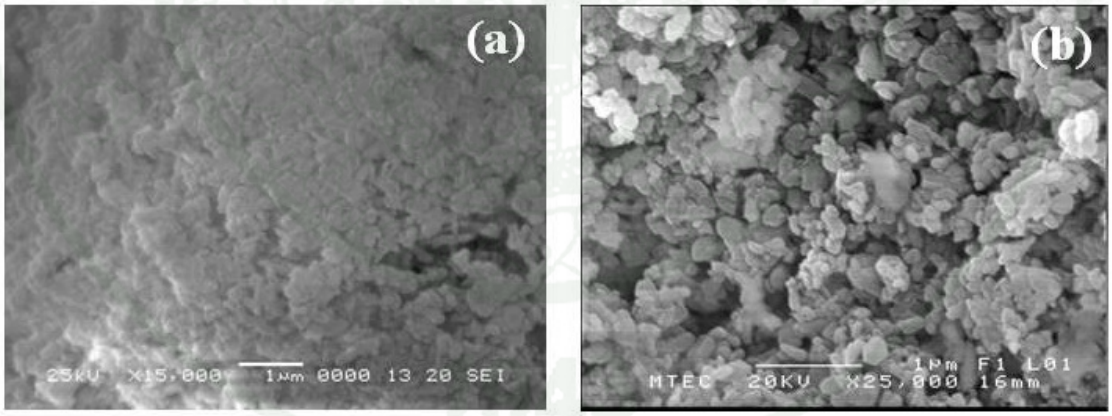

Figure 48 SEM micrographs of synthesized products (a) E_10_250 and (b) high magnification images of E_10_250.

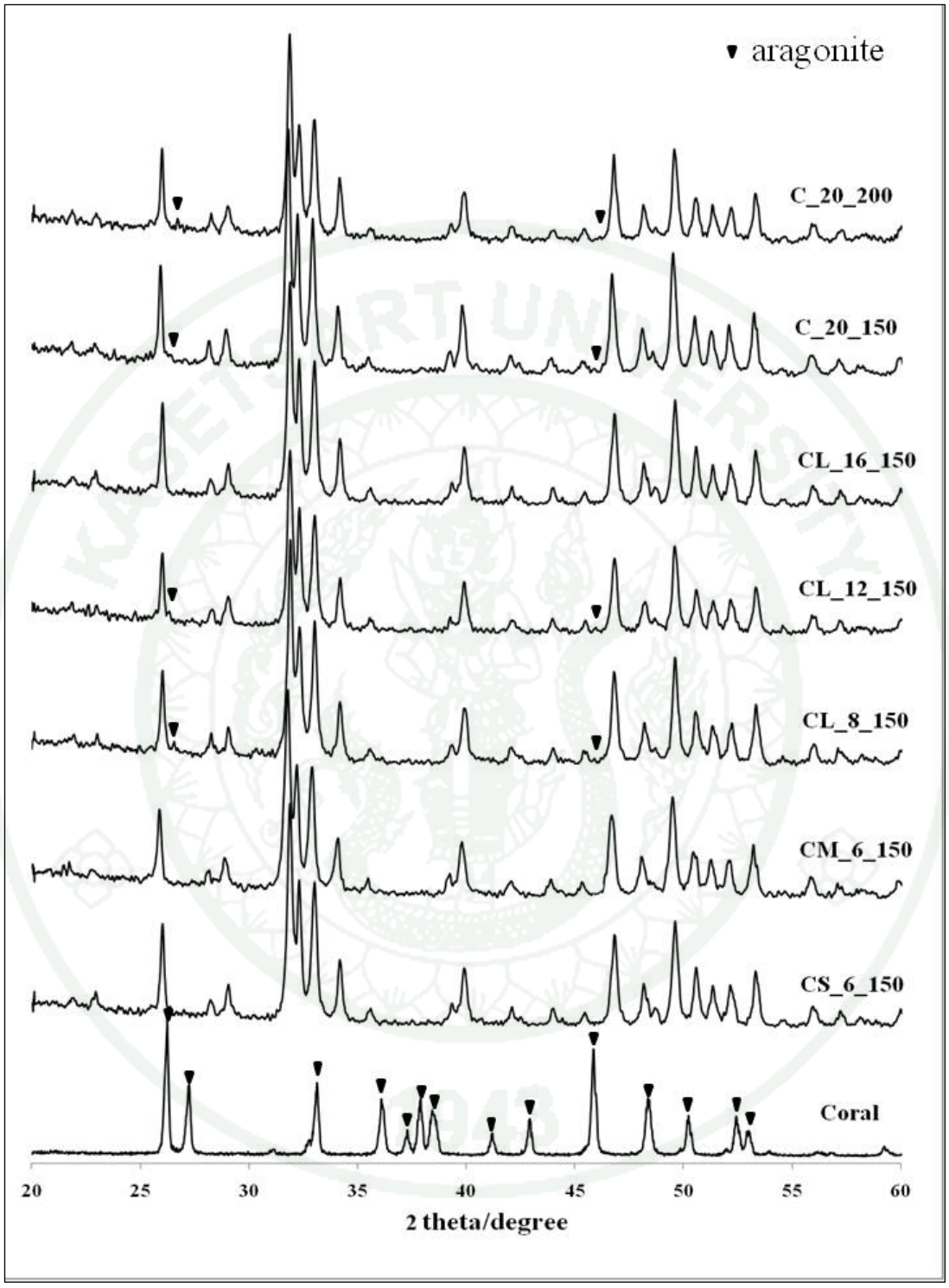

Figure 49 XRD patterns of the synthesized HAp from stag horn coral with different size at different time.

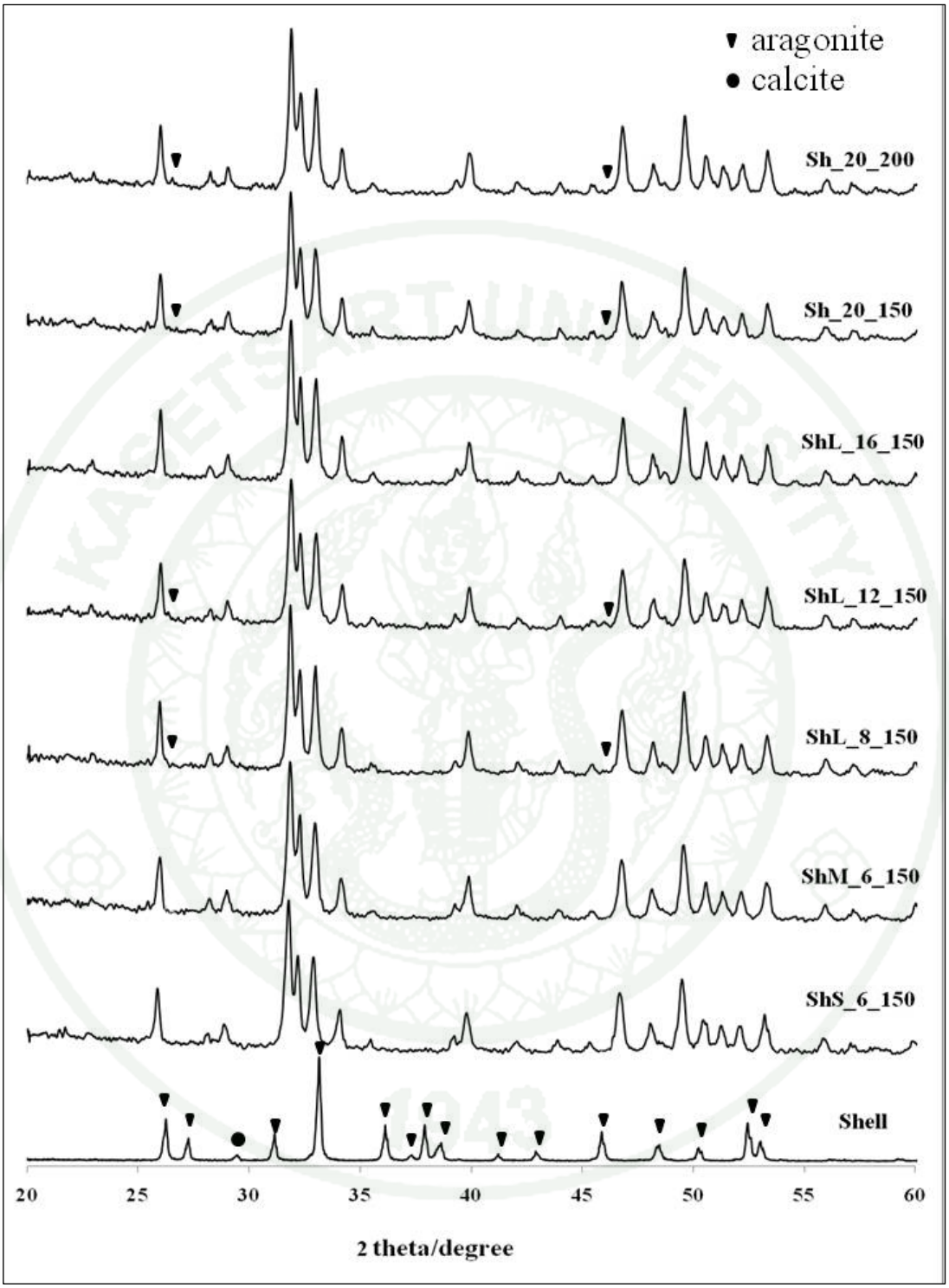

Figure 50 XRD patterns of the synthesized HAp from freshwater shells with different size at different time.

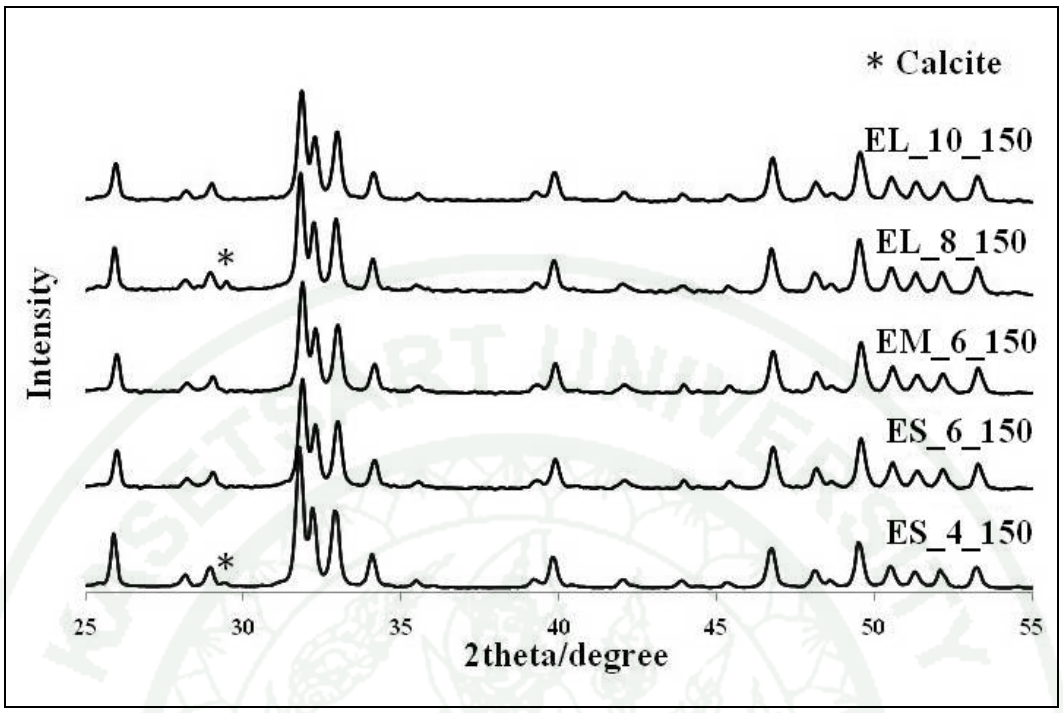

Figure 51 XRD patterns of the synthesized HAp from crocodile eggshells with different size at different time.

(JCPDF 5-0586) were detected, indicating that $CaCO_3$ in eggshells remained. After 10 h treatment of L size, calcite phase was not detected. This result indicated that the reaction time for finer size eggshell powders were less than that for the larger ones.

The surface morphology of synthesized HAp was characterized by SEM as shown in Figure 52 (a, c and d). The transmission electron micrographs demonstrate the formation of rod-like crystals (Fig 52 (b, d and f)). The high resolution of SEM and TEM images of ES_6_150 (Fig 53) show that the rod-like crystals have average size of 50-200 nm.

The size of the crystallite in the synthesized HAp is calculated using the Scherrer's equation. The single peak near 26° in the XRD pattern is chosen for the determination of the FWHM distance (Table 11). The calculated sizes of crystallite in the sample are listed in Table 11. The results show that the sizes of crystallite are between 29.65-37.55 nm.

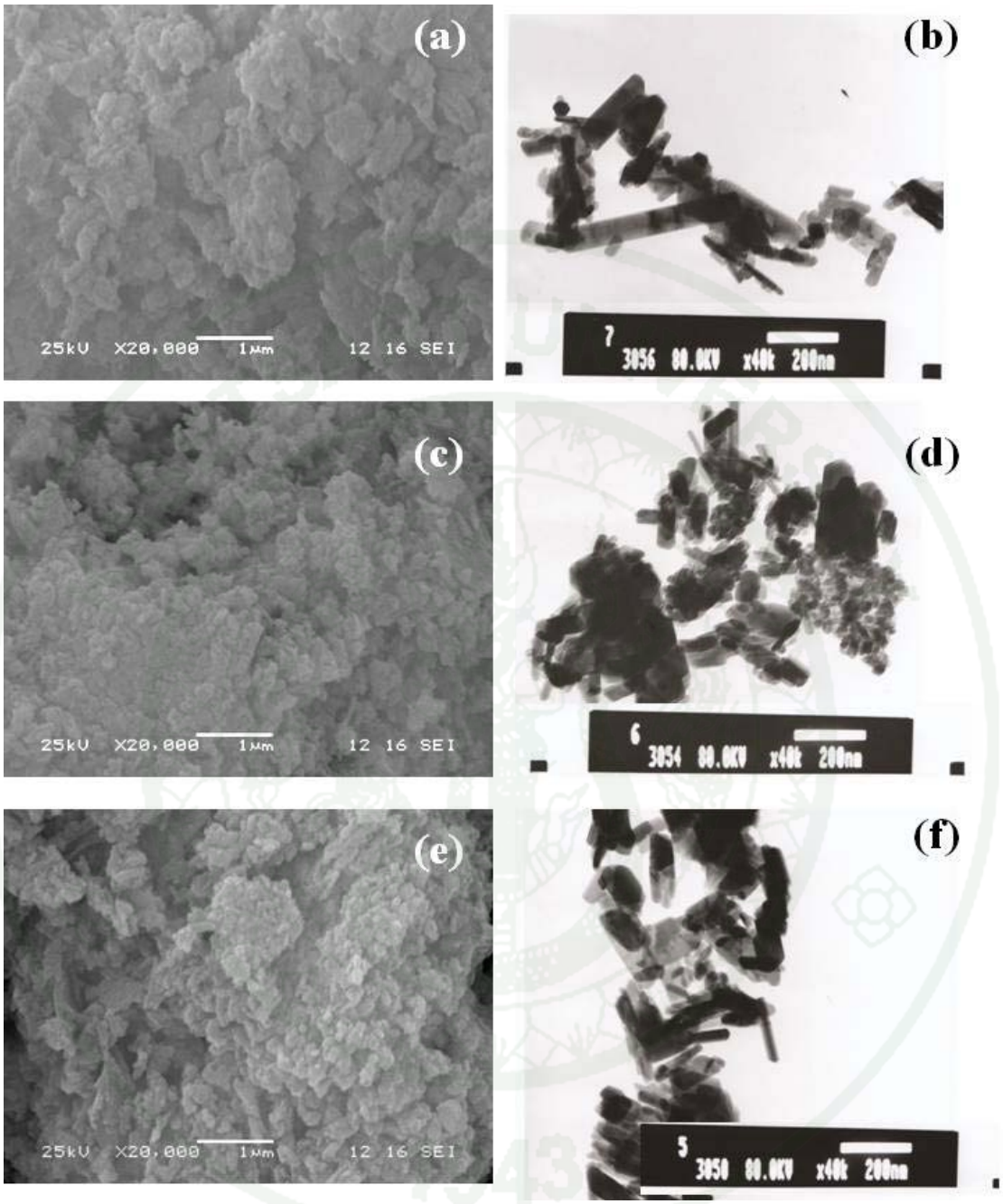

Figure 52 SEM and TEM micrographs of the HAp synthesized from crocodile eggshells with different size and different time (a, b) EL_10_150 (c, b) EM_6_150 and (e,f) ES_6_150.

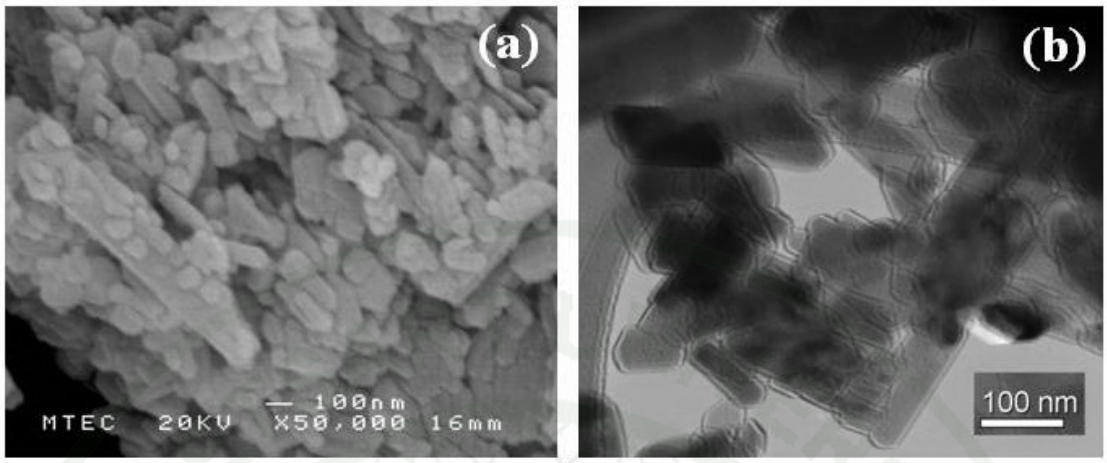

Figure 53 (a) SEM and (b) TEM images of the HAp synthesized from crocodile eggshells with ES_6_150.

Table 11 The crystallite size of synthesized HAp.

Samples	FWHM	Crystallite size (nm)
C_8_250	0.0050	29.65
C_10_250	0.0043	34.93
C_12_250	0.0041	36.27
Sh_8_250	0.0044	33.76
Sh_10_250	0.0041	36.26
Sh_12_250	0.0040	37.55
E_8_250	0.0043	34.93
E_10_250	0.0041	36.65
E_12_250	0.0040	37.06

3 Study of *in vitro* bioactivity

A measure of bioactivity of hydroxyapatite samples was obtained by determining the time required to form a crystalline apatite layer on the surface of

synthesized hydroxyapatite immersed in SBF at body temperature (37 ºC). Figure 54 shows SEM images of calcined HAp (HTib_750W) after soaking in SBF for 0, 1, 2, 3, 4, 5 and 6 days. Figure 55 shows SEM images of synthesized HAp (ES_6_150) after soaking in SBF for 0, 1, 2, 3 and 4 days. Before soaking in SBF solution, both of HTib_750W and ES_6_150 show smooth and homogeneous surface (Fig 54a and 55a). The surface of synthesized (ES_6_150) sample became net-like structure in 3 days while the calcined (HTib_750W) sample took 5 days. The *in vitro* bioactivity tests with SBF showed that the synthesized hydroxyapatite have excellent biomineralization ability. The new generated hydroxyapatite rapidly formed onto the surface of the synthesized HAp after immersion in SBF for one day and their surface was completely covered with flake-like hydroxyapatite after soaking for 3 days (Fig 55e). The SEM image of cross-section fracture of the ES_6_150 disc soaking in SBF for 3 days illustrates the flake-like crystals of the new growth hydroxyapatite (Fig 56a). The flake-like crystals were confirmed as hydroxyapatite by using EDS pattern (Fig 56b) and XRD (Fig 57). The result suggests that the synthesized hydroxyapatite from crocodile eggshell is more bioactive than calcined bone hydroxyapatite. It means that the hydroxyapatite which are synthesized from Ca-based natural materials are more bioactive than that from crocodile bone.

These results support fairly well with the assumptions about the suitability of the produced hydroxyapatite -scaffolds for use in biomedicine with regard to the microstructure, the evolution of the phases and the substitutions in the hydroxyapatite lattice.

4. The *In vitro* study of antibiotic drug delivery

The physicochemical properties of HAp samples used in this part are shown in Table 12.

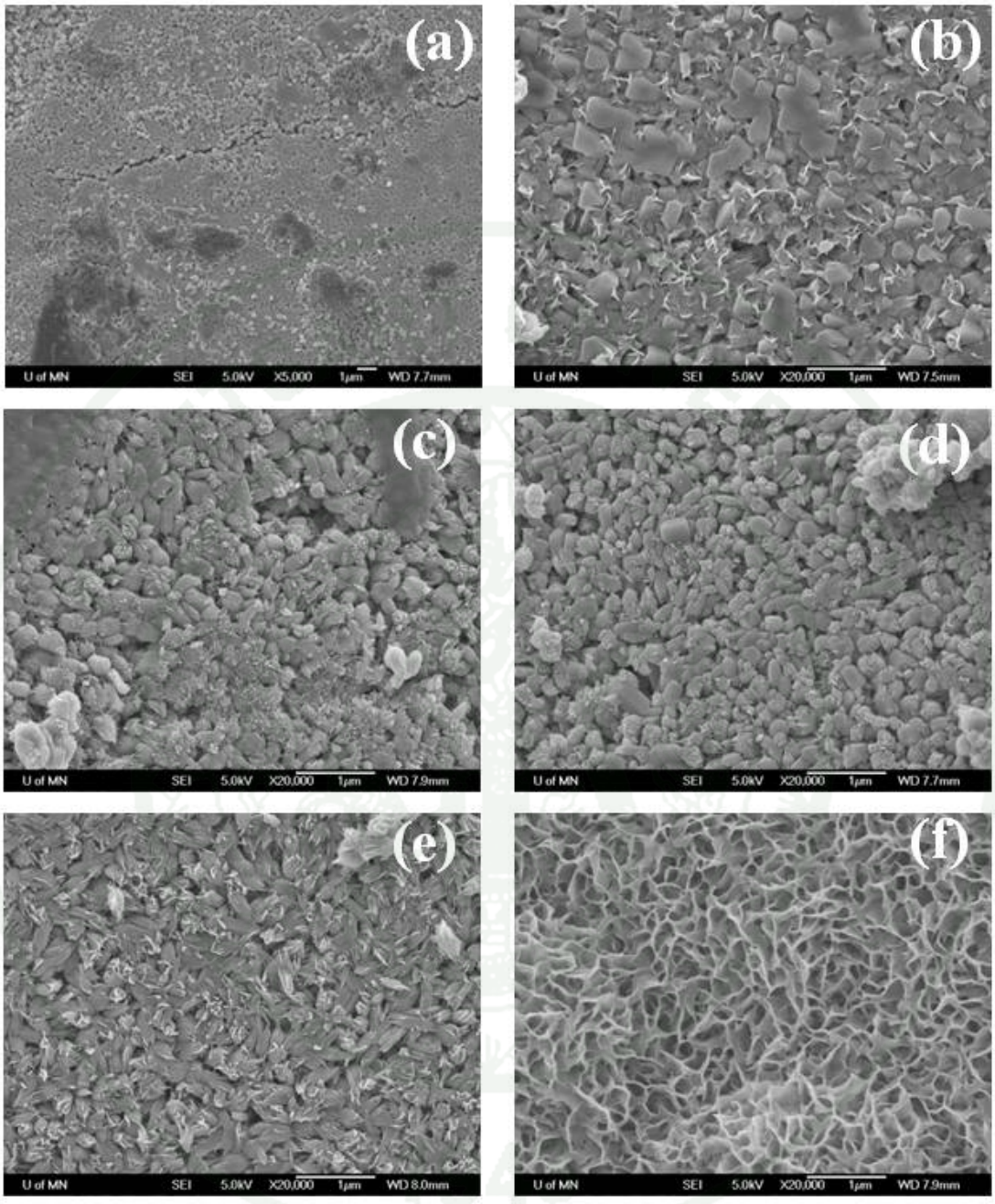

Figure 54 The surface morphologies of the HTib_750W soaking in SBF at 37ºC for (a) 0 day (b) 1 day (c) 2 days (d) 3 days (e) 4 days and (f) 5 days.

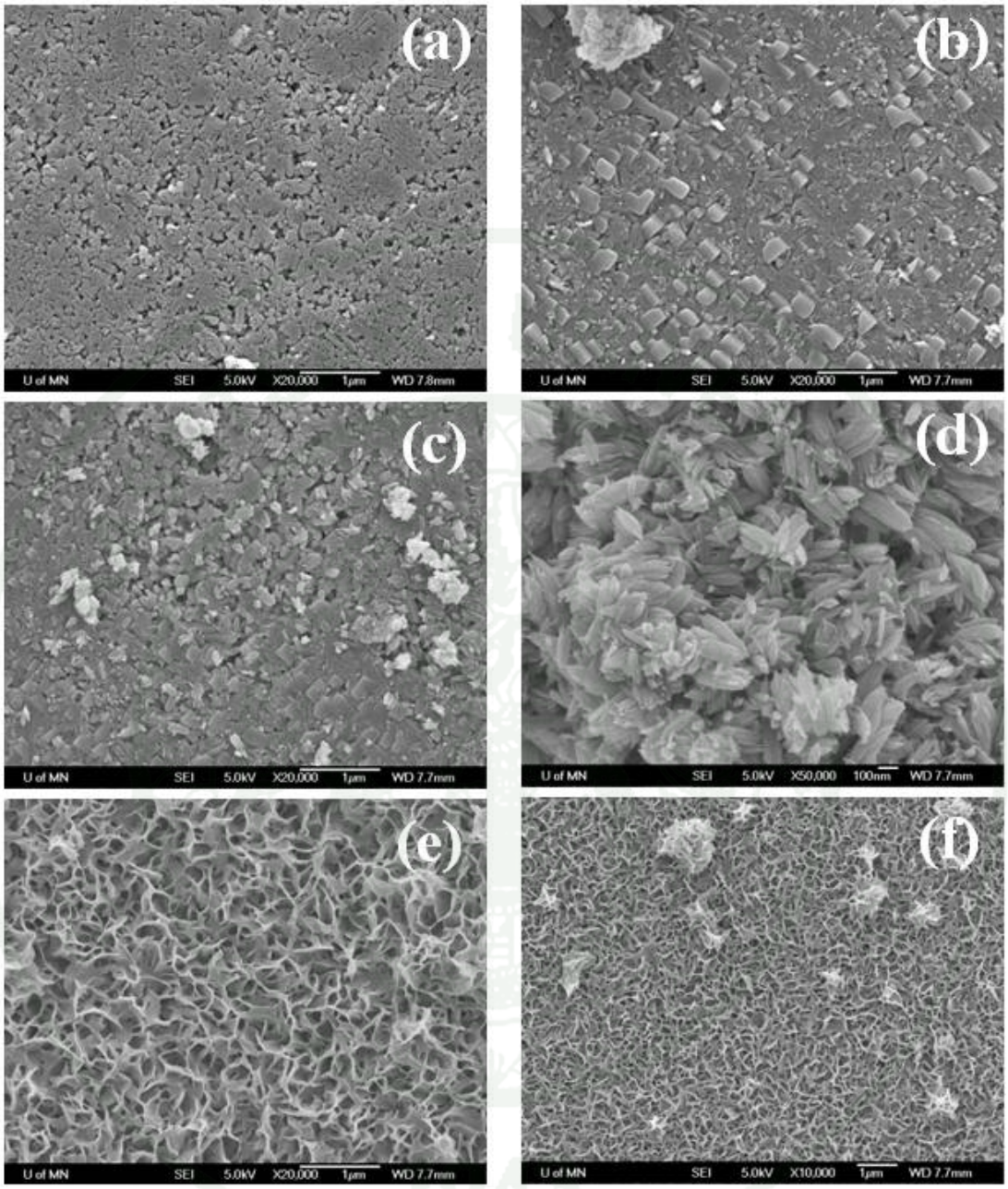

Figure 55 The surface morphologies of the ES_6_150 disc soaking in SBF at 37ºC (a) 0 day (b) 1 day (c) 2 days (d) 2 days (higher magnification) (e) 3 days and (f) 4 days.

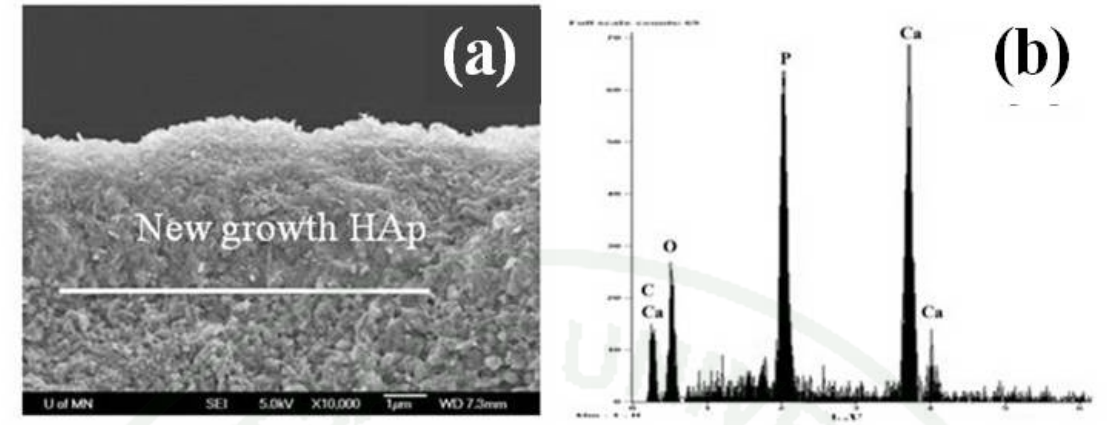

Figure 56 (a) SEM image of cross-section fracture through the ES_6_150 disc soaking in SBF for 3 day and (b) EDS analysis of the flake-like crystal on the surface of specimens.

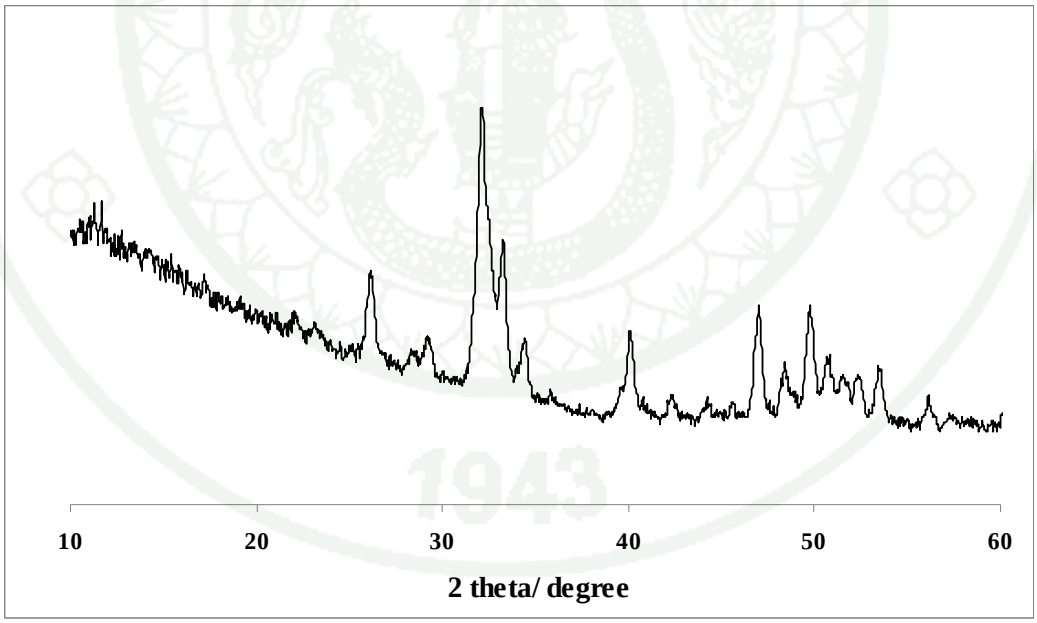

Figure 57 XRD pattern of surface of the ES_6_150 disc soaking in SBF for 3 days.

Table 12 Physicochemical properties of samples.

Samples	Surface Area (m^2/g)	Average Pore Size (nm)	Pore Volume (cm^3/g)	Concentration of drug in sample (%)	
				TC	VM
HTib_750W	1.84	39.77	0.183	44.58	33.57
HTW_750W	5.83	81.74	0.119	47.59	34.94
ES_6_150	20.86	54.22	0.283	45.55	36.05
EM_6_150	24.22	48.68	0.295	44.09	34.85
EL_6_150	22.5	30.18	0.169	38.14	33.41

4.1 Calibration curves

The absorbance (Abs) of six standard solutions are listed in Table 13 and plotted versus the concentration as shown in Figure 58-61

4.2 Drug loading

It was found that the amount of drug in the filtrate obtained after washing the HAp residue during the drug loading process could not be detected. Thus assuming that all drug left after loading was in the centrifugate.

The amount of tetracycline and vancomycin loading in the hydroxyapatite samples are summarized in Table 14. The percentages of loading drug in hydroxyapatite samples are calculated as follow.

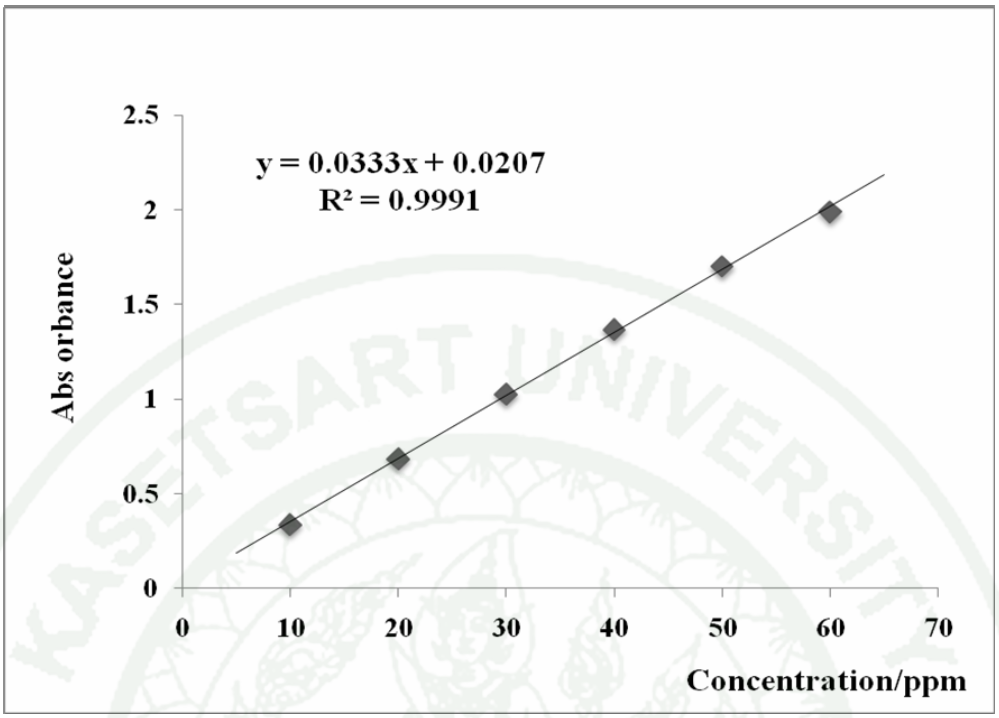

Figure 58 The calibration curve for the determination of tetracyclin in water.

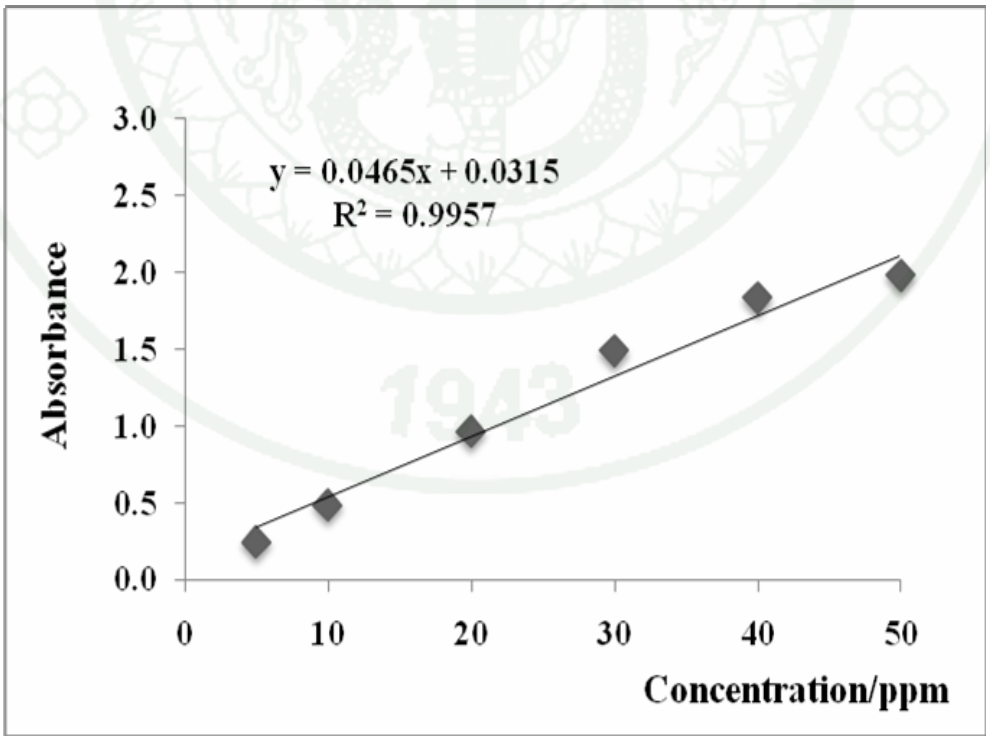

Figure 59 The calibration curve for the determination of tetracycline in SBF.

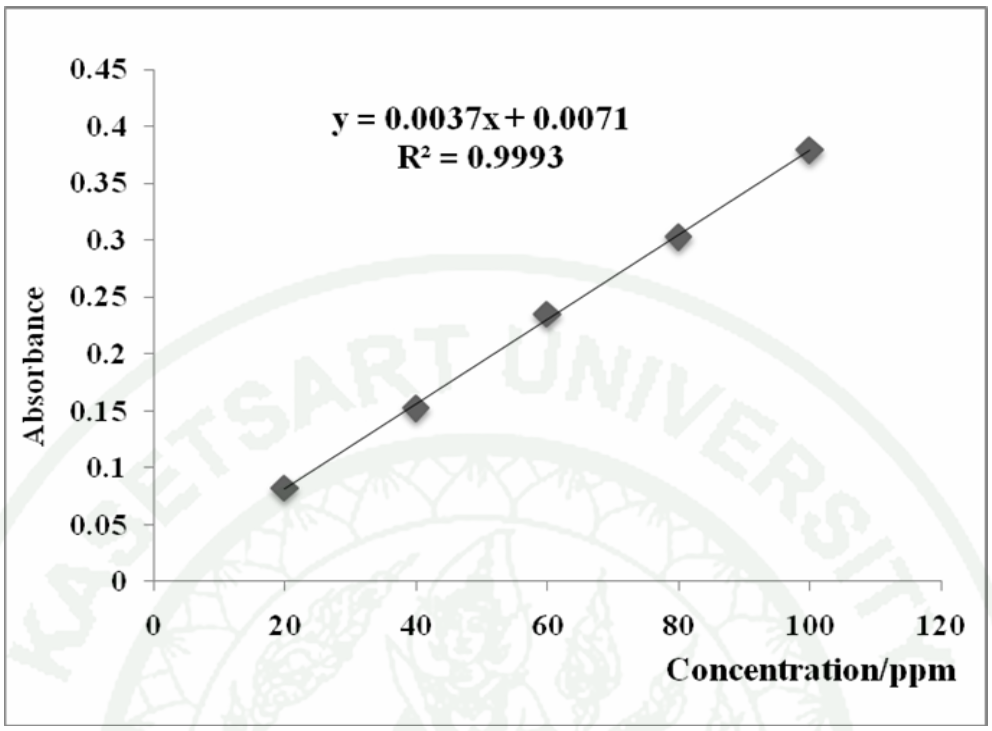

Figure 60 The calibration curve for the determination of vancomycin in water.

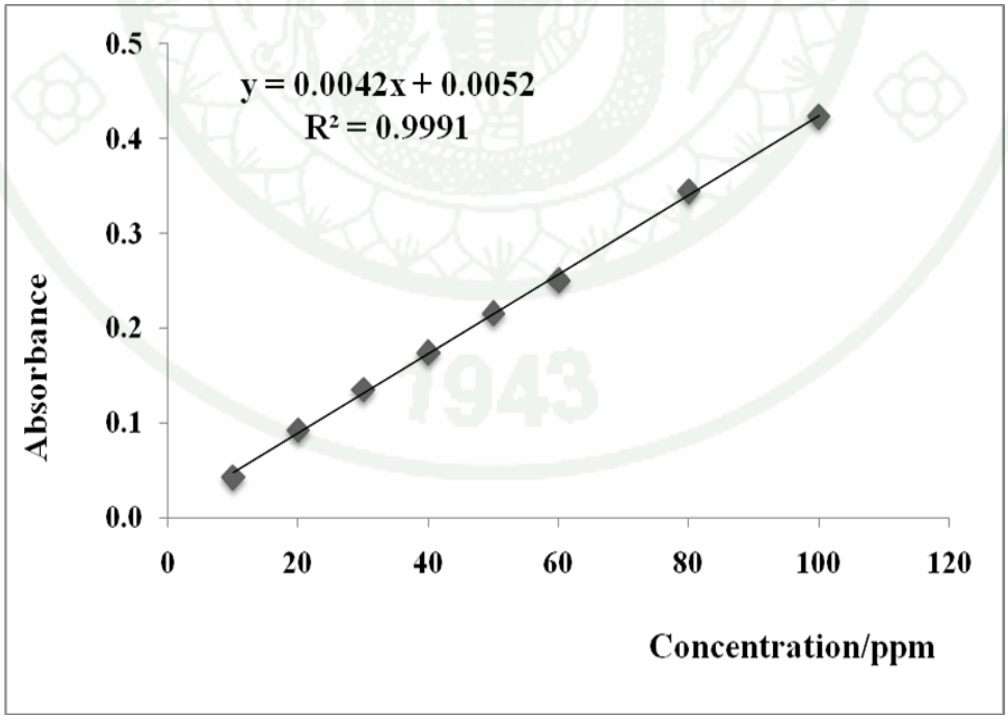

Figure 61 The calibration curve for the determination of vancomycin in SBF.

Weight of HTib_750W sample used in drug loading is 2.0001 g. At wavelength 364 nm the absorbance of tetracycline before loading and after loading are 1.3012 and 0.9078 respectively, which corresponding to 1922.67 ppm and 1065.59 ppm respectively.

The loading drug = 1922.67 - 1065.59 = 857.08 ppm.

$$\% \text{ drug loading } = \frac{857.08}{1922.67} x100 = 44.58$$

The concentration of loading drug = 857.08 mg/l

= 857.08 μg/ml

The amount of loading drug in 5 ml of starting drug solution

= 857.08 *x* 5 μg/ml

= 4285.4 μg

The amount of loading drug in 2.001 g of HAp = 4285.4 μg

Thus, the amount of loading drug per gram HAp $= \frac{4285.4}{2.0001} = 2141.6$ μg/g

4.3 Drug releasing

The absorbance of releasing TC and VM in SBF solution at every two hours were listed in Appendix Table B1 and B2, respectively. The corresponding concentrations of releasing TC and VM are shown in Appendix Table B3 and B4.

The percentages of loading drug in HAp samples are calculated as follow. The loaded HTib_750W sample is chosen as an example of calculation.

Weight of loaded HTib_750W sample used in the drug releasing process is 0.4002 g. At wavelength 366 nm the absorbance of tetracycline releasing from the

HTib_750W sample in SBF solution as the function of time for three trials and their corresponding concentrations are shown in Appendix Table B1 and B3.

The concentrations of releasing tetracycline before dilution are listed in Appendix Table B6. The average accumulative amounts of releasing TC in 5 ml SBF solution are shown in Appendix Table B8. The total amount of releasing tetracycline within 24 hours is summarized in Table 15.

The total amount of releasing drug = 721.5806 μg

Weight of loaded HAp = 0.4002 g

$$\text{The releasing drug per gram HAp} = \frac{721.5806}{0.4002}\ \mu g/g$$

And the loading drug per gram HAp =2141.6 μg/g

$$\text{Therefore} \quad \%\ \text{drug releasing} = \left(\frac{721.5806}{0.4002}\right)\left(\frac{100}{2141.6}\right) = 84.16$$

The average and cumulative amounts of releasing VM in 5 ml SBF solution are listed in Appendix Table B9 and B10, respectively.

The percentage of loading and releasing of tetracycline and vancomycin in the samples are summarized

Table 13 The absorbance data for the calibration curve.

ıncentration	Absorbance											
(ppm)	TC in water			TC in SBF			VM in water			VM in SBF		
	I	II	average	I	II	average	I	II	average	I	II	average
5	-	-	-	0.2477	0.2489	0.2483	-	-	-	-	-	-
10	0.3331	0.3441	0.3386	0.4888	0.4900	0.4894	-	-	-	0.0392	0.0450	0.0421
20	0.6793	0.6957	0.6875	0.9656	0.9675	0.9695	0.0817	0.0830	0.0824	0.0915	0.0927	0.0921
30	1.0128	1.0444	1.0286	1.4948	1.4945	1.4947	-	-	-	0.1326	0.1371	0.1349
40	1.3826	1.3605	1.3715	1.8398	1.8392	1.8395	0.1503	0.1547	0.1525	0.1730	0.1749	0.1739
50	1.7106	1.7008	1.7057	1.9848	1.9833	1.9840	-	-	-	0.2149	0.2160	0.2154
60	1.9857	1.9996	1.9927	2.4560	2.4521	2.4540	0.2380	0.2327	0.2354	0.2555	0.2451	0.2503
80	-	-	-	-	-	-	0.3077	0.2987	0.3032	0.3514	0.3370	0.3442
100	-	-	-	-	-	-	0.3870	0.3720	0.3795	0.4104	0.4355	0.4230

Table 14 The calculation of drug loading in hydroxyapatite.

Sample	ight of Ap (g)	y (Abs)	Concentration of drug (ppm)	Dilution factor	Concentration in drug solution (ppm)	Loading drug (µg/ml)	% drug loading	ding drug per gram of HAp in 5 ml drug solution (µg/g)
Tetracycline before loading	-	1.3012	38.4535	50	1922.67	-	-	-
HTib_750W	2.0001	0.9078	26.6396	40	1065.59	857.04	44.58	2142.61
HTW_750W	2.0003	0.8596	25.1922	40	1007.69	914.85	47.59	2287.12
ES_6_150	2.0003	0.8923	26.1742	40	1046.97	875.57	45.55	2188.94
EM_6_150	1.9998	0.9156	26.8739	40	1074.96	847.80	44.09	2119.51
EL_6_150	2.0000	1.0109	29.7357	40	1189.43	733.24	38.14	1833.11
Vancomycin before loading	-	0.2501	65.66216	30	1969.86	-	-	-
HTib_750W	2.0010	0.2492	65.42568	20	1308.51	664.82	33.57	1652.55
HTW_750W	2.0012	0.2442	64.08108	20	1281.62	689.66	34.94	1719.58
ES_6_150	2.0015	0.2402	62.98649	20	1259.73	710.19	36.05	1774.01
EM_6_150	2.0002	0.2445	64.17297	20	1283.46	688.91	34.85	1715.84
EL_6_150	2.0003	0.2498	65.58378	20	1311.6757	659.79	33.41	1645.23

Table 15 Calculation of percentage of drug releasing.

Sample	Weight of Loaded HAp (g)	Total amount of releasing drug (μg)	Releasing drug per gram HAp (μg/g)	Loading drug per gram HAp (μg/g)	% drug releasing
Tetracycline					
HTib_750W	0.4002	721.5806	1803.20	2142.61	84.16
HTW_750W	0.4001	726.6631	1816.20	2287.12	79.41
ES_6_150	0.4005	582.0251	1453.25	2188.94	66.39
EM_6_150	0.4001	544.5161	1360.84	2119.51	64.21
EL_6_150	0.4001	244.3011	610.60	1833.11	33.31
Vancomycin					
HTib_750W	0.4013	620.0397	1545.08	1652.55	93.49
HTW_750W	0.4012	659.4841	1643.78	1719.58	95.58
ES_6_150	0.4000	506.5079	1266.27	1774.01	71.37
EM_6_150	0.4000	664.4048	1661.01	1715.84	96.81
EL_6_150	0.4004	544.7619	1360.54	1645.23	82.70

Table 16 The percentages of loading and releasing of tetracycline and vancomycin in the samples.

Samples	wt % loading		wt % releasing	
	TC	VM	TC	VM
HTib_750W	44.58	33.57	84.16	93.49
HTW_750W	47.59	34.94	79.41	95.58
ES_6_150	45.55	36.05	66.39	71.37
EM_6_150	44.09	34.85	64.21	96.81
EL_6_150	38.14	33.41	33.31	82.70

Figure 62 shows the cumulative release profile of TC in SBF. The TC release profiles of HTib_750W and HTW_750W showed a similar release behavior for the whole period. The initial step was fast release followed by a relatively slow release. The TC release rate of ES_6_150, EM_6_150 and EL_6_150 were significantly lower than that of HTib_750W and HTW_750W. The amounts of releasing TC in samples are between 84.16 wt % - 33.31 wt % of total TC loading (Table 15). Fig 63 shows the cumulative release profile of VM in SBF. The release profile of VM was similar to that of the TC releasing behavior. The amounts of releasing VM in samples are between 96.81- 71.37 wt % (Table 15). It was obvious that the total percentage of releasing of vancomycin was higher than that of tetracycline (Fig 64-65). The vancomycin structure is large and bulky which affect the amount of drug loading in materials.

In generally, the release behavior can be separated into two stages: an initial fast release followed by a slow release pattern. The fast release is mainly caused by the dissolution of the drug which is physically adsorbed in hydroxyapatite, and the slow release may be attributed to the chemically adsorbed drugs.

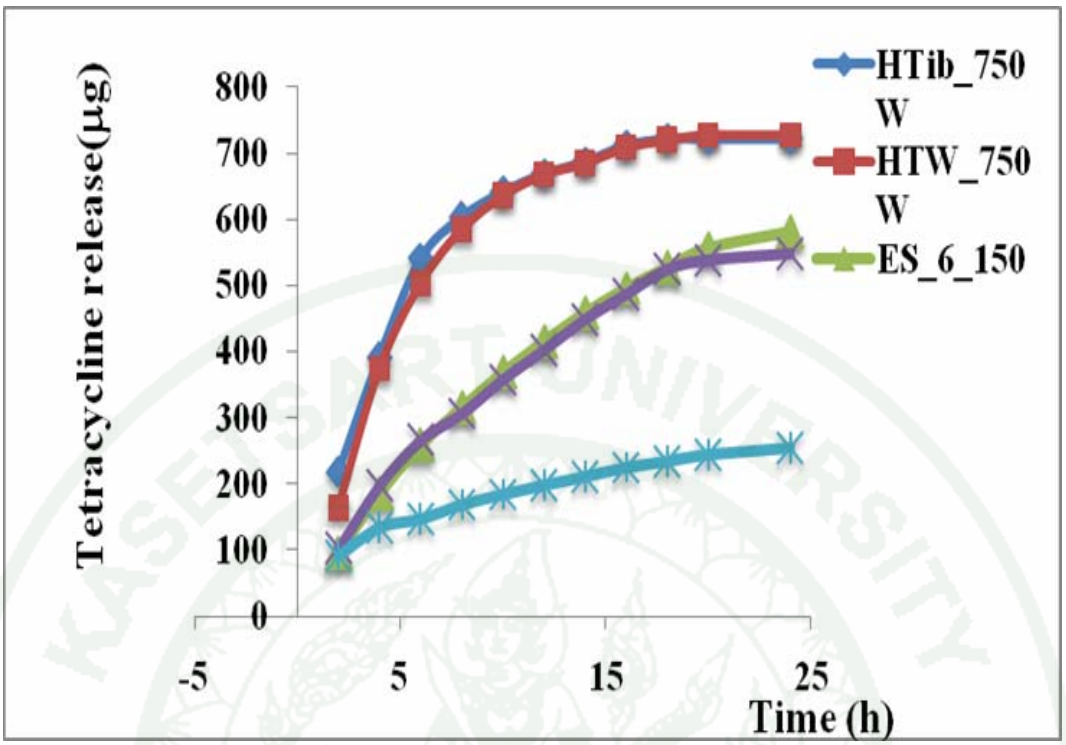

Figure 62 The cumulative release profiles of tetracycline as a function of time in SBF at 37 °C.

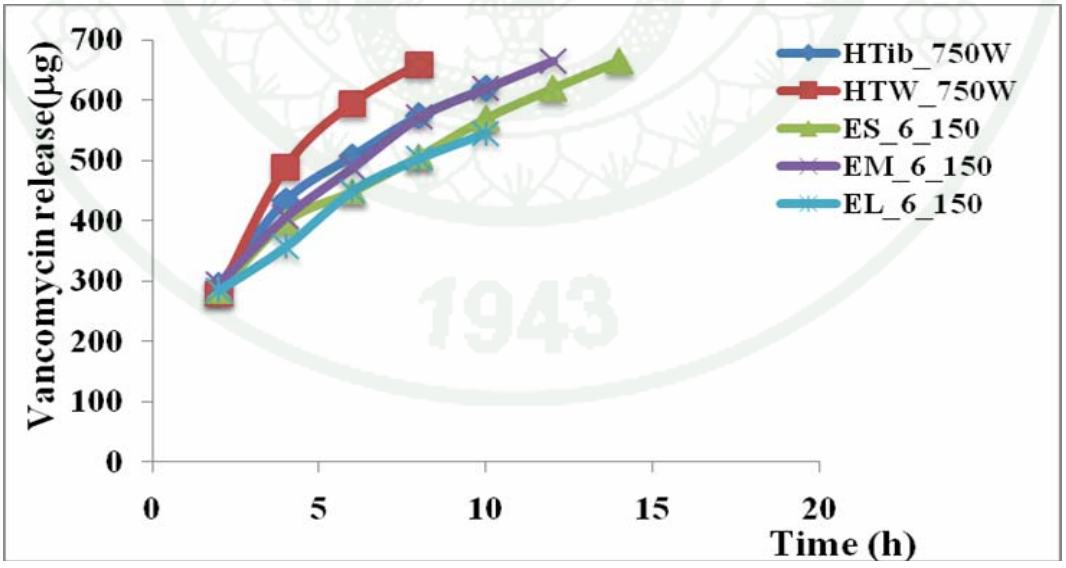

Figure 63 The cumulative release profiles of vancomycin as a function of time in SBF at 37 °C.

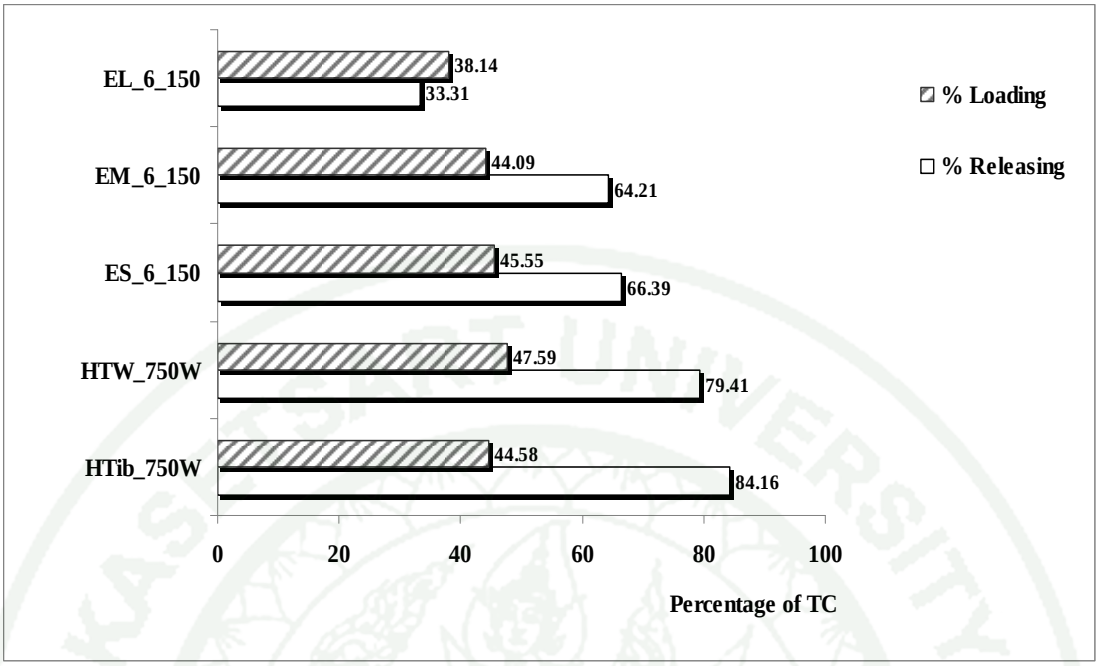

Figure 64 The percentage of loading and releasing of tetracycline in the samples.

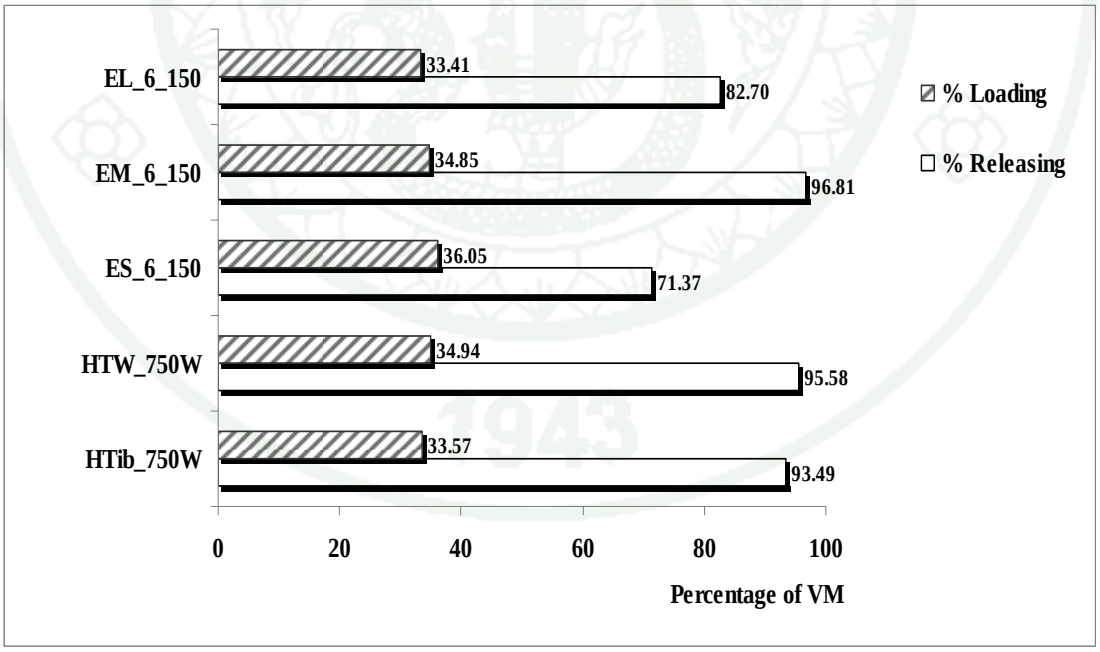

Figure 65 The percentage of loading and releasing of vancomycin in the samples.

CONCLUSION

Crocodile bone of *Crocodylus siamensis* was calcined at 750 °C giving bone hydroxyapatite (BHAp) with high purity. The microstructure analysis shows that the bone hydroxyapatite from tibia bone has a larger grain size than that from tail bone. The high purity hydroxyapatites (HAp) were successfully synthesized from *Acropora Formosa* coral, *Hyriopsis myersiana* freshwater shell and crocodile eggshell by hydrothermal process. It was found that the reaction time of hydrothermal reactions decreases as size of the powder samples. The sizes of crystallite in the hydrothermally synthesized hydroxyapatite are between 29.65 - 37.55 nm. The sizes of crystallite in bone hydroxyapatite increases as the heating temperature.

The *in vitro* bioactivity study in SBF at 37 °C reveals that the time required to form the flake-like crystals layer in SBF solution was only 3 days for HAp from calcium based natural materials, compared to 5 days for BHAp. Accordingly, the BHAp is less bioactive than the HAp.

Two antibacterial drugs which are tetracycline and vancomycin are used in the study of *in vitro* drug delivery behavior of the bone hydroxyapatite (HTib_750w and HTW_750W) and the synthesized hydroxyapatite (ES_6_150, EM_6_150 and EL_6_150). It is found that there is a correlation between the pore size and efficiency of drug loading of the studied hydroxyapatites. The amount of loading drug increases as the pore size. In addition the size and shape of drug molecule affect the amount of drug loading in sample. Vancomycin whose structure is large and bulky may not fit into the pores, thus less percentage of drug loading than tetracycline. The release profiles for both drugs show that the release behavior consists of two stages: the initial step was fast release followed by a relatively slow release.

LITERATURE

Andres-Verg, M., C. Fernndez-Gonzlez and M. Martnez-Gallego. 1998. Hydrothermal synthesis of calcium deficient hydroxyapatites with controlled size and homogeneous morphology. **J. Eur. Ceram. Soc.** 18: 1245-1250.

Aoki, H. 1991. **Science and Medical Applications of Hydroxyapatite**. Takayama Press System Center Co.,Inc, Tokyo.

_____. 1994. **Medical Applications of Hydroxyapatite**. Ishiyaku Euro America, St. Louis, Tokyo.

Arm, D.M., A.F. Tencer, S.D. Bain and D. Celino. 1996. Effect of controlled release of platelet-derived growth factor from a porous hydroxyapatite implant on bone ingrowth. **Biomaterials** 17: 703-709.

Atlan, G., N. Balmain, S. Berland, B. Vidal, E. Lopez. 1997. Reconstruction of human maxillary defects with nacre powder: histological evidence for bone regeneration. **C. R. Acad. Sci. Paris** 320: 253-258.

_____, O. Dellattre, S. Berland, A. LaFaou, G. Nabias, D. Cot, E. Lopez. 1999. Interface between bone and nacre implants in sheep. **Biomaterials** 20: 1017-1022.

Beganskienė, A., O. Dudko, R. Sirutkaitis and R. Giraitis. 2003. Water based sol-gel synthesis of hydroxyapatite. **Mater. Sci.** 9: 383-386.

Belt, H.v.d., D. Neut, W. Shcenk, J.R. Horn, H.C.v.d. Mei and H.J. Busscher. 2001. Stephylococcus aureus biofilm formation on different gentamicin-loaded polymethylmethacrylate bone cements. **Biomaterials** 22: 1607-1611.

Boonyang, U., P. Chaopanich, A. Wongchaisuwat, P. Senthongkaew and S. Siripaisarnpipat. 2010. Effect of phosphate Precursor on the production of hydroxyapatite from crocodile eggshells. **J. Biomim. Biomater. Tissue Eng.** 5: 31-37.

Cao, L.-Y., C.-B. Zhang and J.-F. Huang. 2005. Synthesis of hydroxyapatite nanoparticles in ultrasonic precipitation. **Ceram. Inter.** 31: 1041-1044.

Chattopadhyay, P., S. Pal, A.K. Wahi, L. Singh and A. Verma. 2007. Synthesis of crystalline hydroxyapatite from coral (*Gergonacea sp*) and cytotoxicity evaluation. **Trends Biomater. Artif. Organs** 20: 142-144.

Cheng, K., G. Shen, W. Weng, G. Han, J.M.F. Ferreira and J. Yang. 2001. Synthesis of hydroxyapatite/fluoroapatite solid solution by a sol-gel method. **Mater. Lett.** 51: 37-41.

Cho, S., K. Nakanishi, T. Kokubo, N. Soga, C. Ohtsuki and T. Nakamura. 1995. Dependence of apatite formation on silica gel on its structure: effect of heat treatment. **J. Am. Ceram. Soc.** 78: 1769-1974.

Christoffersen, J., M.R. Christoffersen, R. Larsen and I.J. Møller. 1991. Regeneration by surface-coating of bone char used for defluoridation of water. **Water Res.** 25: 227-229.

Cosijns, A., C. Vervaet, J. Luyten, S. Mullens, F. Siepmann, L. Van Hoorebeke, B. Masschaele, V. Cnudde and J.P. Remon. 2007. Porous hydroxyapatite tablets as carriers for low-dosed drugs. **Eur. J. Pharm. Biopharm.** 67: 498-506.

Descamps, M., J.C. Hornez and A. Leriche. 2009. Manufacture of hydroxyapatite beads for medical applications. **J. Eur. Ceram. Soc.** 29: 369-375.

Duncan, C.P. and B.A. Masri. .1994. The role of antibiotic-loaded cement in the treatment of an infection after a hip replacement. **J. Bone Joint Surg. Am**. 76: 1742-1751.

Fathi, M.H. and A. Hanifi. 2007. Evaluation and characterization of nanostructure hydroxyapatite powder prepared by simple sol–gel method. **Mater. Lett.** 61: 3978-3983.

Feng, W., L. Mu-Sen, L. Yu-Peng and Q. Yong-Xin. 2005. A simple sol-gel technique for preparing hydroxyapatite nanopowder. **Mater. Lett.** 59: 916-919.

Gautier, H., G. Daculsi and C. Merle. 2001. Association of vancomycin and calcium phosphate by dynamic compaction: in vitro characterization and microbiological activity. **Biomaterials** 22: 2481-2487.

Gbureck, U., E. Vorndran and J.E. Barralet. 2008. Modeling vancomycin release kinetics from microporous calcium phosphate ceramics comparing static and dynamic immersion conditions. **Acta Biomater.** 4: 1480-1486.

Herliansyah, M.K., M. Hamdi, A. Ide-Ektessabi, M.W. Wildan and J.A. Toque. 2009. The influence of sintering temperature on the properties of compacted bovine hydroxyapatite. **Mater. Sci. Eng. C** 29: 1674-1680.

Higuchi, T. 1961. Rate of release of medicaments from ointment bases containing drugs in suspensions. **J. Pharm. Sci.** 50: 874-875.

_____. 1963. Mechanism of sustained-action medication. **J. Pharm. Sci.** 52: 1145-1147.

Hu, J., J.J. Russell, B. Ben-Nissan and R. Vago. 2001. Production and analysis of hydroxyapatite from Australian corals via hydrothermal process. **J. Mater. Sci. Lett.** 20: 85-87.

Innes, J.K., R. Vago and B. Ben-Nissan. 2003. Hydrothermal conversion and sol-gel coating of Red Sea. **Key Eng. Mater**. 240-242: 43-46.

Ioku, K., G. Kawachi and S. Sasaki. 2006. Hydrothermal preparation of tailored hydroxyapatite. **J. Mater. Sci.** 41: 1341-1344.

_____, S. Yamauchi, H. Fujimori, S. Goto and M. Yoshimura. 2002. Hydrothermal preparation of fibrous apatite and apatite sheet. **Solid State Ionics** 151: 147-150.

Itokazu, M., Y. Wenyi, T. Aoki, A. Ohara and N. Kato. 1998. Synthesis of antibiotic-loaded interporous hydroxyapatite blocks by vacuum method and in vitro drug release testing. **Biomaterials** 19: 817-819.

Joosten, U., A. Joist, G. Gosheger, U. Liljenqvist, B. Brandt and C. von Eiff. 2005. Effectiveness of hydroxyapatite-vancomycin bone cement in the treatment of Staphylococcus aureus induced chronic osteomyelitis. **Biomaterials** 26: 5251-5258.

Joris, S.J. and C.H. Amberg. 2002. Nature of deficiency in nonstoichiometric hydroxyapatites. I. Catalytic activity of calcium and strontium hydroxyapatites. **J. Phys. Chem.** 75: 3167-3171.

Kasikron research center. **K-Econ analysis**. November, 2004.

Kim, Y.G., D.S. Seo and J.K. Lee. 2008. Dissolution of synthetic and bovine bone-derived hydroxyapatites fabricated by hot-pressing. **Appl. Surface Sci.** 255: 589-592.

Kokubo, T. and H. Takadama. 2006. How useful is SBF in predicting in vivo bone bioactivity? **Biomaterials** 27: 2907-2915.

Lee, S.J. and S.H. Oh. 2003a. Fabrication of calcium phosphate bioceramics by using eggshell and phosphoric acid. **Mater. Lett.** 57: 4570-4574.

_____. 2003b. Synthesis of biocompatible calcium phosphate powders by using an eggshell. **Key Eng. Mater.** 240-242: 35-38.

Lemos, A.F., J.H.G. Rocha, S.S.F. Quaresma, S. Kannan, F.N. Oktar, S. Agathopoulos and J.M.F. Ferreira. 2006. Hydroxyapatite nano-powders produced hydrothermally from nacreous material. **J. Euro. Ceram. Soc.** 26: 3639-3646.

Lewis, K., U. Boonyang, L. Evans, S. Siripaisarnpipat and B. Ben-Nissan. 2006. A comparative study of Thai and Australian crocodile bone for use as a potential biomaterial. **Key Eng. Mater.** 309-311: 15-18.

Liu, J., K. Li, H. Wang, M. Zhu and H. Yan. 2004. Rapid formation of hydroxyapatite nanostructures by microwave irradiation. **Chem. Phys. Lett.** 396: 429-432.

_____, X. Ye, M. Zhu, B. Wang and H. Yan. 2003. The influence of pH and temperature on the morphology of hydroxyapatite synthesized by hydrothermal method. **Ceram. Inter.** 29: 629-633.

Lopez, E., B. Vidal, S. Berland, G. Camprasse, C. Silve. 1992. Demonstation of the capacity of nacre to induce bone formation by human osteoblasts maintained in vitro. **Tissue Cell**. 24: 667-679.

Mann, S. 2001. **Biomaterialization principles and concepts in bioinorganic materials chemistry**. Oxford University Press, New York.

Matsumoto, T., M. Okazaki, M. Inoue, S. Yamaguchi, T. Kusunose, T. Toyonaga, Y. Hamada and J. Takahashi. 2004. Hydroxyapatite particles as a controlled release carrier of protein. **Biomaterials** 25: 3807-3812.

Mizushima, Y., T. Ikoma, J. Tanaka, K. Hoshi, T. Ishihara, Y. Ogawa and A. Ueno. 2006. Injectable porous hydroxyapatite microparticles as a new carrier for protein and lipophilic drugs. **J. Controlled Release** 110: 260-265.

Monmaturapoj, N. 2008. Nano-size hydroxyapatite powders preparation by wet-chemical precipitation route. **J. Metals Mater Miner.** 18: 15-20.

Murugan, R. and S. Ramakrishna. 2006. Production of ultra-fine bioresorbable carbonated hydroxyapatite. **Acta Biomater.** 2: 201-206.

Nasiri-Tabrizi, B., P. Honarmandi, R. Ebrahimi-Kahrizsangi and P. Honarmandi. 2009. synthesis of nanosize sigle-crystal hydroxyapatite via mechanochemical method. **Mater. Lett.** 63: 543-546.

Nayar, S. and A. Guha. 2009. Waste utilization for the controlled synthesis of nanosized hydroxyapatite. **Mater. Sci. Eng. C** 29: 1326-1329.

Neut, D., H.v.d. Belt, I.S.J.R.v. Horn, H.C.v.d. Mei and H.J. Busscher. 2001. Biomaterial-associated infection of gentamicin-loaded PMMA beads in orthopaedic revision surgery. **J. Antimicro. Chemo.** 47: 885-891.

Ni, M. and B.D. Ratner. 2003. Nacre surface transformation to hydroxyapatite in phosphate buffer solution. **Biomaterials** 24: 4323-4331.

Ogiso, M. 1998. Reassessment of long-term use of dense HA as dental implant: case report. **J. Biomed. Mater. Res. Appl. Biomater**. 43: 318-320.

Ooi, C.Y., M. Hamdi and S. Ramesh. 2007. Properties of hydroxyapatite produced by annealing of bovine bone. **Ceram. Inter.** 33: 1171-1177.

Otsuka, M., Y. Matsuda, T. Kokubo, S. Yoshihara, T. Nakamura and T. Yamamuro. 1994. A novel skeletal drug delivery system using self-setting bioactive glass bone cement. III: the in vitro drug release from bone cement containing indomethacin and its physicochemical properties. **J.Controlled Release** 31: 111-119.

Palazzo, B., M.C. Sidoti, N. Roveri, A. Tampieri, M. Sandri, L. Bertolazzi, F. Galbusera, G. Dubini, P. Vena and R. Contro. 2005. Controlled drug delivery from porous hydroxyapatite grafts: An experimental and theoretical approach. **Mater. Sci. Eng. C** 25: 207-213.

Parhi, P., A. Ramanan and A.R. Ray. 2004. A convenient route for the synthesis of hydroxyapatite through a novel microwave-mediated metathesis reaction. **Mater. Lett.** 58: 3610-3612.

_____. 2006. Synthesis of nano-sized alkaline-earth hydroxyapatites through microwave assisted metathesis route. **Materials Letters** 60: 218-221.

Pham, H.H., P. Luo, F. Genin and A.K. Dash. 2002. Synthesis and characterization of hydroxyapatite-ciprofloxacin delivery systems by precipitation and spray drying technique. **AAPS Pharm. Sci. Tech.** 3: E1.

Prabakaran, K., A. Balamurugan and S. Rajeswari. 2005. Development of calcium phosphate based apatite from hen's eggshell. **Bull. Mater. Sci.** 28: 115-119.

_____. and S. Rajeswari. 2006. Development of hydroxyaptite from natural fish bone through heat treatment. **Trends Biomater. Artif. Organs** 20: 20-23.

Rauschmann, M.A., T.A. Wichelhaus, V. Stirnal, E. Dingeldein, L. Zichner, R. Schnettler and V. Alt. 2005. Nanocrystalline hydroxyapatite and calcium sulphate as biodegradable composite carrier material for local delivery of antibiotics in bone infections. **Biomaterials** 26: 2677-2684.

Rhee, S.H. 2002. Synthesis of hydroxyapatite via mechanochemical treatment. **Biomaterials** 23: 1147-1152.

Rivera, E.M., M. Araiza, W. Brostow, V.M. Castano, J.R. Diaz-Estrada, R. Hernandez and J.R. Rodriguez. 1999. Synthesis of hydroxyapatite from eggshells. **Mater. Lett.** 41: 128-134.

Rivera, E.M., R. Curiel and R. Rodriguez. 2003. Selectivity in hydroxyapatite synthesis from eggshell using different thermal treatments. **Mater. Res. Innov.** 7: 85-90.

Rocha, J.H.G., A.F. Lemos, S. Agathopoulos, P. Valério, S. Kannan, F.N. Oktar and J.M.F. Ferreira. 2005. Scaffolds for bone restoration from cuttlefish. **Bone** 37: 850-857.

_____, S. Kannan, S. Agathopoulos and J.M.F. Ferreira. 2005. Hydroxyapatite scaffolds hydrothermally grown from aragonitic cuttlefish bones. **J. Mater. Chem.** 15: 5007-5011.

Rossi, S., A.O. Azghani and A. Omri. 2004. Antimicrobial efficacy of a new antibiotic-loaded poly(hydroxybutyric-co-hydroxyvaleric acid) controlled release system. **J. Antimicro. Chemo.** 54: 1013-1018.

Roy, M.D. and S. Linnehan. 1974. Hydroxyapatite formed from coral skeletal carbonate by hydrothermal exchange. **Nature** 247: 220-222.

Ruksudjarit, A., K. Pengpat, G. Rujijanagul and T. Tunkasiri. 2008. Synthesis and characterization of nanocrystalline hydroxyapatite from natural bovine bone. **Current Appl. Phys.** 8: 270-272.

Sanosh, K.P., M.-C. Chu, A. Balakrishnan, T.N. Kim and S.-J. Cho. 2009. Utilization of biowaste eggshells to synthesize nanocrystalline hydroxyapatite powders. **Mater. Lett.** 63: 2100-2102.

Sasikumar, S. and R. Vijayaraghavan. 2006. Low temperature synthesis of nanocrystalline hydroxyapatite from egg shells by combustion method. **Trends Biomater. Artif. Organs** 19: 70-73.

Schlatterer, B., R. Baeker and K. Schlatterer. 2004. Improved purification of b-lactoglobulin from acid whey by means of ceramic hydroxyapatite chromatography with sodium fluoride as a displacer. **J. Chromatogr. B** 807: 223-228.

Seebacher, F., P. Elsworth and C. Franklin. 2003. Ontogenetic changes of swimming kinematics in a semi-aquatic (*Crocodylus porosus*). **Aust. J. Zoology** 51: 15.

Shen, Y., J. Zhu, H. Zhang and F. Zhao. 2006. In Vitro osteogenic activity of pearl. **Biomaterials** 27: 281-287.

Silve, C., E. Lopez, B. Vidal, D.C. Smity, S. Camprasse, G. Camprasse, G Couly. 1992. Nacre initiates biomineralization by human osteoblasts maintained *in vitro*. **Calcif. Tissue Int.** 51: 363-369.

Siripaisarnpipat, S., A. Wongchaisuwat, B. Pitiyont, N. Boonyaprapat, N. Jongjaitate. 2005. Chemical analysis of composition of shell and freshwater pearl from Thai Amblemid mussel. pp. 187-304. *In* research report Development of freshwater pearl culture in Thailand. Kasetsart University.

Sivakumar, M., T.S.S. Kumar, K.L. Shantha and K.P. Rao. 1996. Development of hydroxyapatite derived from Indian coral. **Biomaterials** 17: 1709-1714.

_____, I. Manjubala and K. Panduranga Rao. 2002. Preparation, characterization and in-vitro release of gentamicin from coralline hydroxyapatite-chitosan composite microspheres. **Carbohydrate Polymers** 49: 281-288.

Slosarczyk, A., J. Szymura-Oleksiak and B. Mycek. 2000. The kinetics of pentoxifylline release from drug-loaded hydroxyapatite implants. **Biomaterials** 21: 1215-1221.

Suchanek, W. and M. Yoshimura. 1998. Processing and properties of hydroxyapatite-based biomaterials for use as hard tissue replacement implants. **J. Mater. Res.** 13: 94-117.

Sudo, A., M. Hasegawa, A. Fukuda and A. Uchida. 2008. Treatment of Infected Hip Arthroplasty With Antibiotic-Impregnated Calcium Hydroxyapatite. **J. Arthroplasty** 23: 145-150.

Suen, R.-B., S.-C. Lina and W.-H. Hsu. 2004. Hydroxyapatite-based immobilized metal affinity adsorbents for protein purification. **J. Chromatogr. A** 1048: 31-39.

Sung, Y.-M., J.-C. Lee and J.-W. Yang. 2004. Crystallization and sintering characteristics of chemically precipitated hydroxyapatite nanopowder. **J. Cryst. Growth** 262: 467-472.

Takahashi, H., M. Yashima, M. Kakihana and M. Yoshimura. 2001. A differential scanning calorimeter study of the monoclinic ($P2_1/b$) ↔ hexagonal ($P6_3/m$) reversible phase transition in hydroxyapatite. **Thermochimica Acta** 371: 53-56.

Teller, M., U. Gopp, H.-G. Neumann and K.-D. Kuhn. 2006. Release of gentamicin from bone regenerative materials: an *In Vitro* study. **J. Biomed. Mater. Res. B: Appl. Biometer.** 81: 23-29.

Toriyama, M., A. Ravaglioli, A. Krajewski, G. Celotti and A. Piancastelli. 1996. Synthesis of hydroxyapatite-based powders by Mechano-Chemical method and their sintering. **J. Euro. Ceram. Soc.** 16: 429-436.

Vagenas, N.V., A. Gatsouli and C.G. Kontoyannis. 2003. Quantitative analysis of synthetic calcium carbonate polymorphs using FT-IR spectroscopy. **Talanta** 59: 831-836.

Vecchio, K.S., X. Zhang, J.B. Massie, M. Wang and C.W. Kim. 2007. Conversion of bulk seashells to biocompatible hydroxyapatite for bone implants. **Acta Biomater.** 3: 910-918.

Wahlig, H., E. Dingeldein, R. Bergmann and K. Reuss. 1978. The release of gentamicin from polymethylmethacrylate beads. **J. Bone Joint Surgery** 60-B: 270-275.

Wang, M. 2004a. Bioactive ceramic-polymer composites for tissue replacement. 1-29. *In* Hin, T. S., **Engineering Materials for Biomedical Applications**. Springer Berlin Heidelberg, New York.

_____. 2004b. Bioactive materials and processing. 1-82. *In* Shi, D., **Biomaterials and tissue engineering**. Springer Berlin Heidelberg, New York.

_____. 2004c. Biological and medical physics biomedical engineering. *In* Shi, D., **Biomaterials and tissue engineering**. Springer Berlin Heidelberg, New York.

Wang, X., H. Fan, Y. Xiao and X. Zhang. 2006. Fabrication and characterization of porous hydroxyapatite/β-tricalcium phosphate ceramics by microwave sintering. **Mater. Lett.** 60: 455-458.

Webb, E., D. Amarasiriwardena, S. Tauch, E. F. Green, J. Jones, A. H. Goodman. 2005. Inductively coupled plasma-mass (ICP-MS) and atomic emission spectrometry (ICP-AES): Versatile analytical techniques to identify the archived elemental information in human teeth. **Microchemical J.** 81: 201-208.

Wood, D.J., R.J. Minns and A. Strover. 1990. Replacement of the rabbit medial meniscus with a polyester-carbon fibre bioprosthesis. **Biomaterials** 11: 13-16.

Woodard, J.R., A.J. Hilldore, S.K. Lan, C.J. Park, A.W. Morgan, J.A.C. Eurell, S.G. Clark, M.B. Wheeler, R.D. Jamison and A.J. Wagoner Johnson. 2007. The mechanical properties and osteoconductivity of hydroxyapatite bone scaffolds with multi-scale porosity. **Biomaterials** 28: 45-54.

Xu, Y., D. Wang, L. Yang and H. Tang. 2001. Hydrothermal conversion of coral into hydroxyapatite. **Mater. Charact.** 47: 83-87.

Yeong, K.C.B., J. Wang and S.C. Ng. 1999. Fabricating densified hydroxyapatite ceramics from a precipitated precursor. **Mater. Lett.** 38: 208-213.

Yoshimura, M. and H. Suda. 1994a. Hydrothermal processing of hydroxyapatite: past, present, and future. pp. 45-72. *In* Brown, P. W. and Constantz, B., **Hydroxyapatite and related materials**. CRC Press Inc., Boca Raton Ann Arbor London Tokyo.

Yoshimura, M. and H. Suda. 1994b. Hydrothermal synthesis of biocompatible whiskers. **J. Mater. Sci.** 29: 3399-3402.

_____, P. Sujaridworakun, F. Koh, T. Fujiwara, D. Pongkao and A. Ahniyaz. 2004. Hydrothermal conversion of calcite crystals to hydroxyapatite. **Mater. Sci. Eng. C** 24: 521-525.

Zaremba, C.M., D.E. Morse, S. Mann, P.K. Hansma and G.D. Stucky. 1998. Aragonite-hydroxyapatite conversion in gastropod (abalone) nacre. **Chem. Mater.** 10: 3813-3824.

Zhang, F., Z.-H. Zhou, S.-P. Yang, L.-H. Mao, H.-M. Chen and X.-B. Yu. 2005. Hydrothermal synthesis of hydroxyapatite nanorods in the presence of anionic starburst dendrimer. **Mater. Lett.** 59: 1422-1425.

Zhang, H., Y. Yan, Y. Wang and S. Li. 2002. Morphology and formation mechanism of hydroxyapatite whiskers from moderately acid solution. **Mater. Res.** 6: 111-115.

Zhang, X. and K.S. Vecchio. 2006. Creation of dense hydroxyapatite (synthetic bone) by hydrothermal conversion of seashells. **Mater. Sci. Eng. C** 26: 1445-1450.

Zhu, S.H., B.Y. Huang, K.C. Zhou, S.P. Huang, F. Liu, Y.M. Li, Z.G. Xue and Z.G. Long. 2004. Hydroxyapatite nanoparticles as a novel gene carrier. **J. Nanoparticle Res.** 6: 307-311.

APPENDICES

Appendix A

Determination of FWHM

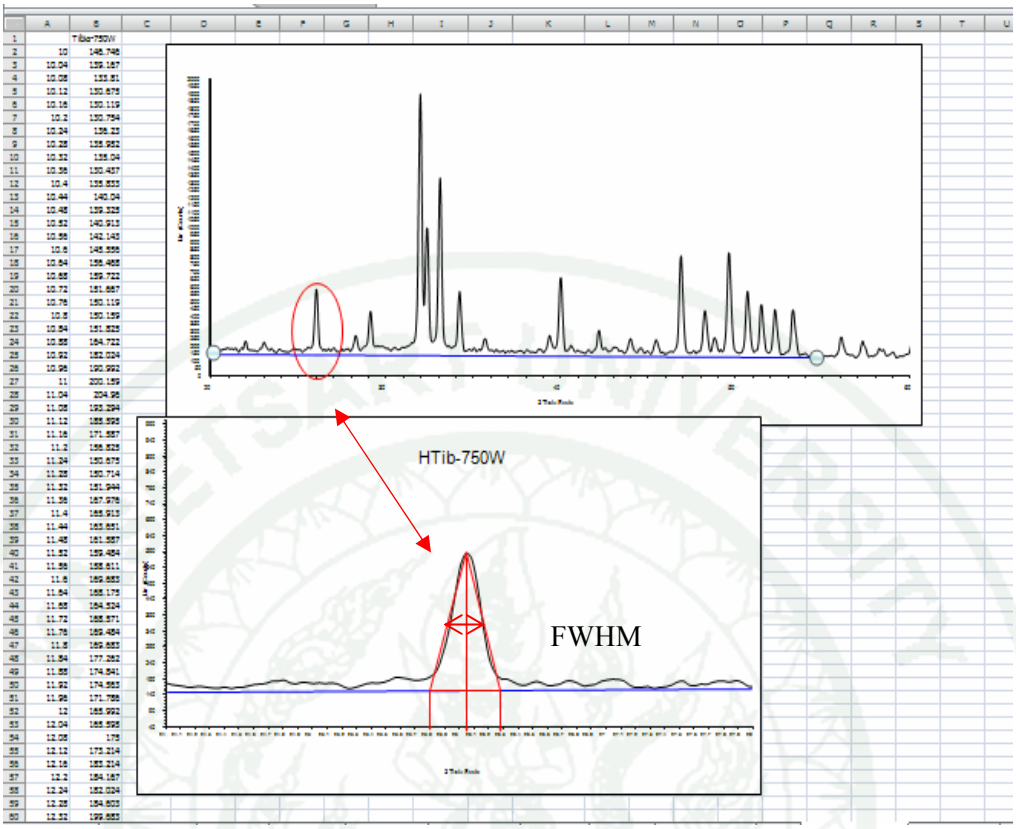

Appendix Figure A1 The determination of FWHM.

Appendix B

Calculation of drug releasing

Appendix Table B1 The absorbance of releasing tetracycline as a function of time.

Time (h)	Absorbance								
	HTib_750W			HTW_750W			ES_6_150		
	I	II	III	I	II	III	I	II	III
2	0.7450	0.2120	).6550	0.6290	0.2570	0.5540	0.2800	0.4830	0.3840
4	0.6770	).5490	).4860	0.8510	0.6090	0.5860	0.3430	0.5370	0.4580
6	0.6760	).9780	).5120	0.7670	0.6290	0.5020	0.3890	0.3700	0.3560
8	0.4560	).8380	).5650	0.8200	0.9100	0.6370	0.6250	0.4860	0.5760
10	0.1690	).5910	).4020	0.3390	0.7400	0.4450	0.5450	0.4860	0.5350
12	0.0749	).4690	).3220	0.0931	0.6110	0.2860	0.3950	0.5077	0.5030
14	0.0382	).3240	).2300	0.0723	0.4030	0.0980	0.3940	0.4450	0.4620
16	0.2850	).3050	).2010	0.2940	0.3490	0.1110	0.3590	0.3320	0.4350
18	-	).1780	).1540	-	0.2300	0.1510	0.3320	0.3501	0.2950
20	-	-	-	-	0.2310	-	0.2730	0.2980	0.3400
24	-	-	-	-	-	-	0.2980	0.257	0.1930

Appendix Table B1 (Continued)

Time (h)	Absorbance					
	EM_6_150			EL_6_150		
	I	II	III	I	II	III
2	0.6260	0.3750	0.5190	0.4110	0.5780	0.3810
4	0.5050	0.4420	0.4820	0.1960	0.2800	0.2210
6	0.3890	0.3050	0.3500	0.1080	0.1850	0.1560
8	0.4250	0.3240	0.4640	0.2170	0.2928	0.1890
10	0.5670	0.4970	0.4640	0.1870	0.1880	0.1530
12	0.4190	0.4440	0.4740	0.1400	0.1650	0.1790
14	0.4220	0.4627	0.5030	0.1230	0.1610	0.1760
16	0.3740	0.4040	0.3720	0.1490	0.1370	0.1850
18	0.3912	0.4201	0.3310	0.1310	0.1280	0.1050
20	0.2010	0.1105	0.1860	0.1453	0.1010	-
24	0.1310	-	0.1110	0.1149	0.1400	-

Appendix Table B2 The absorbance of releasing vancomycin as a function of time.

Time (h)	Absorbance								
	HTib_750W			HTW_750W			ES_6_150		
	I	II	III	I	II	III	I	II	III
2	0.3360	0.2810	).3752	0.2410	0.3520	0.3270	0.3710	0.3360	0.2249
4	0.2090	).1030	).1287	0.1829	0.1596	0.2410	0.1050	0.1563	0.1325
6	0.0592	).0654	).0772	0.0830	0.1698	0.0975	0.0428	0.0400	0.0586
8	0.0672	).0635	).0532	0.0623	0.0953	0.0611	0.0553	0.0486	0.0578
10	0.0771	).0653	).0495	0.0373	0.0333	0.0298	0.0744	0.0480	0.0523
12	0.0382	).0453	0.322	-	-	-	0.0504	0.0397	0.0503
14	-	-	-	-	-	-	0.0394	0.0449	0.0465
16	-	-	-	-	-	-	-	-	-
18	-	-	-	-	-	-	-	-	-
20	-	-	-	-	-	-	-	-	-
24	-	-	-	-	-	-	-	-	-

Appendix Table B2 (Continued)

Time (h)	Absorbance					
	EM_6_150			EL_6_150		
	I	II	III	I	II	III
2	0.3350	0.3730	0.2510	0.2630	0.2410	0.2090
4	0.1090	0.0889	0.0965	0.0637	0.0536	0.0598
6	0.0752	0.0390	0.0777	0.0729	0.0923	0.0830
8	0.0744	0.0863	0.0652	0.0498	0.0265	0.0456
10	0.450	0.0450	0.0464	0.0291	0.0437	0.0398
12	0.0552	0.0352	0.0399	-	0.0261	0.0268
14	0.0252	0.0243	0.0298	-	-	-
16	-	-	-	-	-	-
18	-	-	-	-	-	-
20	-	-	-	-	-	-
24	-	-	-	-	-	-

Appendix Table B3 The concentration of releasing tetracycline as a function of time.

Time (h)	Concentration (ppm)								
	HTib_750W			HTW_750W			ES_6_150		
	I	II	III	I	II	III	I	II	III
2	15.3441	3.8817	3.4086	12.8495	4.8495	11.2366	5.3441	9.7097	7.5806
4	13.8817	1.1290	9.7742	17.6237	12.4194	11.9247	6.6989	10.8710	9.1720
6	13.8602	0.3548	0.3333	15.8172	12.8495	10.1183	7.6882	7.2796	6.9785
8	9.1290	7.3441	1.4731	16.9570	18.8925	13.0215	12.7634	9.7742	11.7097
10	2.9570	2.0323	7.9677	6.6129	15.2366	8.8925	11.0430	9.7742	10.8280
12	0.9333	9.4086	5.2473	1.3247	12.4624	5.4731	7.8172	10.2409	10.1398
14	0.1441	5.2903	4.2688	0.8774	7.9892	1.4301	7.7957	8.8925	9.2581
16	5.4516	5.8817	3.6452	5.6452	6.8280	1.7097	7.0430	6.4624	8.6774
18	-	3.1505	2.6344	-	4.2688	2.5699	6.4624	6.8516	5.6667
20	-	-	-	-	4.2903	-	5.1935	5.7312	6.6344
24	-	-	-	-	-	-	5.7312	5.6817	3.4731

Appendix Table B3 (Continued)

Time (h)	Concentration (ppm)					
	EM_6_150			EL_6_150		
	I	II	III	I	II	III
2	12.7849	7.3871	10.4839	8.1613	11.7527	7.5161
4	10.1828	8.8280	9.6882	3.5376	5.3441	4.0753
6	7.6882	5.8817	6.8495	1.6452	3.3011	2.6774
8	8.4624	6.2903	9.3011	3.9892	5.6194	3.3871
10	11.5161	10.0108	9.3011	3.3441	3.3656	2.6129
12	8.3333	8.8710	9.5161	2.3333	2.8710	3.1720
14	8.3978	9.2731	10.1398	1.9677	2.7849	3.1075
16	7.3656	8.0108	7.3226	2.5269	2.2688	3.3011
18	7.7355	8.3570	6.4409	2.1398	2.0753	1.5806
20	3.6452	1.6989	3.3226	2.4473	1.4946	-
24	2.1398	-	1.7097	1.7935	2.3333	-

Appendix Table B4 The concentration of releasing vancomycin as a function of time.

Time	Concentration (ppm)														
	HTib_750W					HTW_750W					ES_6_150				
	I	II	III	average	±RSD	I	II	III	average	±RSD	I	II	III	average	±RSD
2	54.95	5.14	.29	58.46	0.09	56.36	54.00	57.57	55.98	0.03	63.29	54.95	52.31	56.85	0.10
4	31.86	.29	.40	28.18	0.16	42.31	39.14	44.24	41.90	0.06	21.38	24.07	23.17	22.87	0.06
6	12.86	.33	.14	14.78	0.15	18.74	22.52	21.98	21.08	0.10	8.95	8.29	12.71	9.98	0.24
8	14.76	.88	.43	13.36	0.13	11.21	16.69	10.93	12.94	0.25	11.93	10.33	12.52	11.60	0.10
10	9.98	17	.55	9.23	0.20	-	-	-	-	-	16.48	10.19	11.21	12.63	0.27
12	-	-	-	-	-	-	-	-	-	-	10.76	8.21	10.74	9.90	0.15
14	-	-	-	-	-	-	-	-	-	-	8.14	9.45	9.83	9.14	0.10
16	-	-	-	-	-	-	-	-	-	-	-	-	-	-	-
18	-	-	-	-	-	-	-	-	-	-	-	-	-	-	-
20	-	-	-	-	-	-	-	-	-	-	-	-	-	-	-
24	-	-	-	-	-	-	-	-	-	-	-	-	-	-	-

Appendix Table B4 (Continued)

Time (h)	Concentration (ppm)									
	EM_6_150					EL_6_150				
	I	II	III	average	±RSD	I	II	III	average	±RSD
2	54.71	63.76	58.52	59.00	0.08	61.38	56.14	53.29	56.94	0.07
4	24.71	19.93	21.74	22.13	0.11	13.93	16.29	13.00	14.40	0.12
6	16.67	15.19	17.26	16.37	0.07	16.12	20.74	18.52	18.46	0.13
8	16.78	19.31	14.29	16.69	0.15	10.62	12.21	9.62	10.82	0.12
10	9.48	9.48	9.81	9.59	0.02	7.60	9.17	8.24	8.33	0.09
12	11.90	7.14	8.26	9.10	0.27	-	-	-	-	-
14	-	-	-	-	-	-	-	-	-	-
16	-	-	-	-	-	-	-	-	-	-
18	-	-	-	-	-	-	-	-	-	-
20	-	-	-	-	-	-	-	-	-	-
24	-	-	-	-	-	-	-	-	-	-

Appendix Table B5 The dilution factor of releasing tetracycline as a function of time.

Time (h)	Dilution factor								
	HTib_750W			HTW_750W			ES_6_150		
	I	II	III	I	II	III	I	II	III
2	4	4	4	3	3	4	3	2	3
4	3	3	3	3	3	3	3	3	3
6	2	2	2	2	2	2	2	2	2
8	1	1	1	1	1	1	1	1	1
10	1	1	1	1	1	1	1	1	1
12	1	1	1	1	1	1	1	1	1
14	1	1	1	1	1	1	1	1	1
16	1	1	1	1	1	1	1	1	1
18	-	1	1	-	1	1	1	1	1
20	-	-	-	-	1	-	1	1	1
24	-	-	-	-	-	-	1	1	1

Appendix Table B5 (Continued)

Time (h)	Dilution factor					
	EM_6_150			EL_6_150		
	I	II	III	I	II	III
2	2	2	2	2	2	2
4	2	2	2	2	2	2
6	2	2	2	1	1	1
8	1	1	1	1	1	1
10	1	1	1	1	1	1
12	1	1	1	1	1	1
14	1	1	1	1	1	1
16	1	1	1	1	1	1
18	1	1	1	1	1	1
20	1	1	1	1	1	-
24	1	1	1	1	1	-

Appendix Table B6 The concentration of releasing tetracycline before dilution.

Time (h)	Concentration (ppm)														
	HTib_750W					HTW_750W					ES_6_150				
	I	II	III	average	±RSD	I	II	III	average	±RSD	I	II	III	average	±RSD
2	61.38	15.53	53.63	43.51	0.56	38.55	14.55	44.95	32.68	0.49	16.03	19.42	22.74	19.40	0.17
4	41.65	33.39	29.32	34.79	0.18	52.87	37.26	35.77	41.97	0.23	13.40	21.74	18.34	17.83	0.24
6	27.72	40.71	20.67	29.70	0.34	31.63	25.70	20.24	25.86	0.22	15.38	14.56	13.96	14.63	0.05
8	9.13	17.34	11.47	12.65	0.33	16.96	18.89	13.02	16.29	0.18	12.76	9.77	11.71	11.42	0.13
10	2.96	12.03	7.97	7.65	0.59	6.61	15.24	8.89	10.25	0.44	11.04	9.77	10.83	10.55	0.06
12	0.93	9.41	6.25	5.53	0.77	1.31	12.46	5.47	6.42	0.88	7.82	10.24	10.14	9.40	0.15
14	0.14	6.29	4.27	3.57	0.88	0.88	7.99	1.43	3.43	1.15	7.80	8.89	9.26	8.65	0.09
16	5.45	5.88	3.65	4.99	0.24	5.65	6.83	1.71	4.73	0.57	7.04	6.46	8.68	7.39	0.16
18	-	3.15	2.63	1.93	0.88	-	4.27	2.57	2.28	0.94	6.46	6.85	5.57	6.33	0.10
20	-	-	-	-	-	-	4.29	-	-	-	5.19	5.73	6.63	5.85.	0.12
24	-	-	-	-	-	-	-	-	-	-	5.73	5.68	3.47	4.96	0.26

Appendix Table B6 (Continued)

Time (h)	Concentration (ppm)									
	EM_6_150					EL_6_150				
	I	II	III	average	±RSD	I	II	III	average	±RSD
2	25.57	14.77	20.97	20.44	0.26	16.32	23.51	15.03	18.29	0.20
4	20.37	17.66	19.38	19.13	0.07	7.08	10.69	8.15	8.64	0.20
6	15.38	11.76	13.70	13.61	0.13	1.65	3.30	2.68	2.54	0.33
8	8.46	6.29	9.30	8.02	0.19	3.99	5.62	3.39	4.33	0.20
10	11.52	10.01	9.30	10.28	0.11	3.34	3.37	2.61	3.11	0.05
12	8.33	8.87	9.52	8.91	0.07	2.33	2.87	3.17	2.79	0.10
14	8.40	9.27	10.14	9.27	0.09	1.97	2.78	3.11	2.62	0.16
16	7.37	8.01	7.32	7.57	0.05	2.53	2.27	3.30	2.70	0.08
18	7.74	8.36	6.44	7.51	0.13	2.14	2.08	1.58	1.93	0.06
20	3.65	1.70	3.32	2.89	0.36	2.45	1.49	-	1.31	0.46
24	2.14	-	1.71	1.28	0.88	1.79	2.33	-	1.38	0.35

Appendix Table B7 The average amounts of releasing tetracycline in 5 ml SBF solution (μg).

Time (h)	Average amount (μg)				
	HTib_750W	HTW_750W	ES_6_150	EM_6_150	EL_6_150
2	217.56	163.41	96.99	102.19	91.43
4	173.92	209.84	89.14	95.66	43..19
6	148.49	129.28	73.15	68.06	12.71
8	63.24	81.45	57.08	40.09	21.66
10	38.26	51.24	52.74	51.38	15.54
12	27.65	32.10	47.00	44.53	13.96
14	17.84	17.16	43.24	46.35	13.10
16	24.96	23.64	36.97	37.83	13.49
18	9.64	11.40	31.63	37.56	9.66
20	-	7.15	29.27	14.44	9.85
24	-	-	-	-	-

Appendix Table B8 The cumulative amounts of releasing tetracycline in 5 ml SBF solution (μg).

Time (h)	Cumulative amount (μg)				
	HTib_750W	HTW_750W	ES_6_150	EM_6_150	EL_6_150
2	217.56	163.41	96.99	102.19	91.43
4	391.49	373.24	186.13	197.85	134.62
6	539.98	502.53	259.28	265.91	147.33
8	603.23	583.98	316.36	306.00	168.99
10	641.49	635.22	369.10	357.38	184.53
12	669.14	667.32	416.10	401.92	198.45
14	686.97	684.48	459.34	448.27	211.59
16	711.94	708.11	496.32	486.10	225.08
18	721.58	719.51	527.95	523.66	234.74
20	721.58	726.66	557.22	538.10	244.60
24	721.58	726.66	557.22	538.10	244.60
Total amount of releasing TC within 24 hours	721.58	726.66	557.22	538.10	244.60

Appendix Table B9 The average amounts of releasing vancomycin in 5 ml SBF solution (μg).

Time (h)	Average amount (μg)				
	HTib_750W	HTW_750W	ES_6_150	EM_6_150	EL_6_150
2	292.30	279.88	284.25	295.00	284.68
4	140.91	209.48	114.37	110.63	72.02
6	73.89	105.40	49.92	81.87	92.30
8	66.79	64.72	57.98	83.45	54.09
10	46.15	-	63.13	47.94	41.67
12	-	-	49.52	45.52	-
14	-	-	45.71	-	-
16	-	-	-	-	-
18	-	-	-	-	-
20	-	-	-	-	-
24	-	-	-	-	-

Appendix Table B10 The cumulative amounts of releasing vancomycin in 5 ml SBF solution (μg).

Time (h)	Cumulative amount (μg)				
	HTib_750W	HTW_750W	ES_6_150	EM_6_150	EL_6_150
2	292.30	279.88	284.25	295.00	284.68
4	433.21	489.37	398.61	405.63	356.71
6	507.10	594.76	448.53	487.50	449.01
8	573.89	659.48	506.51	570.95	503.10
10	620.04	659.48	569.64	618.89	544.76
12	620.04	659.48	619.17	664.40	543.04
14	620.04	659.48	664.88	664.40	543.04
16	-	-	-	-	-
18	-	-	-	-	-
20	-	-	-	-	-
24	-	-	-	-	-
Total amount of releasing VM within 14 hours	620.04	659.48	664.88	664.40	543.04

CIRRICULUM VITAE

NAME : Miss Upsorn Boonyang

BIRTH DATE : September 03, 1981

BIRTH PLACE : Udonthani, Thailand

EDUCATION :

YEAR	INSTITUTE	DEGREE/DIPLOMA
2003	Thammasat Univ.	B.Sc. (Chemistry)

PUBLICATIONS : K. Lewis, U. Boonyang, L. Evans, S. Siripaisarnpipat, B. Ben-Nissan. "A Comparative Study of Thai and Australian Crocodile Bone for use as a Potential Biomaterial" Key Eng. Mater. Vols. 309-311 (2006) 15-8.

U. Boonyang, P. Chaopanich, A. Wongchaisuwat, P. Senthongkaew, S. Siripaisarnpipat. "Effect of Phosphate Precursor on the Production of Hydroxyapatite from Crocodile Eggshells" J. Biomim. Biomater. Tissue Eng. Vol.5 (2010)31-7.

PETTY PATENT : ดร.สุธาทิพย์ ศิริไพศาลพิพัฒน์ และ อัปสร บุญยัง "กรรมวิธีการผลิตสารไฮดรอกซีอะปาไทต์จากวัสดุธรรมชาติที่มีแคลเซียมเป็นองค์ประกอบหลัก" อนุสิทธิบัตรเลขที่ 4281/2550

SCHOLARSHIP : The Royal Golden Jubilee PhD, Research Assistantship from the Thailand Research Fund (TRF) 2004-2009

RGJ-CHE-PhD-SW, Research Fund from Walailak University 2005-2008